AD NUMBER

AD822784

LIMITATION CHANGES

TO:

Approved for public release; distribution is unlimited. Document partially illegible.

FROM:

Distribution authorized to U.S. Gov't. agencies and their contractors; Critical Technology; JUN 1967. Other requests shall be referred to Army Electronics Command, Attn: AMSEL-KL-TG, Fort Monmouth, NJ. Document partially illegible. This document contains export-controlled technical data.

AUTHORITY

USAEC ltr dtd 16 Jun 1971

AD

SU-IPR Report No. 156

TECHNICAL REPORT ECOM-00482-11

Electrostatic Waves in Bounded Hot Plasmas

by

Masayuki Omura

June 1967

ECOM

UNITED STATES ARMY ELECTRONICS COMMAND · FORT MONMOUTH, N.J.
CONTRACT DA-28-0[illegible]AC-00482(E)

INSTITUTE FOR PLASMA RESEARCH
STANFORD ELECTRONICS LABORATORIES
STANFORD UNIVERSITY · STANFORD, CALIFORNIA

NOTICES

Disclaimers

The findings in this report are not to be construed as an official Department of the Army position, unless so designated by other authorized documents.

The citation of trade names and names of manufacturers in this report is not to be construed as official Government indorsement or approval of commercial products or services referenced herein.

Disposition

Destroy this report when it is no longer needed. Do not return it to the originator.

Technical Report ECOM-00482-11

June 1967

ELECTROSTATIC WAVES IN BOUNDED HOT PLASMAS

by

Masayuki Omura

SUIPR REPORT NO. 156

Technical Report

Contract DA 28-043 AMC-00482(E)

Prepared by

Institute for Plasma Research
Stanford University
Stanford, California

ABSTRACT

This report deals with the study of electrostatic waves in bounded hot plasmas and, except for a few dc measurements, is theoretical.

The study is broadly divided into two parts. The first section investigates waves in a diode system with no dc magnetic field applied. A dc analysis of the equilibrium plasma produced within a thermionic diode is undertaken to provide a basis for the rf analysis, and expected plasma densities in the diode are computed for a variety of practical situations. Electrostatic wave resonances in the diode are predicted by using the hydrodynamic model for the nonuniform plasma. The impedance of a uniform plasma diode is obtained by using a kinetic model of the plasma. This model enables us to take into account the end plate electron absorption loss, a process similar to that which causes end plate diffusion in the Q-machine. The absorption loss is found to have a large effect on the impedance of the diode.

The second part of the report deals with the study of guided waves along a cylindrical column of Maxwellian plasma in a magnetic field. A dc study of the plasma column is first conducted. Theoretical density and current profiles are obtained and are compared with the measured results. Since an rf analysis using a self-consistent dc solution is complicated involved, the plasma column is approximated by a uniform plasma with a sharp boundary and no drift. To obtain the rf fields in such a column, a plane-wave solution for an infinite Maxwellian plasma in an applied magnetic field is first obtained. By superimposing infinitely many plane waves, the fields within the column are constructed, and by matching the appropriate fields at the boundary, a dispersion relation is derived.

The solutions to the dispersion relation reveal the existence of a new type of unstable waves. When only the electrons are assumed to respond to the electric field, the surface waves which propagate when $\omega_{ce} < \omega_{pe}$ are found to be unstable. When the ion motion is included, additional unstable surface waves are obtained whenever $\omega_{ci} < \omega_{pi}$. A study of the instability shows that it is due to finite Larmor radii effects and is driven by the transverse energy of the particles.

While the "electron" surface wave instability is relatively weak and can easily be stabilized by making $\omega_{ce} > \omega_{pe}$, the "ion" surface wave instability is found to be very strong, and the stabilizing condition of $\omega_{ci} > \omega_{pi}$ is not easily attained in high density plasmas such as those in fusion machines. Thus, the unstable ion surface waves may have a serious effect on the containment of the fusion plasma.

CONTENTS

CONTENTS (Continued)

TABLE

ILLUSTRATIONS

SYMBOLS

a	waveguide radius
a_n	expansion coefficient
$\bar{A}$	vector potential
b	plasma radius
$\bar{B}(r)$	magnetic field
$\bar{B}_1(r)$	perturbed magnetic field
$\bar{B}_1(r,\omega)$	spectrum of the perturbed magnetic field
$\bar{B}_0$	applied dc magnetic field
c	speed of light
$\bar{D}_1(r,\omega)$	spectrum of the perturbed displacement field
$\bar{\bar{D}}(r)$	permittivity
e	electron charge
e_j	charge of the j^{th} species
$\bar{E}(r)$	electric field
$\bar{E}_0$	dc electric field
$\bar{E}_1(r)$	perturbed electric field
$\bar{E}_1(r,\omega)$	spectrum of the perturbed electric field
$E_{1z}(r), E_{1\theta}(r), E_{1r}(r)$	perturbed electric field in the z, θ, r directions
$f_0(\bar{v})$	dc electron velocity distribution function
$f_1(r,\bar{v},t)$	perturbed electron distribution function
$f_j(r,\bar{v})$	dc velocity distribution function for the j^{th} species in a plasma column
$F(k)$	elliptic integral of the first kind
I_n	Bessel polynomial
$\bar{k}$	$\bar{B}_1(r,\omega)/B_0$

$H_n^{(2)}(x)$	Hankel function
i	$\sqrt{-1}$
$\hat{i}_x, \hat{i}_y, \hat{i}_z$	unit vectors along x, y and z axis
$\bar{I}$	unit tensor
$\bar{I}_t$	total current density
$I_n = I_n(x)$	modified Bessel function
$\bar{J}_p(x,t)$	perturbed conduction current
$J_{\phi j}$	azimuthal current due to the j^{th} species
J_+, J_-	ion and electron emission currents
$K(\zeta)$	complete elliptic integral of the first kind
$\bar{k}$	wave number
$k_x, k_y, k_z, k_\rho, k_\parallel$	components of the wave number
$\bar{L} = \bar{L}(\omega)$	gyro-tensor $\bar{L}(\omega) = \int_0^\infty \bar{D}(\omega')d\omega'$
$\bar{M}$	magnetization vector
m	electron mass
m_j	mass of the j^{th} species
n	integer
n_0	dc electron density
$n_+(x), n_i(r)$	ion density
$n_-(x), n_e(r)$	electron density
$\hat{n}$	unit vector along the dc magnetic field
$N_j(r)$	density per unit length for the j^{th} species
p	k_ρ
p_z	$i\left(\frac{\omega}{\omega_c} - n\right)$
$\bar{P}$	polarization vector (perturbed)
P_0, P_1	zero and first oder pressure
$R(\omega)$	reflection coefficient

r	radius
r_m	$\sqrt{8\kappa T/m_i\omega_{ci}^2}$
r_o	cathode radius
$\vec{r}$	coordinate vector in r,-θ plane
t	time
T	temperature
$T_\perp, T_\parallel$	transverse and longitudinal temperature
$\vec{u}_o$	drift velocity
v	velocity in one dimension
$\vec{v}$	velocity vector
v_θ	electron thermal speed, $\sqrt{\kappa T/m}$
$v_{\theta j}$	thermal speed of the j^{th} species
v_p	phase velocity
v_o	velocity of the spherical shell plasma
$V(r), V(x)$	dc potential
$\vec{x}$	coordinate vector
x,y,z	linear coordinates
$Z_n = Z(\zeta_n)$	Hilbert transform of gaussian
α	$n_+(0)/n_-(0)$
β	$n_+(L)/n_-(L)$
$\gamma_e, \gamma_a, \gamma_i$	arrival rates of electrons, atoms and ions
Γ	$\sqrt{(\omega^2-\omega_p^2)/v_o^2}$
δ	$\sqrt{1-\alpha^2}$
ϵ_o	free space permittivity
$\overleftrightarrow{\epsilon}$	relative dielectric tensor

ϵ_{ij}	elements of the dielectric tensor
ζ_n	$(\omega-n\omega_c)/\sqrt{2}\, k_{\parallel} v_\theta$
η	normalized dc potential, $eV/\kappa T$
κ	Boltzmann's constant, 1.38044×10^{-23} joules/^oK
$\lambda_D, \lambda_{DO}, \lambda_{DL}, \lambda_a$	Debye lengths, $\lambda_D = v_\theta/\omega_p$
λ	$\sqrt{2}\, k_\perp v_\theta/\omega_c$
$\vec{\xi}, \xi$	dummy variables
$\overleftrightarrow{\pi}$	electric susceptibility tensor for the electrons
$\overleftrightarrow{\pi}_j$	electric susceptibility tensor for the j^{th} species
π_{ij}	elements of the susceptibility tensor
ρ, ρ'	normalized radius
ρ_1	perturbed charge density
$\rho(x,\xi), \sigma(\lvert x\rvert)$	conductivity kernels
φ	dummy variable
$\emptyset[\ ]$	rf potential
$\psi(a,b;x)$	confluent hypergeometric function of the second kind
μ_i, μ_e, μ_a	emission rates of ions, electrons and neutrals
μ_o	free space permeability
$\overleftrightarrow{\mu}(\varphi)$	tensor relating $\vec{B}$ to $\vec{M}$
ω	angular frequency
$\omega_p, \omega_{po}, \omega_{pe}$	electron plasma frequency, $\sqrt{n_e e^2/m\epsilon_o}$
ω_c, ω_{ce}	electron cyclotron frequecy, eB_o/m
ω_{pi}	ion plasma frequency $\sqrt{n_i e^2/m_i \epsilon_o}$
ω_{ci}	ion cyclotron frequency eB_o/m_i
$\overleftrightarrow{\omega}_j = \vec{i}_z \omega_j$	rotational vector for the j^{th} species of a plasma column

ω_H	$\sqrt{(\omega_c^2 + \omega_p^2)/2}$
ω_{H1}	ion hybrid frequency $\frac{1}{\omega_{H1}^2} = \frac{1}{\omega_{p1}^2 \omega_{c1}^2} + \frac{1}{\omega_{ce}^2}$

ACKNOWLEDGMENT

I would like to express my sincere gratitude to Dr. Heinrich Derfler for his invaluable guidance and interest during all phases of this work. I am also indebted to Dr. Thomas C. Simonen for his cooperation and assistance throughout the course of this study, to Professor O. Buneman for his valuable comments, and to Professor L. Moll for reading the manuscript.

My gratitude is also expressed to Mrs. Elaine Christensen for her expert help in preparing the manuscript.

Last but not least, I would like to express heartfelt thanks to my wife, Claire, for her untiring support and encouragement.

I. INTRODUCTION

The object of this study is an investigation of electrostatic waves in bounded hot plasmas. While the bulk of prior work on electrostatic waves is restricted to infinitely extended plasmas, our study emphasizes the effects due to finite plasma boundary. Originally we hoped to avoid complications due to instabilities by restricting our work to near equilibrium plasmas. Yet in the study of a perfectly Maxwellian magnetoplasma column, we discovered unstable surface waves which are due to finite Larmor radii effects.

Plasmas in perfect thermostatic equilibrium are generated inside a black body, and our work on the subject of equilibrium plasma generation and the waves in such plasmas is summarized in Section A below. A near equilibrium column of plasma is obtained in a magnetic field between electron and ion emitting end plates. Prior work on electrostatic waves in such plasma columns and our own work which lead to the discovery of unstable waves is summarized in Section B. A brief review of known instabilities in Section C places the newly discovered instability into proper perspective.

A. PLASMAS IN PERFECT THERMOSTATIC EQUILIBRIUM

Theory and interpretation of experimental data on plasmas often suffer because the deviations from equilibrium are not known exactly. A situation in which all of the constituents are in equilibrium may be found inside a black body. A study of the dc states of an equilibrium plasma bounded by thermionically emitting walls is undertaken in Chapter II. An earlier work by Nottingham[1] considers the diode geometry consisting of two parallel infinite walls emitting only electrons. In such a system the electron density within the diode space was found to be highly nonuniform and became very low at a distance of a few Debye lengths away from the wall. We show that under equilibrium conditions a small amount of ions emitted from a thermionic emitter can neutralize the electron space charge to form a plasma in the diode space. This is illustrated by computations based on diode walls made from pure refractory metals. The effects of enhanced ion emission from the walls due to the

introduction of alkali vapor in the diode space are also examined. Some experimental measurements for a sodium plasma are given and compared with the theoretical prediction.

Electrostatic waves within the equilibrium plasma diode are studied in Chapter III. The nonuniform sheath effects are investigated by means of the hydrodynamic model of the plasma. Previously the hydrodynamic model was used by Weissglas[2] and later by Parker[3] to explain the Dattner[4] resonances in a nonuniform plasma column. As opposed to these previous works on free boundary sheaths, our study is directed to the cathode sheaths bounded by an emitter.

In the second part of Chapter III we present a study of end plate loss effects by using a kinetic model of the plasma. The end plate losses are due to the same mechanism which causes end plate diffusion in a plasma column such as that produced in the Q-machine.[5] When particles in the magnetized plasma column are absorbed by the end plate and re-emitted with different guiding centers, the net result is a diffusion of the particles away from the column. In the diode system consisting of infinite parallel planes, we are not concerned with diffusion, but the process of absorption and re-emission causes rf energy loss in the diode. An electron emitted from the wall acquires rf energy as it traverses the diode space, and the entire energy is lost as it is absorbed at the other wall. Previous work by Hall[6] used kinetic theory in considering a plasma capacitor but assumed perfect reflection of the particles at the boundary and thereby neglected the end plate loss effects. In our study we include the absorption effect at the end plate, but because of the extreme complexity of kinetic analysis, we were able to study only the case of a uniform plasma in the diode space.

B. ELECTROSTATIC WAVES IN A PLASMA COLUMN

In a practical plasma the emitting plates are not infinite in extent. In fact, plasmas are often produced between two circular emitting plates which are separated by a distance several times greater than the plate radius. Confinement of the plasma in such a column is achieved by applying a magnetic field along the axis. A dc study of such a column of magnetized plasma is given in Chapter IV. Theoretical density and

current profiles are computed from an appropriate solution to the Boltzmann equation and a comparison is made with some experimental results. The study indicates that the plasma column may be approximated by a uniform plasma with a sharp boundary. To simplify the study of waves in the plasma column, it is essential to assume that the column is uniform.

In 1957 Gould and Trivelpiece[7] used the cold plasma model to predict electrostatic wave propagation along a uniform plasma column such as the one shown in Fig. 1.1. The dispersion relations for cylindrically symmetic waves along such a column are shown in Fig. 1.2. When $\omega_c > \omega_p$, propagation is confined within two frequency ranges, $0 \leq \omega \leq \omega_p$ and $\omega_c < \omega < \sqrt{\omega_p^2 + \omega_c^2}$. Whether the plasma completely fills the waveguide or not, these passbands are unaltered as long as $\omega_c > \omega_p$. However, when $\omega_c < \omega_p$, filled and unfilled waveguides have different passbands. For the completely filled waveguide, the two passbands are $0 < \omega < \omega_c$ and $\omega_p < \omega < \sqrt{\omega_p^2 + \omega_c^2}$. When the plasma does not fill the waveguide, the upper passband is as before $\left(\omega_p < \omega < \sqrt{\omega_p^2 + \omega_c^2}\right)$, but the lowest order mode of the low-frequency band propagates in the band $0 < \omega < \sqrt{(\omega_p^2 + \omega_c^2)/2}$ as shown by the dotted line. This particular mode is a

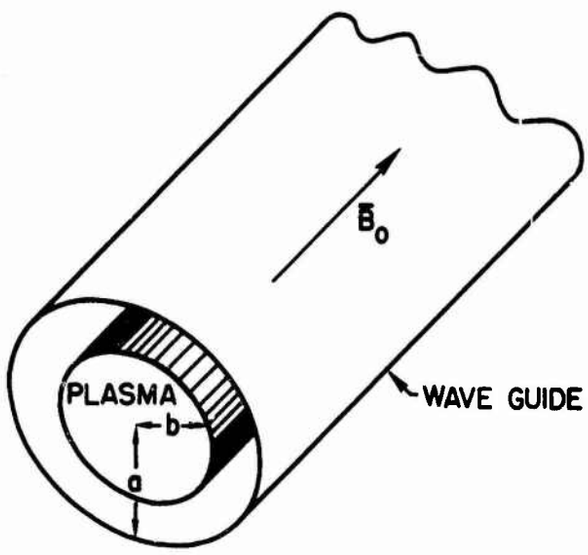

FIG. 1.1. CONFIGURATION OF PLASMA IN A CYLINDRICAL WAVEGUIDE.

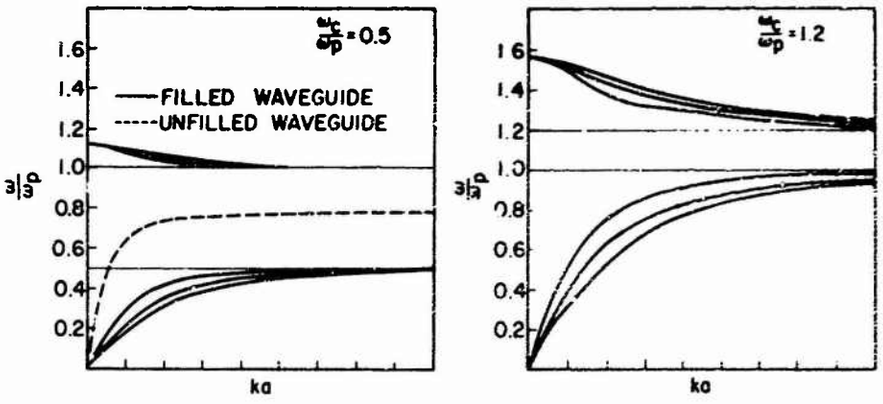

FIG. 1.2. DISPERSION RELATION FOR WAVES IN CYLINDRICAL PLASMA COLUMN. Dispersion relations for waves in a cylindrical column of cold plasma are given for two cases. The diagram on the right shows dispersion relations with $\omega_c = 1.2\ \omega_p$ and on the left dispersion relations with $\omega_c = 0.5\ \omega_p$ are shown. The quantity ka is the product of wavenumber and the waveguide radius.

surface wave in the frequency range $\omega_c < \omega < \sqrt{(\omega_p^2 + \omega_c^2)/2}$ in that the fields are strongest near the edge of the plasma. Such a surface mode cannot be excited in a filled waveguide. In Chapter VI attention is directed toward this surface wave which becomes unstable when the temperature effects are included properly.

Agdur and Weissglas[8] used the hydrodynamic model of the plasma to point out the temperature effects. Later Jayson and Lichtenberg[9] used an electron plasma model with Maxwellian velocity distribution along the magnetic field but with zero transverse temperature to compute dispersion relations for waves in filled waveguides. Kuehl et al[10] used a fully thermal plasma model but with infinite magnetic field to compute the dispersion relation in the identical geometry. The models of Lichtenberg and Jayson and Kuehl et al yield Landau damping of the modes, while the hydrodynamic model does not. The study of waves in fully thermal unbounded magnetoplasma has been conducted by several authors,[11,12] but the waves in a magnetoplasma column have not been treated before due to the extreme computational complexity involved. This paper reports the study of waves in a magnetoplasma column and the discovery of surface wave instabilities.

In preparation for the study of electrostatic-wave propagation in a magnetized plasma column, a dielectric tensor appropriate for an infinitely extended Maxwellian plasma is obtained in Chapter V. Our dielectric tensor is simpler than the "dielectric" tensor presented by Stix.[13] The simplicity of our dielectric tensor results from subdividing the plasma current into polarization and magnetization currents. A cylindrical wave solution appropriate for a uniform column of Maxwellian plasma is synthesized from plane waves and the dispersion relation for the waves is obtained in Chapter VI. At low magnetic fields $(\omega_c < \omega_p)$ the surface wave along the column of a Maxwellian electron plasma is shown to be unstable. The nature of the instability is studied by means of Derfler's stability criteria.[14,15] The surface waves which occur near the ion cyclotron frequency when $\omega_{ci} < \omega_{pi}$ are also found to be unstable. Since the complete analysis is so vast, only the lowest-order cylindrically symmetric mode is numerically analyzed.

C. INSTABILITIES

Plasma instabilities can be divided into two general groups, microinstability and macroinstability. The instabilities which cannot be derived from the standard magnetohydrodynamic equations but which depend on detailed microscopic equations for the plasma are classified as microinstabilities. We are interested primarily in the microinstabilities which occur in a finite geometry.

Among the macroinstabilities in a current carrying plasma are the well-known kink and sausage instabilities which are caused by the interaction of the plasma with its self-magnetic field. Another instability which occurs in a plasma with a directed current is the Kadomtsev instability.[16] The Kelvin-Helmholtz instability[17] occurs in a stratified fluid in which the adjacent layers are in relative motion.

The above instabilities can be obtained from the fluid model of the plasma. The second class of instabilities, the microinstabilities, may be divided into two broad groups. The first are those instabilities which are caused by the peculiarities of the velocity distribution and may be called velocity space instabilities. The second group of instabilities depends on the plasma geometry. A simple example of the first

In preparation for the study of electrostatic-wave propagation in a magnetized plasma column, a dielectric tensor appropriate for an infinitely extended Maxwellian plasma is obtained in Chapter V. Our dielectric tensor is simpler than the 'dielectric' tensor presented by Stix.[13] The simplicity of our dielectric tensor results from subtracting the plasma current into polarization and magnetization currents. A cylindrical wave solution appropriate for a uniform column of Maxwellian plasma is synthesized from plane waves and the dispersion relation for the waves is obtained in Chapter VI. A [illegible] the surface wave along the column of a Maxwellian electron plasma is shown to be unstable. The nature of the instability is studied by means of Dawler's stability criteria.[14,15] The surface waves which occur near the ion cyclotron frequency when $\omega_{ci} \quad \omega_{pi}$ are also found to be unstable. Since the complete analysis is so vast, only the lowest-order cylindrically symmetric mode is numerically analyzed.

C. INSTABILITIES

Plasma instabilities can be divided into two general groups, microinstability and macroinstability. The instabilities which cannot be derived from the standard magnetohydrodynamic equations but which depend on detailed microscopic equations for the plasma are classified as microinstabilities. We are interested primarily in the microinstabilities which occur in a finite geometry.

Among the macroinstabilities in a current carrying plasma are the well-known kink and sausage instabilities which are caused by the interaction of the plasma with its self-magnetic field. Another instability which occurs in a plasma with a directed current is the Kadomtsev instability.[16] The Kelvin-Helmholtz instability[17] occurs in a stratified fluid in which the adjacent layers are in relative motion.

The above instabilities can be obtained from the fluid model of the plasma. The second class of instabilities, the microinstabilities, may be divided into two broad groups. The first are those instabilities which are caused by the peculiarities of the velocity distribution and may be called velocity space instabilities. The second group of instabilities depends on the plasma geometry. A simple example of the first

type of the two-stream instability which occurs when counter streaming of charged particles exists. Velocity space instability occurs also when there is temperature anisotropy in the plasma. Drummond and Tetreault[11] investigated the instabilities of a plasma with zero temperature along the magnetic field but with non-zero velocity in the perpendicular direction. Their model can be considered also as having extreme temperature anisotropy.

Our interest lies primarily with instabilities of the second group. While the velocity space instability is independent of plasma geometry those of the second group require geometric discontinuity. Finally studies of slightly inhomogeneous plasma has been carried out by many authors. Rudakov and Sagdeev[12] and Krall and Rosenbluth[13] independently discovered the so-called universal instabilities which occur when there is a density gradient in the direction perpendicular to the magnetic field. Universal instabilities arise because of resonance between the drift of particles in the inhomogeneous plasma and the phase velocities of the waves. Other papers by Krall and Rosenbluth[14] and Rosenbluth and Simon[15] predict unstable modes near multiples of the ion gyro-frequency in the slightly inhomogeneous plasma.

The surface wave instability which we discovered must also be distinguished from the second group since it is found only when the plasma discontinuity is finite. The surface wave instability however is different from the universal instability. While the waves associated with the universal instability propagate in the direction perpendicular to both the density gradient and the magnetic field, the surface wave propagates along the magnetic field. It is principally governed by the density gradient in the radial direction. The wave with the universal instability must be an extraordinary moding mode while the surface wave instability is found in ordinary and extraordinary waves. Like the universal instability and velocity space instability, the surface wave is not related to any of the resonance instabilities.

There is yet a third type of electrostatic instabilities which is a combination of the velocity space instabilities and the geometrical induced instabilities. Post and Rosenbluth[16] discuss how a two-stream type instability is modified by a weak density and magnetic field gradient. This third type is again unlike the surface wave instability.

II. DC STATES OF HOLLOW CATHODE PLASMA

Gdien plasmas produced in the laboratory differ from a true thermodynamical equilibrium plasma. In such nonequilibrium plasmas the energy distribution of the constituents (electrons, ions, neutrals and radiation) deviates significantly from Boltzmann's probability law (exp - E/KT). These deviations are an apparently inexhaustible source for the discovery of new instabilities, designed by nature to ultimately restore equilibrium. Theory and interpretation of experimental data frequently suffer because the deviations from equilibrium are never known exactly. A situation where all constituents are as close as possible to strict thermodynamic equilibrium may be found within a boundary consisting of walls which thermionically emit electrons, ions, and neutrals. In this chapter we will examine the dc properties of equilibrium plasmas bounded by such thermionically emitting walls. Numerical results are given for some practical situations.

A. PLASMA DIODE

In this section we investigate theoretically the plasma produced between the two infinite plane emitting walls as shown in Fig. 2.1. There is no net dc potential across the diode, and the emitters emit electrons and ions in some known number ratio $\beta^2 = n_+(L)/n_-(L)$, which is fixed by thermodynamic considerations of the material.

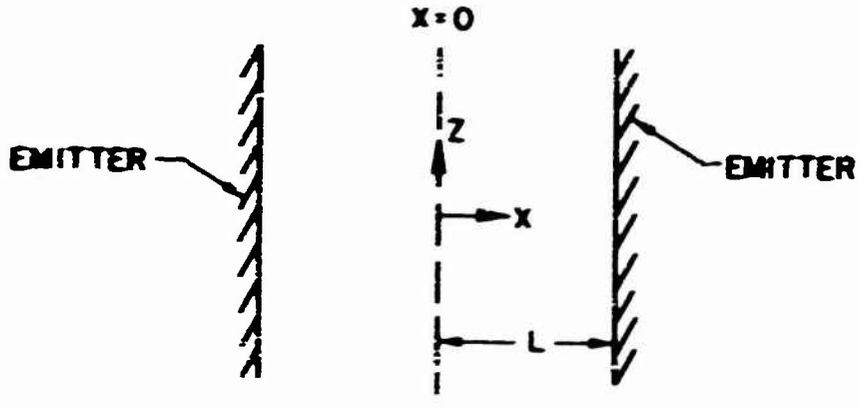

FIG. 2.1. EMITTER GEOMETRY

In the past a great deal of work has been done on diodes consisting of thermionic emitters. The majority of these papers deal with the study of dc and oscillating states with a nonzero dc potential applied across the diode. An early work on the thermionic diode with zero net potential was given by Nottingham,[1] who treated the problem in the absence of ions. Without the ions he found that the electron density was highly nonuniform, and if the spacing was much greater than the Debye length, the density at the midplane was very low. Eichenbaum and Hernqvist[25] included the ion emission but studied the problem using the collisionless Boltzmann equation, never allowing the empty regions of the phase space to fill up. Figure 2.2 illustrates the model used by Eichenbaum and Hernqvist with the shaded region of the ion phase space unfilled. Such a nonequilibrium analysis is not realistic when there is no net potential across the diode. Langmuir[26] examined an equilibrium case but with one of the planes at infinity.

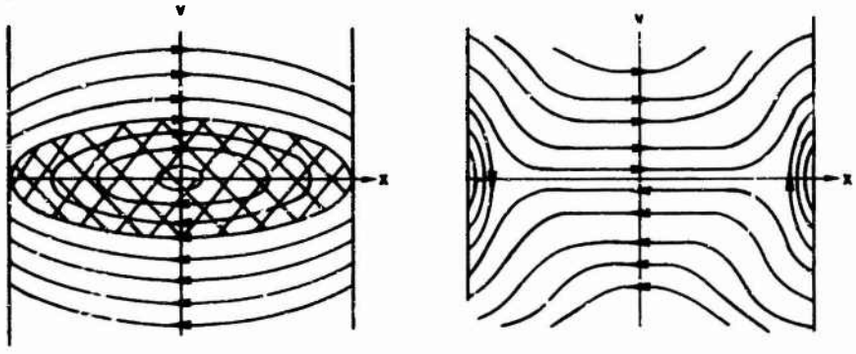

FIG. 2.2. PHASE SPACE SKETCH FOR THE ELECTRONS AND IONS.

In our problem, we assume a strict thermodynamic equilibrium and fill the phase space completely according to Boltzmann's probability law, and hence the scale-height law is used for the electron and ion densities. By taking the potential to be zero at the midplane $(x = 0)$, Poisson's equation becomes

$$\frac{d^2V}{dx^2} = -\frac{e}{\epsilon_o}\left[n_+(x) - n_-(x)\right]$$
$$= -\frac{e}{\epsilon_o}\left\{n_+(0)\,\exp\left[-\frac{eV}{\kappa T}\right] - n_-(0)\,\exp\left[\frac{eV}{\kappa T}\right]\right\} \quad . \qquad (2.1)$$

At this point normalized quantities

$$\xi = \frac{x}{\sqrt{2}\,\lambda_{D0}} ,$$

$$\eta = \frac{eV}{\kappa T}$$

and

$$\alpha^2 = \frac{n_+(0)}{n_-(0)}$$

with the Debye length at $x = 0$,

$$\lambda_{D0} = \left(\frac{\epsilon_o \kappa T}{n_-(0)\, e^2} \right)^{1/2} ,$$

are introduced, and Eq. (2.1) is thus reduced to

$$\frac{d^2\eta}{d\xi^2} = 2[e^{\eta} - \alpha^2 e^{-\eta}] . \qquad (2.2)$$

Let us first consider the case of $\alpha < 1$, the "electron" rich case. The boundary condition at $\xi = 0$ is

$$\eta = 0 , \qquad \eta' = 0 .$$

By introducing a new variable

$$w^2 = e^{\eta} , \qquad (2.3)$$

the solution to Eq. (2.2) is found to be

$$F(\alpha, w) = K(\alpha) - \xi \qquad (2.4)$$

where $F(\alpha,w)$ is the elliptic integral of the first kind[27] with modulus α,

$$F(\alpha,w) = \int_0^w \frac{dt}{\sqrt{(1-t^2)(1-\alpha^2 t^2)}} \qquad (2.5)$$

and $K(\alpha) = F(\alpha,1)$ is the complete elliptic integral. Tables for these integrals are available.[26]

By inverting Eq. (2.4), we obtain

$$w = sn[K(\alpha) - \xi,\alpha] \qquad (2.6)$$

where $sn[K(\alpha) - \xi,\alpha]$ is the Jacobi elliptic function[27] with modulus α and argument $K(\alpha)-\xi$. Hence,

$$\psi = -2 \ln sn[K(\alpha) - \xi,\alpha] . \qquad (2.7)$$

Equation (2.7) enables us to calculate the potential as a function of z provided α is known. Generally, α is a quantity we seek in terms of a similar quantity given at the emitter surface. Let

$$\beta^2 = \frac{n_+(L)}{n_-(L)} .$$

We know from the scale-height law that

$$n_-(L) = n_-(0) \exp(-\tau_L)$$

and

$$n_+(L) = n_+(0) \exp(-\tau_L) .$$

Hence,

$$\frac{n_+(L)}{n_-(L)} = \frac{n_+(0)}{n_-(0)} \exp(-2\tau_L) ,$$

or

$$\beta^2 = \alpha^2 e^{-4\tau_L} .$$

The subscript L denotes quantities evaluated at the surface of the emitter. Since

$$\xi = \frac{x}{\sqrt{2}\, i_{DL}} = \frac{x}{\sqrt{2}\, i_{DL}} \frac{i_{DL}}{i_D} = \frac{x}{\sqrt{2}\, i_{DL}} \left(\frac{n_-(L)}{n_-(L)} \right)^{1/2} = \frac{x}{\sqrt{2}\, i_{DL}} \exp\left(-\frac{\tau_L}{2} \right) = \frac{x}{\sqrt{2}\, i_{DL}} \tau_L ,$$

Eq. (2.4) can be rewritten as

$$\frac{x}{\sqrt{2}\, i_{DL}} = \frac{K(\alpha) - F(\alpha, \varphi)}{\tau_L} . \qquad (2.8)$$

We evaluate Eq. (2.8) at $x = L$ and obtain

$$\frac{L}{\sqrt{2}\, i_{DL}} = \frac{K(\alpha) - F(\alpha, \varphi_L)}{\tau_L} . \qquad (2.9)$$

With Eq. (2.9) a family of curves, L/i_{DL} versus α with τ_L as a parameter, can be plotted as shown in Fig. 2.3. From the graph α can be determined for given values of τ_L and $L/(\sqrt{2}\, i_{DL})$ and, consequently, τ_-/τ_L, x/L and n_-/n_L can be obtained.

The following properties of the Jacobi elliptic function and the elliptic integrals are worth noting here.[24] For $\alpha \to 1$ we have

$$\mathrm{sn}(x, \alpha) \approx \sin x - \frac{\alpha^2}{4} \cos x (x - \sin x \cos x) \ldots \qquad (2.10)$$

$$K(\alpha) \approx \frac{\pi}{2} + \alpha^2 \frac{\pi}{8} \ldots \qquad (2.11)$$

Thus, for $\alpha \to 1$, Eq. (2.7) becomes

$$\tau_- \approx -2 \ln \left[\sin \left(\frac{\pi}{2} - \xi \right) \right]$$

which is the relation obtained by Nottingham for the case of a pure electron cloud.

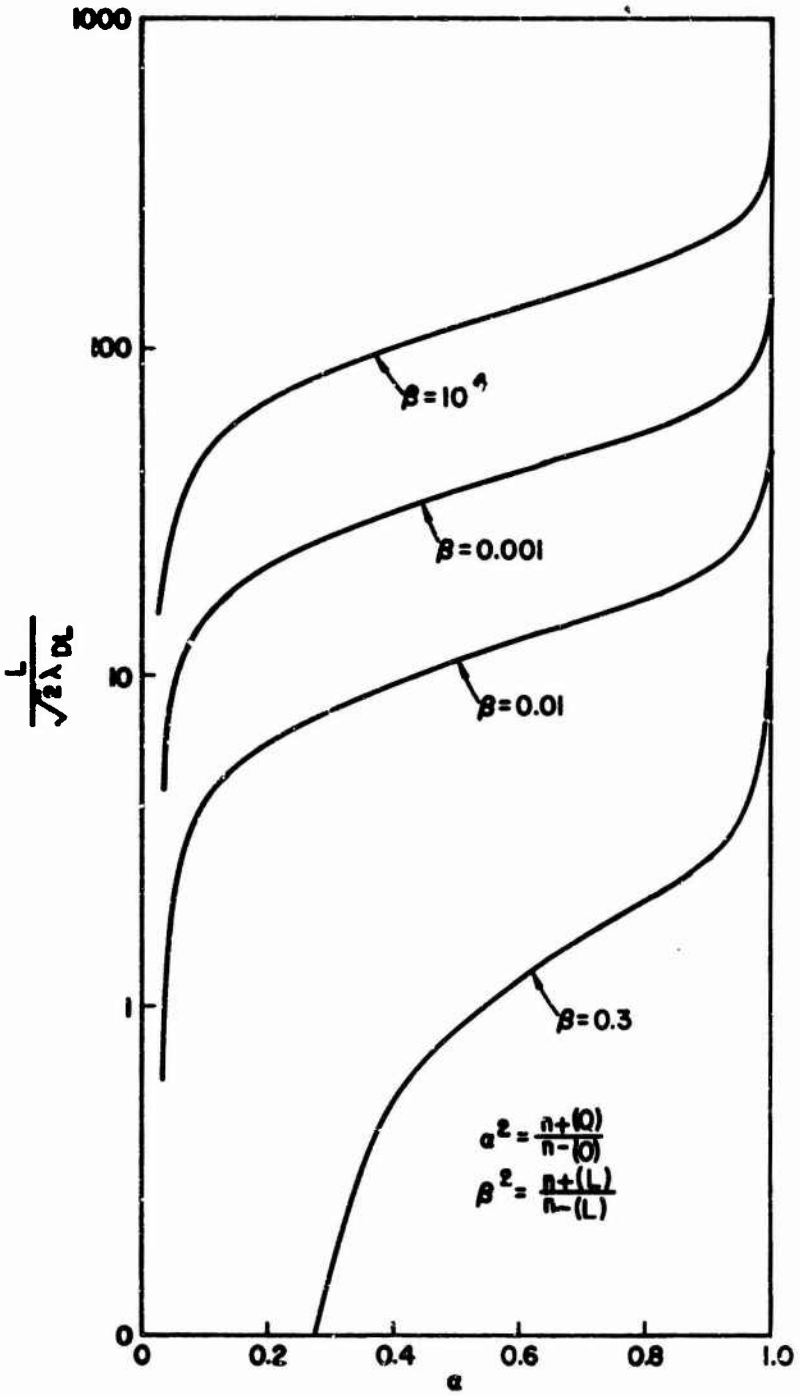

FIG. 2.3. RATIO OF ELECTRON AND ION DENSITY, $\alpha^2 = n_+(0)/n_-(0)$, IN MID-PLANE AS A FUNCTION OF SEPARATION DISTANCE 2L IN UNITS OF DEBYE LENGTH λ_L FOR DIFFERENT VALUES OF $\beta^2 = n_+(L)/n_-(L)$.

For α approaching unity we have

$$sn(u,\alpha) \approx \tanh u + \frac{1}{4}(1-\alpha^2)\,\mathrm{sech}^2 u[\sinh u \cosh u - u] \ldots \quad (2.12)$$

and

$$K(\alpha) \approx \ell n\left[\frac{4}{(1-\alpha)^{1/2}}\right] \ldots \quad (2.13)$$

For small values of w or $\sqrt{\beta/\alpha}$, we also have

$$F(\alpha,w) \approx w - \frac{1}{6} w^2(1+\alpha^2) \ldots \quad (2.14)$$

By shifting the origin to the wall,

$$\xi' = -\xi + L ,$$

using Eq. (2.9) and letting the other wall go to infinity $(\alpha \to 1)$, we obtain from Eq. (2.7)

$$\begin{aligned} \eta &\approx -2\,\ell n\, sn[F(1,\sqrt{\beta}) + \xi', 1] \\ &\approx -2\,\ell n\, sn[\sqrt{\beta} + \xi', 1] \\ &\approx -2\,\ell n\,[\tanh(\sqrt{\beta} + \xi')] \end{aligned} \quad (2.15)$$

which is the result given by Langmuir for the semi-infinite plasma bounded by an emitting plane.

Thus far, we have been concerned with electron rich cases. The ion rich cases can be derived simply be re-defining the parameters α, β, η and λ_{DO} as shown in the table below.

Symbol	Electron Rich	Ion Rich
β^2	$n_+(L)/n_-(L)$	$n_-(L)/n_+(L)$
α^2	$n_+(0)/n_-(0)$	$n_-(0)/n_+(0)$
λ_{DO}^2	$\kappa T\,\epsilon_o/(e^2 n_-(0))$	$\kappa T\,\epsilon_c/(e^2 n_+(0))$
η	$eV/\kappa T$	$-eV/\kappa T$

With the new definitions, the Poisson's equation becomes identical to Eq. (2.2) with $\alpha \leq 1$.

B. NUMERICAL EXAMPLES WITH PURE METAL EMITTERS

To give some idea of the types of densities and potential profiles which can be expected inside a "black body," we give some numerical results based on emission data of pure refractory metals. In practice the quantity $\beta^2 = n_+(L)/n_-(L)$ is not easily obtained because the data on ion emission rate from various metals are scarce. For the numerical computations we use the following empirical formula on ion emission from molybdenum emitter as given by Wright[29] and the Richardson equation for electron emission. Current densities are given in amps per cm^2.

$$\ell n\, J_+ = 28.39 - \frac{e\phi_+}{\kappa T} - 0.453\, \ell n\, T + 6.22 \times 10^{-4} T\,, \qquad (2.16a)$$

$$J_- = AT^2 \exp\left(-\frac{e\phi_-}{\kappa T}\right) \qquad (2.16b)$$

with

$$A = 55 \text{ amp/cm}^2$$

$$\phi_+ = 8.3 \text{ volts}$$

$$\phi_- = 4.37 \text{ volts}\,.$$

In the computation the emitters are assumed to be 1 cm apart. In Fig. 2.4 plots of n_o, $n_+(0)$, $n_-(0)$ and λ_{DO} versus $1/T$ are given. The neutral density n_o is obtained from the data provided by Honig.[30] The graphs show that above 2000 ^oK the space charge is practically neutralized at $x = 0$. For $T < 1800\ ^oK$ the diode space consists almost entirely of electrons, the density is very low and the Debye length is of the order of the diode separation. Figs. 2.5 and 2.6 give potential and density profiles for $T = 2200\ ^oK$.

We were somewhat startled to find that the space charge neutralization requires only a small amount of ion emission from the walls. For the example shown in Fig. 2.6, the ion density at the wall is 10^6/cc, which

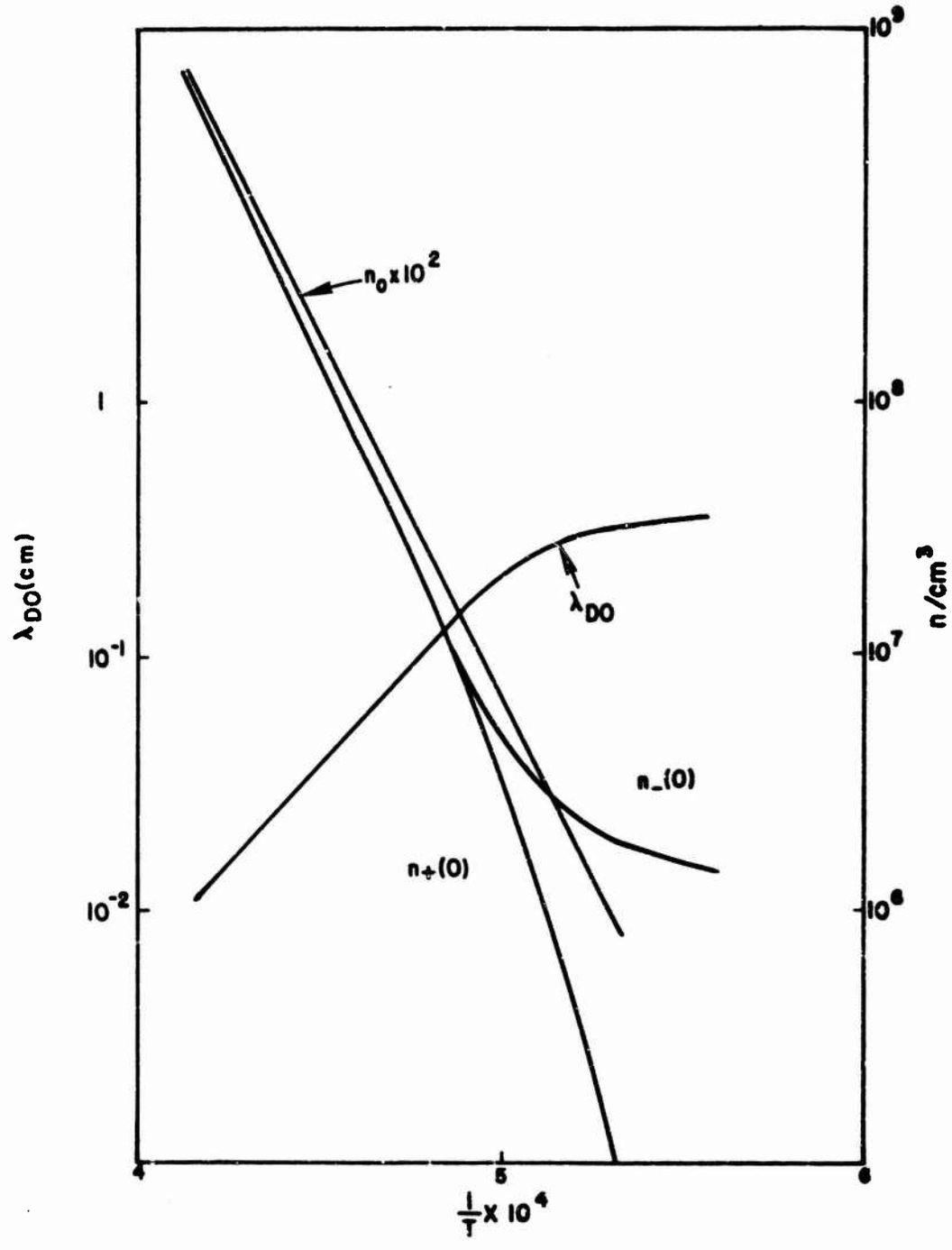

FIG. 2.4. ELECTRON DENSITY, $n_-(0)$, ION DENSITY, $n_+(0)$, DEBYE LENGTH λ_{DO} IN MID-PLANE, AND THE NEUTRAL DENSITY n_o AS A FUNCTION OF 1/T FOR A PURE MOLYBDENUM EMITTER.

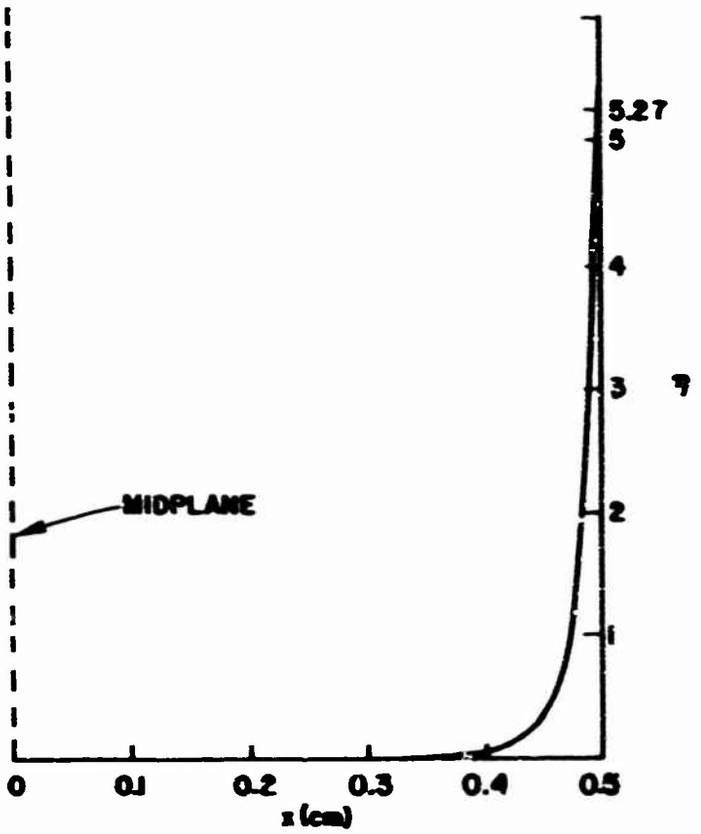

FIG. 2.5. ELECTROSTATIC POTENTIAL $\eta = eV/\kappa T$ AS A FUNCTION OF THE DISTANCE FROM MID-PLANE.

corresponds to an ion current density of 10^{-9} amps/cm^2. Even with such a small ion emission rate, we can derive a neutral plasma whose density is orders of magnitude greater than that predicted by the analysis of Nottingham (ions absent) or Eichenbaum and Hernqvist (nonequilibrium analysis with unfilled regions in phase space).

The midplane electron density, ion density and neutral density versus 1/T for tungsten and niobium are shown in Figs. 2.7 and 2.8. For tungsten the data on the neutral density are obtained from graphs provided by Honig, and the following empirical formula as given by Smith[31] is used to compute the ion density at the tungsten emitter.

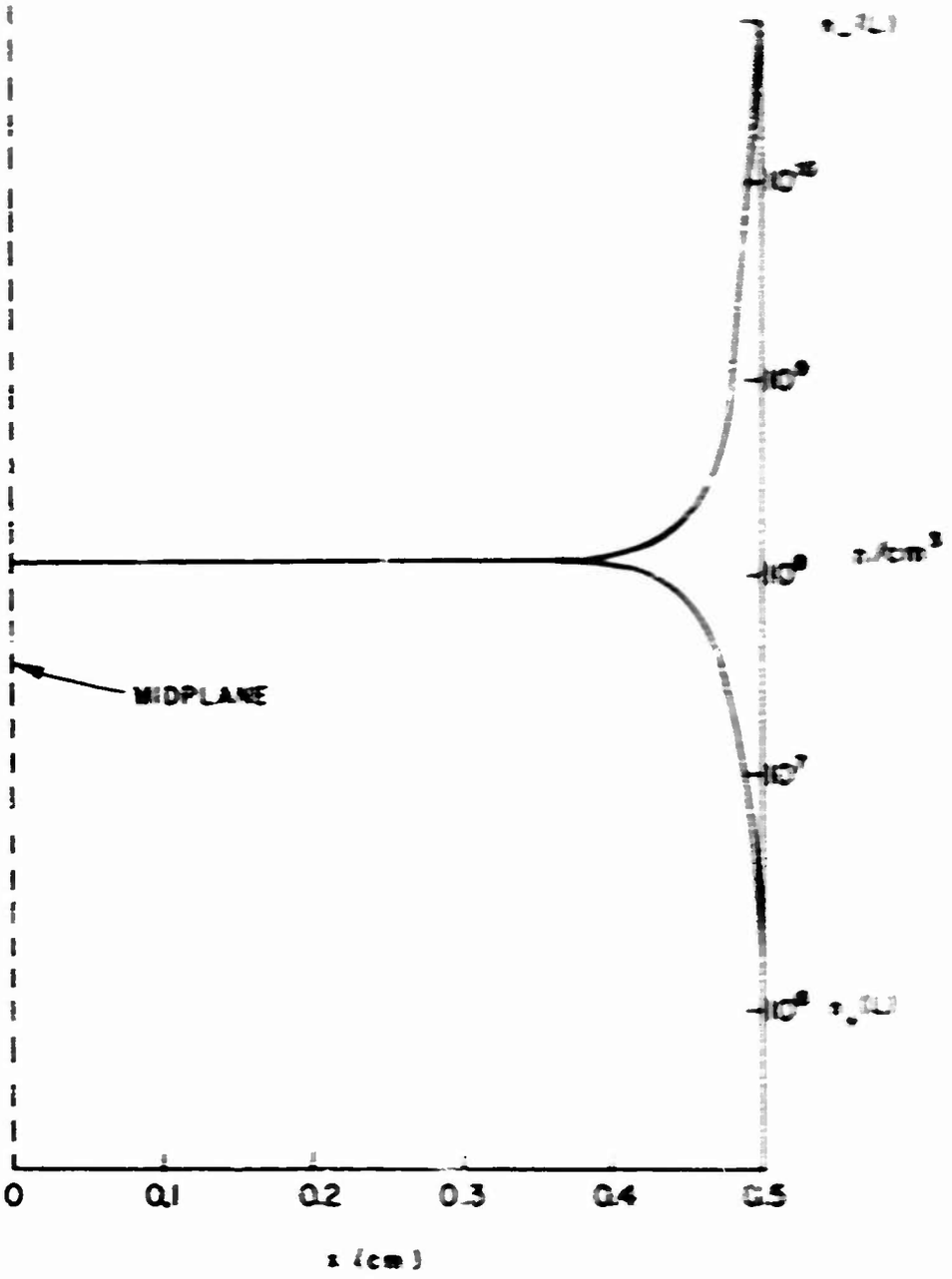

FIG. 2.6. ELECTRON DENSITY $n_e(x)$ AND ION DENSITY $n_+ = n_e$ AS FUNCTIONS OF THE DISTANCE FROM THE MID-PLANE.

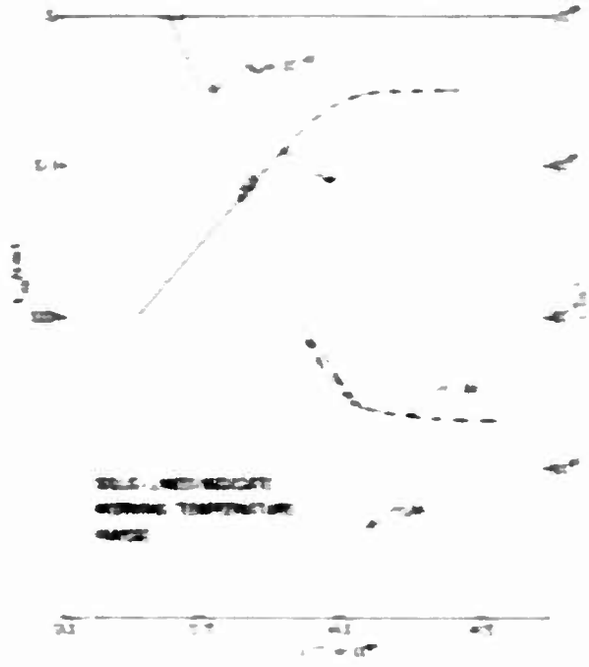

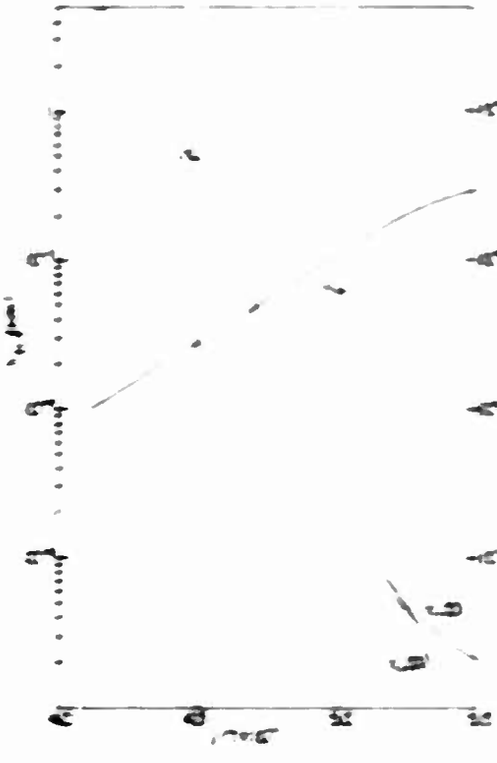

$$\log_{10} j_e = 0.36 \log_{10} T + 1.64 \times 10^{-3} T - \frac{\phi_e}{2.3kT} + 12.4 \qquad (2.17)$$

with $\phi_e = 11.9$ volts. The result for tungsten emitters is qualitatively similar to that of the molybdenum emitter. The calculation for the niobium emitter is based on the ion emission data obtained in the laboratory by the author.[32] The niobium ion emission data obeyed the following empirical relation

$$\ln j_e = 24.1 - \frac{\phi_e}{kT} - 1.2 \ln T - 2 \times 10^{-3} T$$

with $\phi_e = 3.82$ volts. The current densities are given in amps per cm^2. The neutral density for niobium is obtained from vapor pressure data provided by Honeywell.[33]

C. PLASMA PRODUCED INSIDE A SMALL CYLINDRICAL EMITTER

We now consider the cylindrical emitter, as shown in Fig. 2.5, to see the effect of the geometry on the plasma density and the sheath potential. Under the condition

$$\frac{\lambda}{R_e} \ll \frac{\lambda}{r_e} \ll 1 ,$$

Poisson's equation is given as

$$\frac{d^2\chi}{dr^2} + \frac{1}{r}\frac{d\chi}{dr} = -\frac{e}{\epsilon_0}\left[n_+(r) - n_-(r)\right] \qquad (2.18)$$

Again the scale-height law is assumed to govern the density distribution, and hence,

$$\frac{d^2\chi}{dr^2} + \frac{1}{r}\frac{d\chi}{dr} = -\frac{e}{\epsilon_0}\left\{n_+(0)\exp\left[-\frac{e\chi}{kT}\right] - n_-(0)\exp\left[\frac{e\chi}{kT}\right]\right\} \qquad (2.19)$$

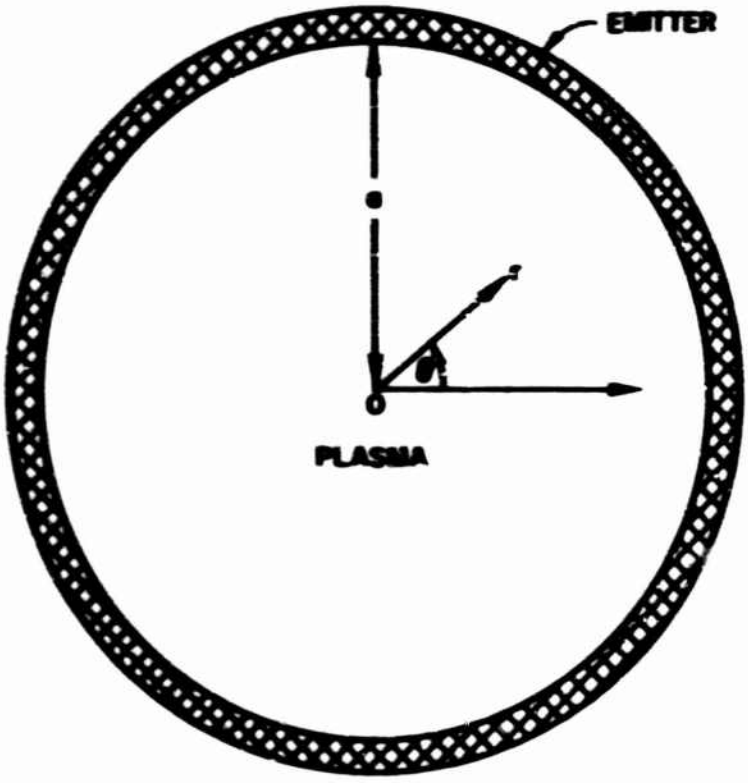

FIG. 2.9. CYLINDRICAL EMITTER OF RADIUS a.

where $n_+(0)$ and $n_-(0)$ are the ion and electron densities at $r = 0$. Normalization similar to those of Section A yields

$$\frac{d^2\eta}{d\xi^2} + \frac{1}{\xi}\frac{d\eta}{d\xi} = e^{\eta} - \alpha^2 e^{-\eta} \qquad (2.20)$$

where

$$\xi = \frac{r}{\lambda_{D0}} = r\sqrt{\frac{e^2 n_-(0)}{\varepsilon_0 kT}} .$$

Equation (2.20) cannot be solved in terms of classical transcendental equations. An analytic solution does exist, however, when the ions are absent ($\alpha = 0$). For this special case the solution is given by

$$\eta = -2\ln\left(1 - \frac{\xi^2}{8}\right) . \qquad (2.21)$$

For the general case of nonzero α, one must resort to numerical integration. The following normalization is found to be convenient for numerical analysis

$$\rho' = \sqrt{\alpha}\,\rho = \frac{r}{\lambda_{DO}}\sqrt{\alpha} = \frac{r}{\lambda_a}\sqrt{\beta}\ , \quad \lambda_a = \sqrt{\frac{\kappa T\,\epsilon_o}{e^2 n_-(a)}}$$

The variable ρ' measures the radius in units of $\lambda_a/\sqrt{\beta}$, which is a known quantity, while the variable ρ is normalized to λ_{DO}, which is not known a priori. Poisson's equation now becomes

$$\frac{d^2\eta}{d\rho'^2} + \frac{1}{\rho'}\frac{d\eta}{d\rho'} = \frac{1}{\alpha}\left[e^{\eta} - \alpha^2 e^{-\eta}\right] \tag{2.22}$$

or by re-arranging the right hand side we have

$$\frac{1}{\rho'}\frac{d}{d\rho'}\left(\rho'\frac{d\eta}{d\rho'}\right) = \frac{1}{\alpha}\left[2\sinh\eta + \delta^2 e^{-\eta}\right] \tag{2.23}$$

where

$$\delta^2 = 1 - \alpha^2$$

Equation (2.23) introduces a parameter δ^2 which is generally a small number directly proportional to the fractional deviation from neutrality at $\rho' = 0$. For computational purposes, we used Eq. (2.23). For a given value of α, a series solution can be obtained for small values of ρ'. Let

$$\eta = a_1\rho' + a_2\rho'^2 + a_3\rho'^3 + a_4\rho'^4 \ldots$$

Then

$$\frac{1}{\rho'}\frac{d}{d\rho'}\left(\rho'\frac{d\eta}{d\rho'}\right) = \frac{a_1}{\rho'} + 4a_2 + 9a_3\rho' + 16a_4\rho'^2 \ldots$$

$$\sinh \eta = a_1 \xi^{-1} + a_2 \xi^{-2} + \left(a_3 + \frac{1}{3} a_1^3\right) \xi^{-3} \ldots$$

and

$$e^{-\eta} = 1 - a_1 \xi^{-1} + \left(\frac{a_1^2}{2} - a_2\right) \xi^{-2} + \left(a_1 a_2 - a_3 - \frac{1}{3} a_1^3\right) \xi^{-3} \ldots$$

By inserting these relations into Eq. (2.23) and equating the coefficients of the like power terms, we get

$$a_{2m+1} = 0 \qquad \text{for } m = 0, 1, 2, 3 \ldots$$

$$a_2 = \frac{\xi^2}{4}$$

$$a_4 = \frac{1}{16} (2 - \xi^2) a_2$$

$$a_6 = \frac{1}{36} \left[(2 - \xi^2) a_4 + \frac{\xi^2 a_2^2}{2} \right]$$

$$a_8 = \frac{1}{64} \left[(2 - \xi^2) a_6 + \frac{a_2^3}{3} - \frac{\xi^2 a_2^3}{2} + \xi^2 a_2 a_4 \right]$$

Using this solution as the starting point, the differential equation is integrated numerically by a SUBALGOL procedure called "Adams Predictor Corrector Method," available at the Stanford Computation Center. The integration procedure is repeated with different values of ξ until the boundary condition at the wall is satisfied. The resulting potential profiles for a molybdenum emitter are shown with the temperature as a parameter in Fig. 2.10. The diameter of the emitters is taken to be 1 cm. The curves show that the density and potential profiles for the cylindrical system look like those of the planar system when the radius is much larger than the Debye length, λ_D.

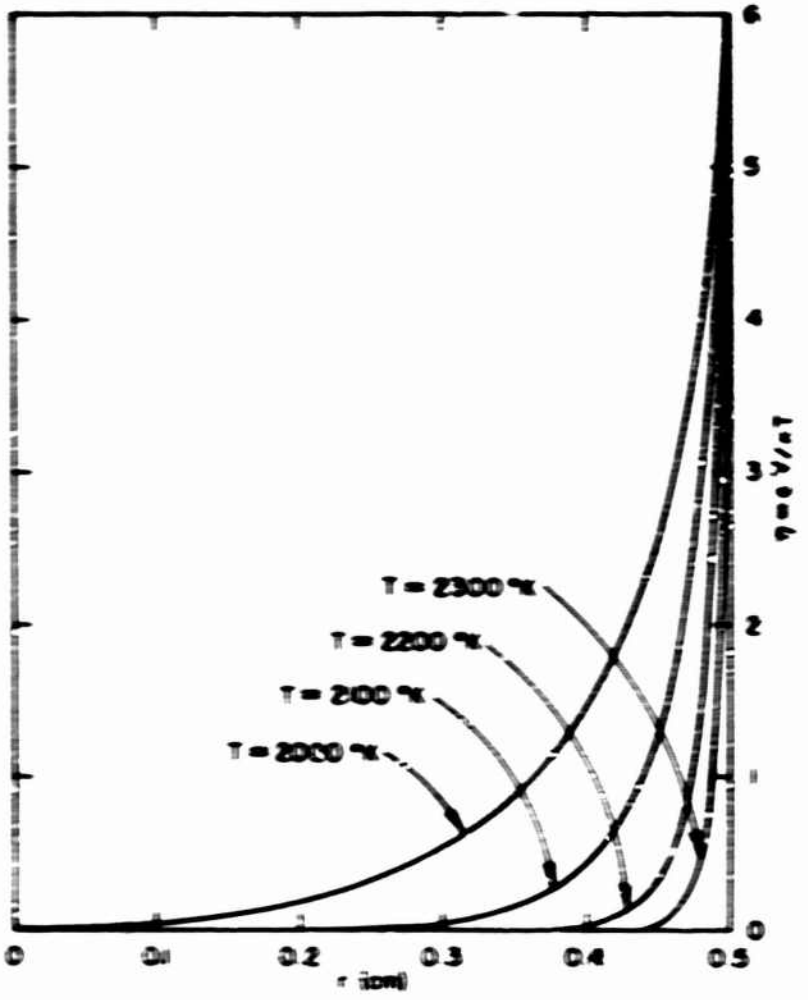

FIG. 2.11. POTENTIAL PROFILES INSIDE A HOLLOW CYLINDRICAL MOLYBDENUM EMITTER FOR DIFFERENT TEMPERATURES.

D. CONTACT IONIZATION PLASMAS

In 1923 Langmuir and Kingdon[34] showed that, when a neutral atom strikes a hot metal whose work function is greater than the ionization potential of the atom, the atom bounces off the metal as an ion with high probability. Since Langmuir's demonstration many papers have been written on this subject, and, in fact, many of the plasma generators designed today are based on this phenomena. An excellent theoretical treatment of the surface phenomena involved with the so-called contact ionization process is given in a recent series of papers by Levine and Gyftopoulos.[35,36,37] They derive the emission rates of the ions, electrons and atoms under thermodynamic equilibrium conditions. The emission rates ν_i, ν_e and ν_a are given in terms of temperature and the

fraction θ of the metal surface covered by a mono-layer of adsorbent. Under steady state conditions, ion and atom emission rates are equated to the arrival rates of the ions and atoms μ_i and μ_a.

$$\nu_a + \nu_i = \mu_a + \mu_i$$

To obtain the steady state coverage, we assume $\nu_i = \mu_i$, and the atom emission rate is equated to the atom arrival rate which is computed from the vapor pressure of the adsorbent material. In this manner, the steady state coverage θ is determined and hence emission rates can be computed. Strictly speaking, our computations violate the thermodynamic equilibrium condition since we assume that the vapor temperature is not necessarily equal to the metal temperature. Using the resulting emission data, we compute the density and potential profiles for several different sets of conditions. Shown in Figs. 2.11 and 2.12 are the profiles for a typical case with cesium vapor and tungsten emitters. Note that the space charge is neutral in the greater portion of the diode space despite the large difference in the electron and ion densities at the wall.

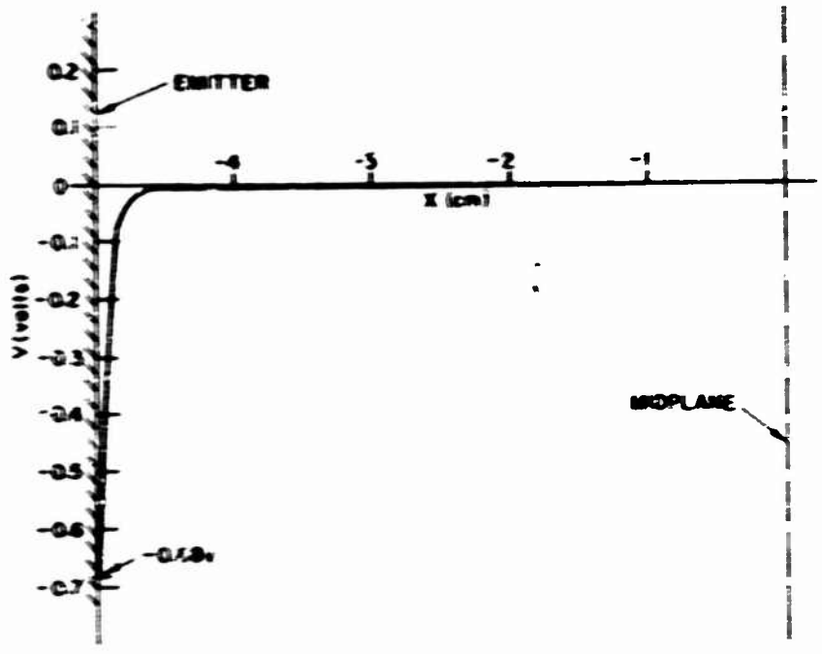

FIG. 2.11. THEORETICAL DC POTENTIAL PROFILE FOR A DIODE WITH TUNGSTEN WALLS AND CESIUM VAPOR. For the computation, the wall temperature was 1300 °K and the vapor temperature was 50 °C. The wall separation was taken to be 1 cm.

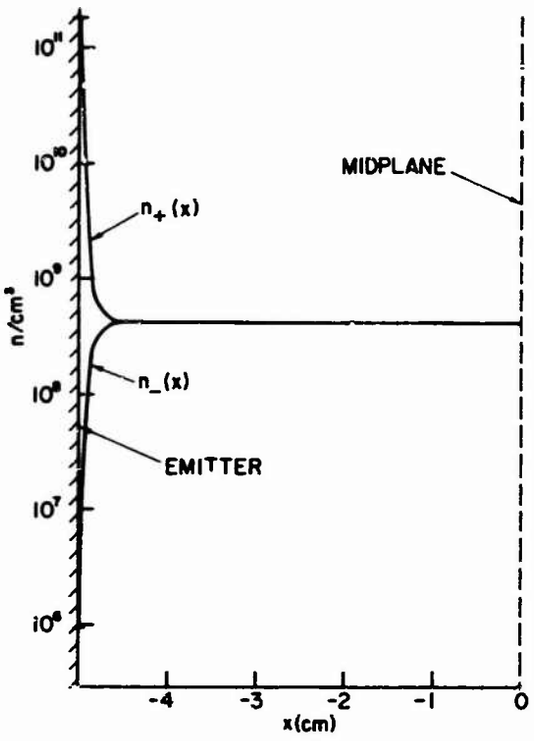

FIG. 2.12. ION AND ELECTRON DENSITY PROFILE. The conditions are identical to those of Fig. 2.11.

The midplane densities for sufficiently large plate separation ($L \gg \lambda_{DO}$) are computed for tantalum emitters with sodium, potassium and cesium vapors. Shown in Figs. 2.13, 2.14 and 2.15 are the midplane plasma frequency and the Debye lengths as functions of emitter temperature with the vapor temperature as a parameter. In the range of emitter temperatures covered, the Ta-Na system is electron rich, the Ta-K system is either electron or ion rich depending on the emitter temperature, and the Ta-Cs system is ion rich. It is interesting to note that even with sodium, whose ionization potential is higher than the work function of tantalum, a good workable plasma can be obtained. The probability of a sodium atom being ionized by tantalum is small, but a sufficiently high number become ionized to neutralize the electron space charge in the diode space.

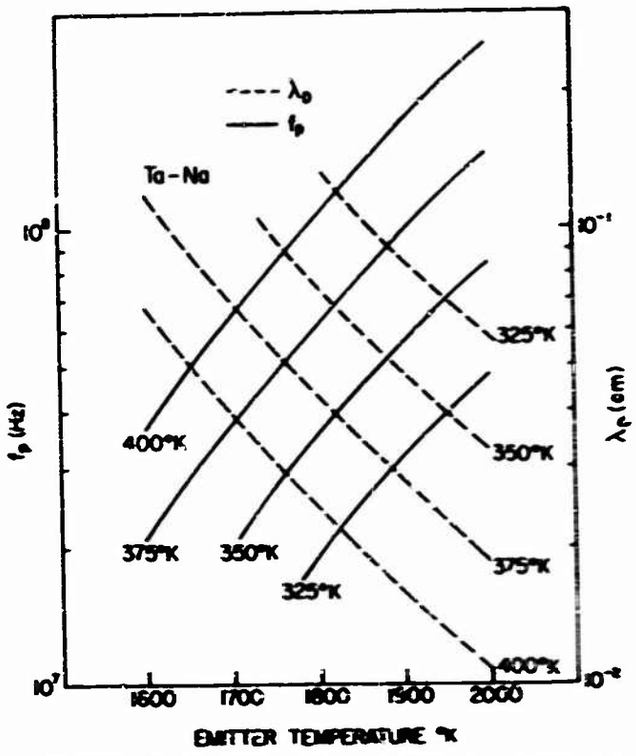

FIG. 2.13. PLASMA FREQUENCY AND THE DEBYE LENGTH FOR A SODIUM PLASMA PRODUCED BETWEEN TWO TANTALUM PLATES VS PLATE TEMPERATURE. Sodium temperature is used as a parameter.

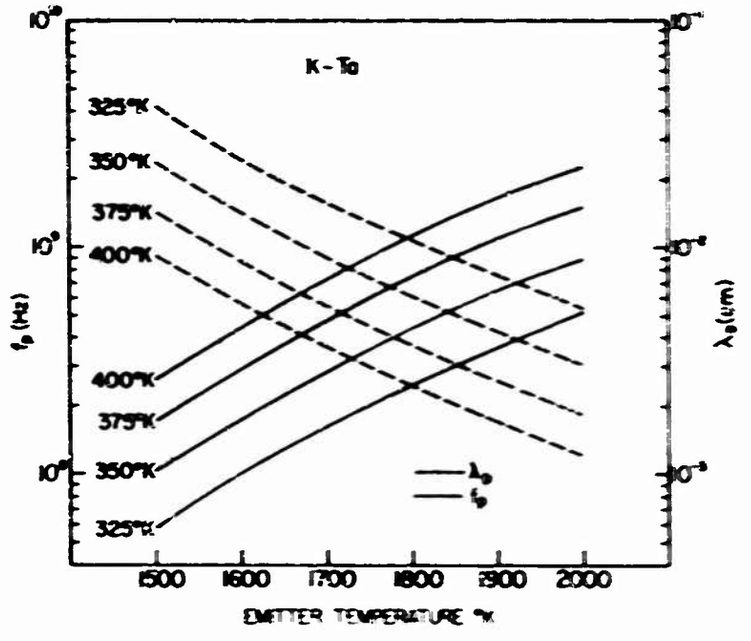

FIG. 2.14. PLASMA FREQUENCY AND THE DEBYE LENGTH FOR A POTASSIUM PLASMA PRODUCED BETWEEN TWO TANTALUM PLATES. The quantities are plotted as functions of tantalum temperature with potassium vapor temperature as a parameter.

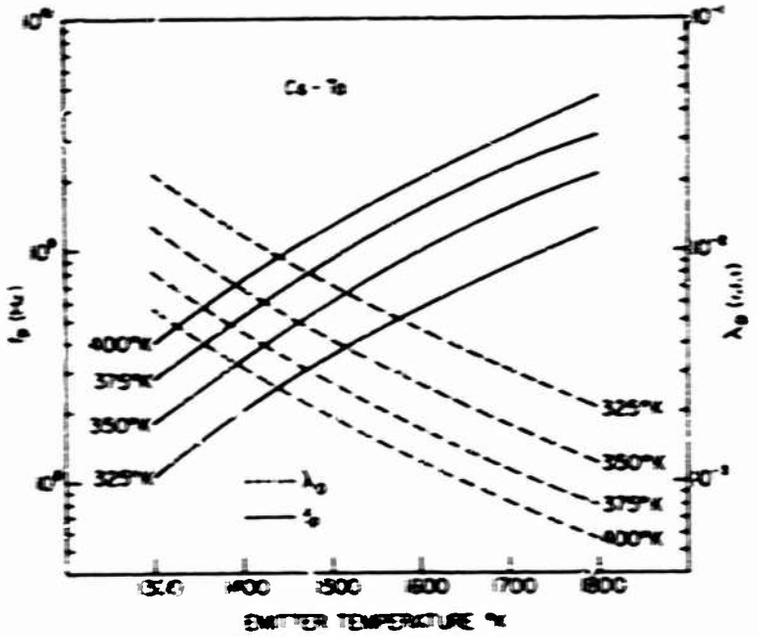

FIG. 2.15. PLASMA FREQUENCY AND THE DEBYE LENGTH FOR A CESIUM PLASMA PRODUCED BETWEEN TWO TANTALUM PLATES. The quantities are given as functions of tantalum temperature with cesium vapor temperature as a parameter.

E. DENSITY MEASUREMENTS WITH SODIUM PLASMA

Sodium plasma is produced in a diode which is described in the schematic drawings of Figs. 2.16 and 2.17. The diode consists of two circular tantalum buttons of diameter 1.6 inches seperated by 1 inch. The buttons are heated by electron bombardment, and the whole tube is immersed in an oil bath to keep the tube temperature uniform and low. Provision is made also to vary the oil bath temperature. The two gridded probes are for the Langmuir wave measurements discussed elsewhere.[3] The density is measured by a Langmuir probe consisting of a long wire of 15/1000 inch diameter. The probe is provided with an accurate meter which indicates the probe distance from the center line, and provisions are made to permit angular motion of the probes as well. The buttons are surrounded by heat shields which also act as guard rings. To confine the plasma in the radial direction and make the diode closely approximate an infinite system, an axial magnetic field is applied.

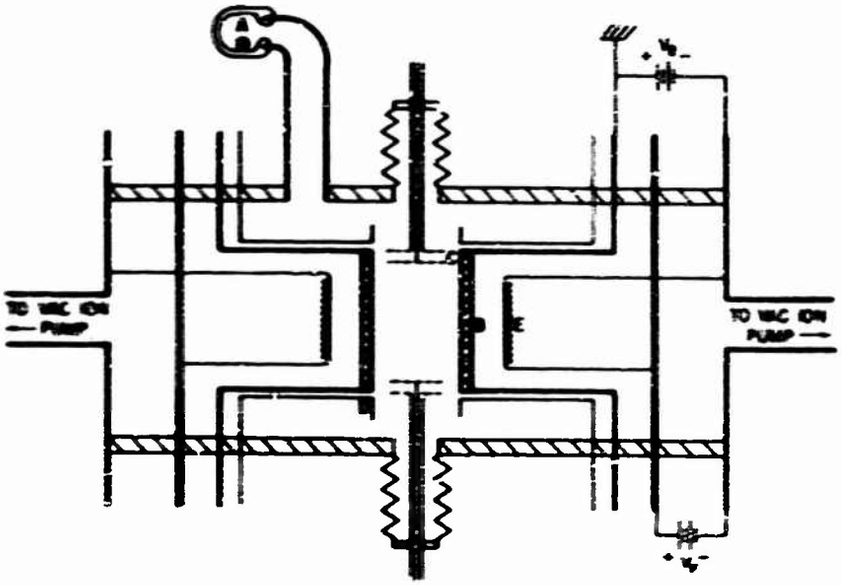

FIG. 2.16. SCHEMATIC DRAWING OF THE PLASMA TUBE. A = sodium vapor source; B = tantalum plates; C = gridded probe; D = heat shield (guard ring); E = bombarder filament; V_B = bombarder power supply; V_F = filament power supply.

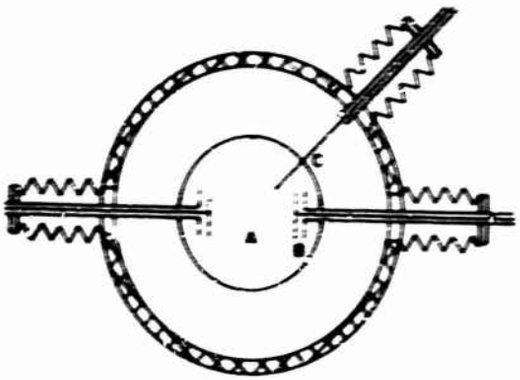

FIG. 2.17. SCHEMATIC DRAWING OF THE PROBE SYSTEM. A = tantalum plate; B = gridded probe; C = Langmuir probe.

The plasma density is found to be highly dependent on the guard-ring potential, as was noted also by Cutler.[39] The curves of Fig. 2.1[illegible] show the probe characteristics for various guard-ring potentials with a magnetic field of 3[illegible] gauss applied. Shown in Fig. 2.1[illegible] are the experimental and theoretical plasma frequencies as functions of the button temperature. The data are taken with the probe tip 2 mm from the center line, the guard ring biased positive and an axial magnetic field of 3[illegible] gauss applied. In the analysis of the data, we take that portion of the probe which is inside the cathode radius to compute the effective area of the probe. Hence, this method gives only the average density of the plasma. Nevertheless, the agreement between the theory and the experiment is good.

With the oil bath temperature at 3[illegible] °K, the neutral sodium density computed from vapor pressure data is 3 × 1[illegible] /cc. The plasma density with the button temperature at 2[illegible] °K is 2 × 1[illegible] /cc, which represents 4[illegible] percent ionization. Higher percentage ionization can be achieved at higher button temperatures. When a hard sphere model is used for sodium atom, the electron neutral collision frequency is about 3 MHz, while the plasma frequency is about 3 MHz for the conditions above.

From the measurements we can conclude that the sodium plasma is well-suited for low density quiescent plasma experiments. Undesirable effects, such as disappearance of the vapor source, shorting of the electrodes due to sodium coating and corrosion, are not noticeable. We believe that this is the first sodium plasma produced by the resonance ionization process. On the basis of our computations, Derfler and Simonen[35] decided to use the Na-Ta system in their Landau damping experiment.

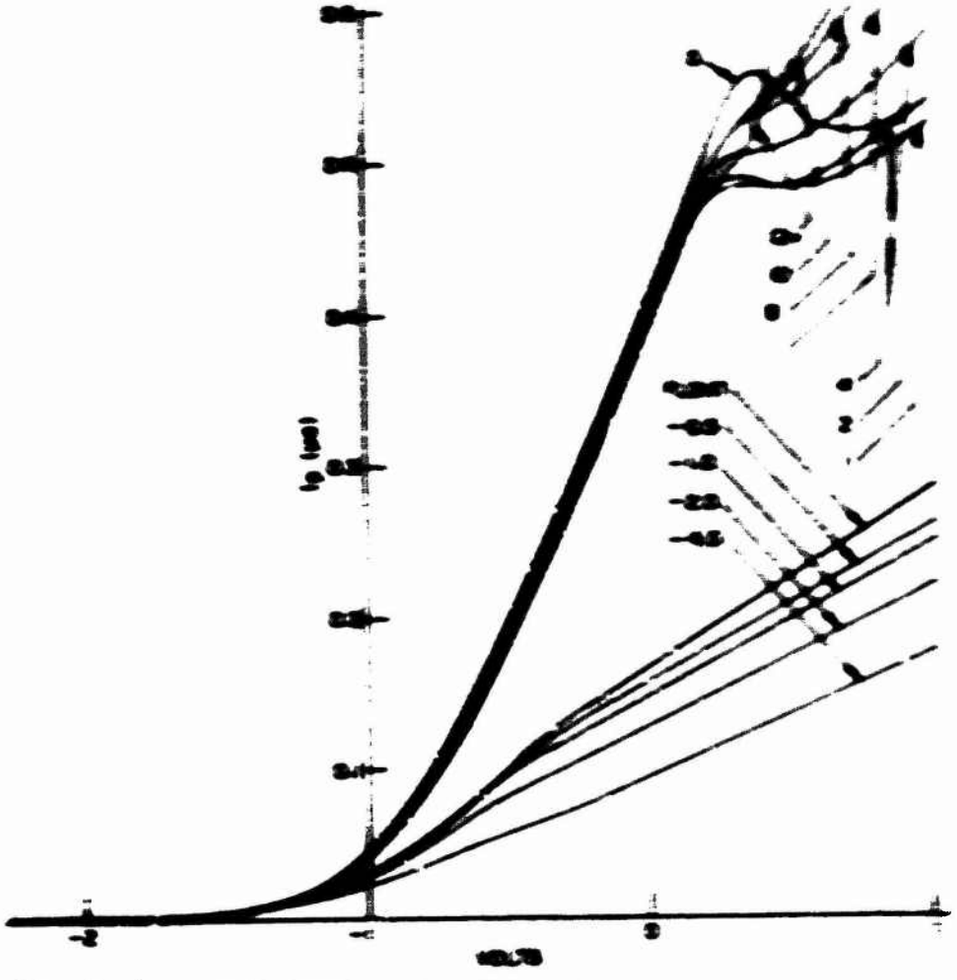

FIG. 2.14. PROBE CURVES FOR VARIOUS GUARD-RING POTENTIAL. The emitter temperature was at 1[illegible]°K and the magnetic field was 3K gauss. Probe tip was 1.2 cm from the tube axis.

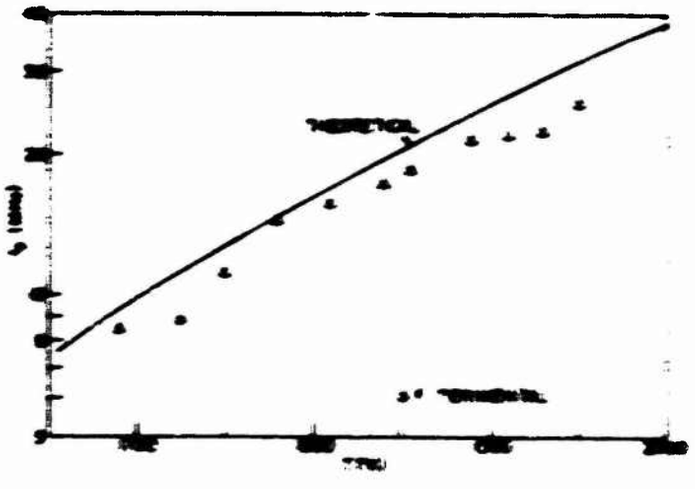

FIG. 2.15. EXPERIMENTAL AND THEORETICAL PLASMA FREQUENCIES VS HOTTOM TEMPERATURE. The coil both temperature was 3[illegible]°K.

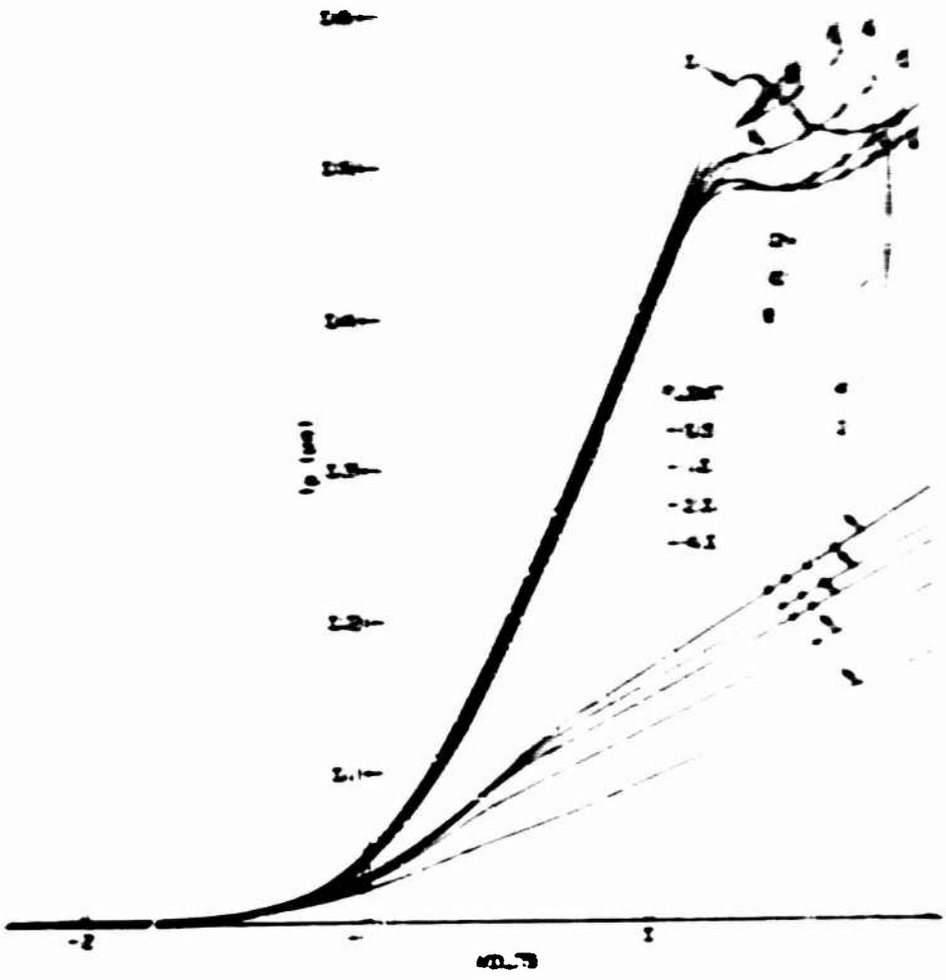

FIG. [illegible]. PROBE CURVES FOR VARIOUS DIODE-BIAS POTENTIALS. The emitter temperature was [illegible] and the temperature [illegible] were [illegible]. Probe [illegible] was [illegible] from the plane axis.

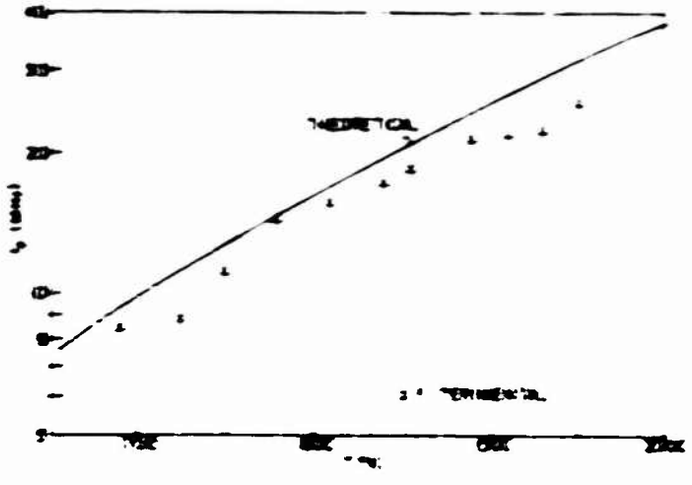

FIG. [illegible]. EXPERIMENTAL AND THEORETICAL PLASMA FREQUENCIES VS EMITTER TEMPERATURE. The [illegible] emitter temperature was [illegible].

and [illegible]

[illegible]

[illegible]

[illegible]

Equation [illegible] the [illegible] which was used in the previous chapter to derive the [illegible] of the [illegible]. The equation of state

[illegible]

[illegible]

[illegible]

and [illegible] for the [illegible]

[illegible]

[illegible]

[illegible]

Equation [illegible] and [illegible] equations [illegible] the [illegible] of equations [illegible] equations appropriate for the one [illegible] [illegible] for [illegible] We [illegible] the [illegible] the following [illegible] and [illegible]

[illegible]

and

[illegible]

[illegible] Equation [illegible] the [illegible] equation [illegible]

[illegible]

$$\left[\frac{\partial}{\partial t} + \frac{\partial}{\partial x}\right]\left[\frac{\partial}{\partial t} - \frac{\partial}{\partial x}\right] \; - \; \left[\frac{\partial^2}{\partial t^2} - \frac{\partial^2}{\partial x^2}\right]$$

or

$$\left[\frac{\partial}{\partial t} + \frac{\partial}{\partial x}\right]\left[\frac{\partial}{\partial t} - \frac{\partial}{\partial x}\right] \; - \; \left[\frac{\partial}{\partial t} + \frac{\partial}{\partial x}\right]\left[\frac{\partial}{\partial t} - \frac{\partial}{\partial x}\right]$$

where [illegible] is a function of position and [illegible]. Assuming that [illegible] the solution must satisfy the characteristic equation of the finite [illegible] equation

$$\left[\frac{\partial}{\partial t} + \frac{\partial}{\partial x}\right]\left[\frac{\partial}{\partial t} - \frac{\partial}{\partial x}\right] \; - \; \left[\frac{\partial}{\partial t} + \frac{\partial}{\partial x}\right]\left[\frac{\partial}{\partial t} - \frac{\partial}{\partial x}\right]$$

and the [illegible] is independent of [illegible] and we shall [illegible] in solutions of this equation with [illegible]. The [illegible] of [illegible] in the [illegible] finite [illegible] equation

[illegible] Boundary Conditions

[illegible] boundary conditions are [illegible] to solve [illegible] sufficient to [illegible] the [illegible] at the value [illegible] must result a [illegible] that will be [illegible] from a [illegible] analytic. By [illegible] such [illegible] with [illegible] at the value [illegible] [illegible] the [illegible] The boundary condition of [illegible] is [illegible] from a [illegible] of [illegible] and we shall [illegible] [illegible] However we [illegible] a [illegible] [illegible] in the [illegible] [illegible] [illegible] [illegible]

[illegible] Eigenvalue Case

By [illegible] the [illegible] relations and [illegible]

[illegible] that [illegible] is the [illegible]

$$\frac{\partial}{\partial x} = \frac{\partial}{\partial x} = \frac{\partial}{\partial x}$$

$$= \frac{}{}$$

$$= \frac{}{}$$

$$= \frac{}{}$$

$$\frac{}{} = \frac{}{} \frac{}{} = \frac{}{} \frac{}{}$$

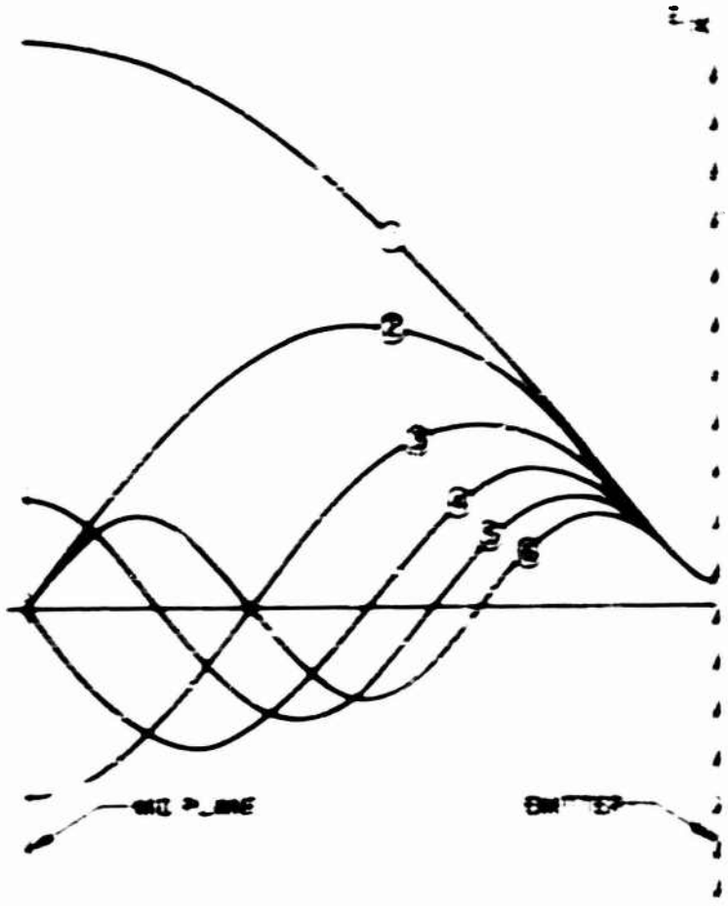

FIG. [illegible] ELECTRIC [illegible] AMPLITUDES OF THE FIRST SIX
RESONANCES FOR RECTANGULAR CAVITIES HAVING [illegible] AS SHOWN
AT [illegible]. Modes are numbered and the corresponding [illegible] are given in Table [illegible].

$$\frac{\quad}{\quad}\left(\frac{\quad}{\quad}\right)$$

where [illegible] is the wavelength and [illegible] the wave number. At resonance we get [illegible] where [illegible] is an integer and hence [illegible] in the uniform case. The quantity [illegible] is a constant for each resonance

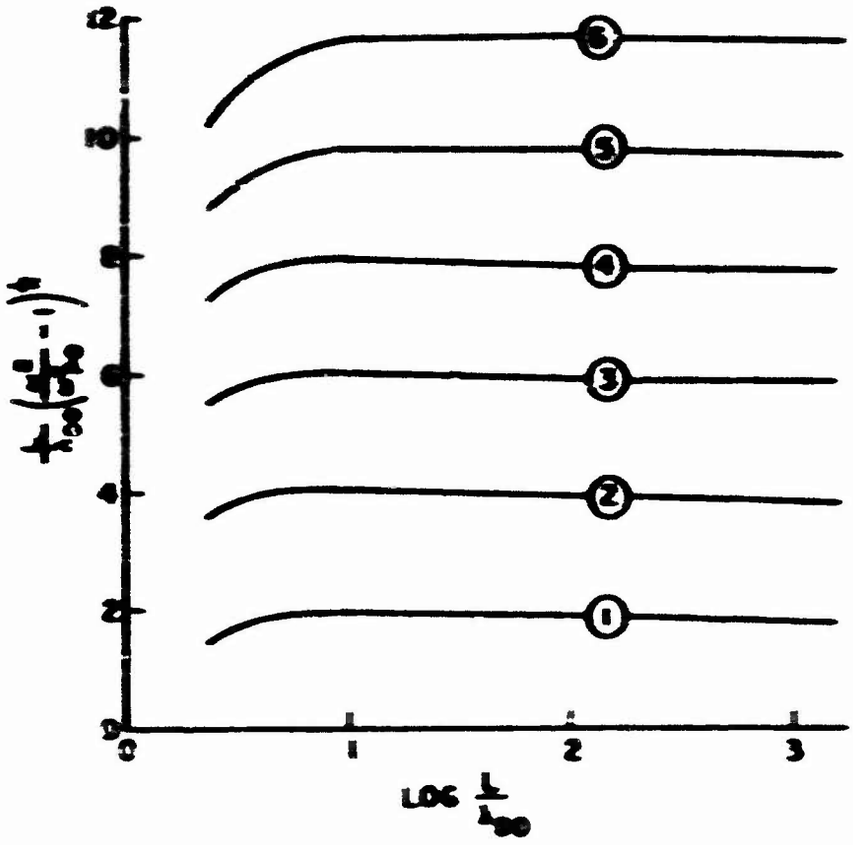

FIG. [illegible] PLOTS OF $\frac{\omega}{\omega_{po}}$ VS $\log \frac{L}{\lambda_{po}}$ FOR THE FIRST SIX MODES.

TABLE 1. THE FIRST SIX RESONANCE FREQUENCIES OF THE PLASMA BETWEEN TWO HELMHOLTZ METTERS AS A FUNCTION OF TEMPERATURE. The electric field is symmetric about $z = 0$. For odd numbered modes and anti-symmetric for the even numbered modes.

		MODE 1	MODE 2	MODE 3	MODE 4	MODE 5	MODE 6
T	ω_{po} [illegible]	ω_1/ω_{po}	ω_2/ω_{po}	ω_3/ω_{po}	ω_4/ω_{po}	ω_5/ω_{po}	ω_6/ω_{po}
15K	1.1[illegible] × 1[illegible]	1.[illegible]	2.[illegible]	3.[illegible]	4.[illegible]	5.[illegible]	6.[illegible]
13K	1.2[illegible] × 1[illegible]	1.[illegible]	2.[illegible]	3.[illegible]	4.[illegible]	5.[illegible]	6.[illegible]
20K	1.9[illegible] × 1[illegible]	1.[illegible]	2.[illegible]	3.[illegible]	4.[illegible]	5.[illegible]	6.[illegible]
21K	4.4[illegible] × 1[illegible]	1.[illegible]	2.[illegible]	3.[illegible]	4.[illegible]	5.[illegible]	6.[illegible]
22K	9.[illegible] × 1[illegible]	1.[illegible]	2.[illegible]	3.[illegible]	4.[illegible]	5.[illegible]	6.[illegible]
23K	2.1[illegible] × 1[illegible]	1.[illegible]	2.[illegible]	3.[illegible]	4.[illegible]	5.[illegible]	6.[illegible]

4. Ion Rich Case

In the ion rich cases Buttner resonances of the cathode sheath are expected since the electron density near the diode walls is low. "Buttner resonances," the resonances observed on a plasma column, are due to nonuniformity in the plasma. As can be seen from Eq. (3.10), propagation occurs when the applied frequency is greater than the plasma frequency, and the wave is "cut off" when $\omega < \omega_p$. If the frequency is adjusted to be above the plasma frequency at the edge of the column but below that at the center, the wave propagates inward to the point where it is cut off due to the increasing electron density and is reflected. If the total phase shift is 2π when the wave returns to the wall, a standing wave will be set up and resonance results. An excellent analysis of these resonances for the positive column of a discharge is given by Parker.[3] Shown in Fig. 3.3 are the rf electric field strengths of the first three modes for the ion rich case corresponding to the dc solution shown in Figs. 2.11 and 2.13. The first resonance occurs at a frequency below the midplane plasma frequency, and the electric field is

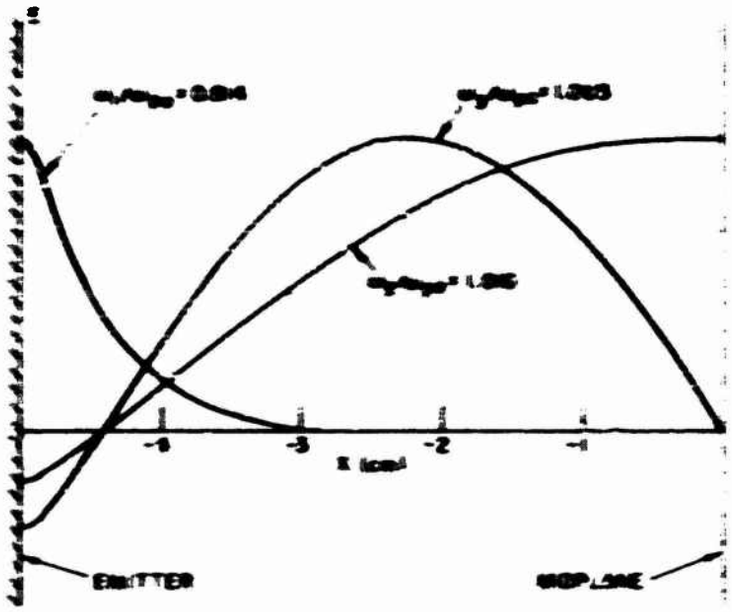

FIG. 3.3. RF ELECTRIC FIELD STRENGTH FOR THE FIRST THREE RESONANCES VS DISTANCE FROM THE MIDPLANE.

concentrated in the sheath region. Clearly this resonance is like the former resonance. The resonance frequency of the second, third and higher order modes are greater than ω_{pe}, and the fields for these penetrate into the plasma. The higher order mode frequencies are very close together and, hence, the modes may not be detectable experimentally. The first and second resonances are spaced far enough apart so that the first resonance may be detectable.

3. END PLATE LOSSES

An electron acquires rf energy from the electric fields as it traverses the diode space, but the entire rf energy is lost when the electron is absorbed by the wall. In this section, a kinetic model of the plasma is used to study this end plate loss effect.

We shall assume that the plasma is uniform within the diode. Then the linearized Boltzmann equation for a uniform one-dimensional collisionless electron plasma is given by

$$\left(\frac{\partial}{\partial t} + v\frac{\partial}{\partial x}\right) f_1(v,x,t) = \frac{e}{m} E(x,t) \frac{\partial f_0}{\partial v} \qquad (3.11)$$

By Laplace transforming in time, we obtain

$$p\, f_1(v,x,p) + v \frac{\partial f_1(v,x,p)}{\partial x} = \frac{e}{m} E(x,p) \frac{\partial f_0}{\partial v} \qquad (3.12)$$

where $p = i\omega$. The general solution to Eq. (3.12) is given by

$$f_1(v,x,p) = f_1(v,0,p) \exp\left[-\frac{px}{v}\right] + \int_0^x E(p,\xi) \frac{e}{mv} \frac{\partial f_0}{\partial v} \exp\left[-\frac{p(x-\xi)}{v}\right] d\xi \,. \qquad (3.13)$$

For the analysis, we shall use the geometry shown in Fig. 3.-. We shall assume further that $f_0(v)$ is a symmetric function of v. In order to make f_1 regular for $\mathrm{Re}(p) > 0$, the arbitrary constant in Eq. (3.13) must be selected so that

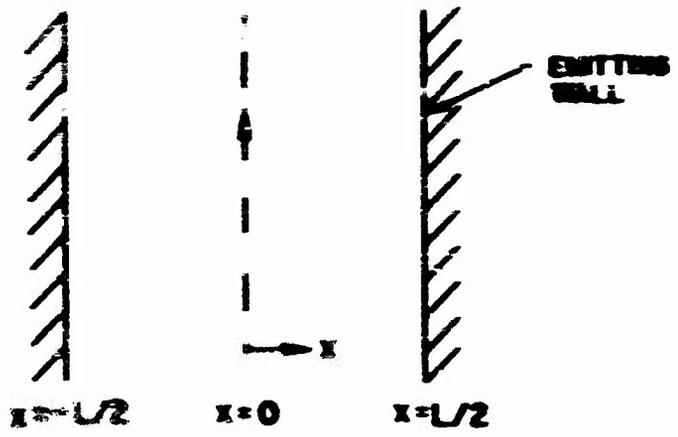

FIG. 3.4. EMITTER GEOMETRY

$$f_1(p,x,v) = f_1\left(p,-\frac{L}{2},v\right)\exp\left[-\frac{p(x+L/2)}{v}\right] + \frac{\sigma_0}{\pi v} f_0(v)\int_{-L/2}^{x} E(p,\xi)\exp\left[-\frac{p(x-\xi)}{v}\right]d\xi \qquad (3.14)$$

and

$$f_1(p,x,-v) = f_1\left(p,\frac{L}{2},-v\right)\exp\left[-\frac{p(L/2-x)}{v}\right] + \frac{\sigma_0}{\pi v} f_0(v)\int_{x}^{L/2} E(p,\xi)\exp\left[+\frac{p(x-\xi)}{v}\right]d\xi \qquad (3.15)$$

where throughout this section we take $v > 0$. To obtain the boundary conditions, we shall assume that a certain fraction $R(v)$ of the particles impinging upon the wall with velocity v is specularly reflected, and the rest perfectly absorbed by the wall. In other words, at $x = -L/2$

$$f_1\left(p,-\frac{L}{2},v\right) = R(v) f_1\left(p,-\frac{L}{2},-v\right) \qquad (3.16)$$

and at $x = L/2$

$$f_1\left(p,\frac{L}{2},-v\right) = R(v) f_1\left(p,\frac{L}{2},v\right) \qquad (3.17)$$

The coefficient $R(v)$ can be a complex number which allows for time delay in reflection. By applying these boundary conditions to Eqs. (3.14) and (3.15), one evaluates $f_1(p, x = L/2, \mp v)$ to obtain

$$f_1(p,x,v) = \frac{\cdots}{\cdots} + \frac{\omega_0 f_0}{2v} \int_{-L/2}^{x} K(p,\xi) \exp\left[-\frac{p(x-\xi)}{v}\right] d\xi \qquad (3.18)$$

and

$$f_1(p,x,-v) = \frac{\cdots}{\cdots} - \frac{\omega_0 f_0}{2v} \int_{x}^{L/2} K(p,\xi) \exp\left[\frac{p(x-\xi)}{v}\right] d\xi \qquad (3.19)$$

From Maxwell's equation we have

$$I_1(p) = J_1(p,x) + p\epsilon_0 E(p,x)$$

$$= p\epsilon_c E(p,x) - e \int_0^\infty v\left\{f_1(p,x,v) - f_1(p,x,-v)\right\} dv \qquad (3.20)$$

where the total current density I_1 in the one dimensional system is known to be independent of x. The quantity I_1 represents the driving current which was assumed to be zero in the study of the lossless plasma resonance in Section IIIA. By using Eqs. (3.18) and (3.19), Eq. (3.20) can be expressed in the following form

$$I_1 = p\epsilon_0 E(p,x) + \int_{-L/2}^{L/2} \sigma(|x-\xi|) E(p,\xi) d\xi + \int_{-L/2}^{L/2} \rho(x,\xi) E(p,\xi) d\xi \qquad (3.21)$$

The coefficient R_1 can be a complex number which allows for time delay in reflection. By applying these boundary conditions to Eqs. (3.2) and (3.3), one evaluates $f_{1,2}(z,t=0)$ to obtain

$$f_{1,2}(z,t=0) = \frac{\omega_p \int_{-\infty}^{\infty} \left[\omega_p \int_{-\infty}^{\infty} \left[\omega_p \int_{-\infty}^{\infty} \right] \right]}{\omega_p \int_{-\infty}^{\infty}}$$

$$= \frac{\omega_p}{2\pi} \int_{-\infty}^{\infty} \left[\omega_p \int_{-\infty}^{\infty} \right] d\omega \qquad (3.4)$$

and

$$f_{1,2}(z,t=0) = \frac{\omega_p \int_{-\infty}^{\infty} \left[\omega_p \int_{-\infty}^{\infty} \right] \left[\omega_p \int_{-\infty}^{\infty} \right]}{\omega_p \int_{-\infty}^{\infty}}$$

$$= \frac{\omega_p}{2\pi} \int_{-\infty}^{\infty} \left[\omega_p \int_{-\infty}^{\infty} \right] d\omega \qquad (3.5)$$

From Maxwell's equations we have

$$\nabla \times \mathbf{H}_2(z,t) = \sigma \mathbf{E}_2(z,t)$$

$$+ \varepsilon \frac{\partial}{\partial t} \mathbf{E}_2(z,t) = \varepsilon \int_{-\infty}^{\infty} \left[\frac{\partial}{\partial t} f_2(z,t-\tau) \right] d\tau \qquad (3.6)$$

where the total current density J_2 in the one dimensional system is known to be independent of z. The quantity J_2 represents the driving current which was assumed to be zero in the study of the unstable plasma resonance in Section III.A. By using Eqs. (3.4) and (3.5), Eq. (3.6) can be expressed in the following form

$$J_2 = \sigma \mathbf{E}_2(z,t) = \int_{-\infty}^{\infty} \left[\omega_p \int_{-\infty}^{\infty} \right] d\omega - \int_{-\infty}^{\infty} \left[\omega_p \int_{-\infty}^{\infty} \right] d\omega \qquad (3.7)$$

where

$$\sigma(x) = -\frac{e^2 n_0}{m} \int_0^\infty f_0(v) \exp\left(-\frac{mvx}{kT}\right) dv \qquad (3.22)$$

and

$$\sigma_{xx}(x) = -\frac{e^2 n_0}{m} \int_0^\infty \frac{\exp\left(-\frac{mvx}{kT}\right)\left[\frac{mv}{kT}\exp\left(-\frac{2mvx}{kT}\right) - \exp\left(-\frac{2mvx}{kT}\right)\right] dv}{\left[1 - e^{-\frac{mvx}{kT}}\right]}$$

$$= -\frac{e^2 n_0}{m} \int_0^\infty \frac{\exp\left(-\frac{mvx}{kT}\right)\left[\frac{mv}{kT}\exp\left(-\frac{2mvx}{kT}\right) - e^{-\frac{2mvx}{kT}}\right] dv}{\left[1 - e^{-\frac{mvx}{kT}}\right]} \qquad (3.23)$$

The quantity $\sigma(x)$ is the conductivity factor for an infinite plasma. For the finite shell system the infinite plasma conductivity factor is modified by an additional reflection term, $\sigma_{xx}(x)$.

The problem is now reduced to solving the integral Eq. (3.13) for the electric field. The general solution to this equation for an arbitrary velocity distribution function is difficult to obtain. To get an idea of how the end plate losses affect the plasma resonances, we shall in the following analysis assume that the plasma has spherical shell distribution of velocities as follows

$$f_0(\vec{v}) = \frac{n_0}{4\pi v_0^2} \delta(|\vec{v}| - v_0) \qquad (3.24)$$

This distribution function when projected into one dimension yields

$$f_0(v) = \frac{n_0}{2v_0} \qquad |v| < v_0$$

$$= 0 \qquad |v| > v_0 \qquad (3.25)$$

By identifying the mean squared velocity to the thermal speed, we obtain the following relation

$$\frac{\sigma_1}{\sigma} = \epsilon_{1r}^{\prime} = \frac{1}{\epsilon_0} \int \epsilon^{\prime} \, dx = \frac{\epsilon_1^{\prime}}{\epsilon_0}$$

One important shortcoming of the 'spherical shell' model is that it does not exhibit Landau damping. However, it does give results which are simple and informative. We shall further simplify the problem by assuming that the reflection coefficient R is real and independent of ω. By inserting Eq. (3.2) into Eqs. (3.22) and (3.23), $\phi(x)$ and $\phi(x,\xi)$ are found to be

$$\phi(x) = -\frac{\epsilon_1^{\prime}}{\beta \epsilon_0} \exp\left(-\frac{\beta x}{\epsilon_0}\right) \qquad (3.27)$$

$$\phi(x,\xi) = -\frac{\epsilon_1^{\prime}}{\beta \epsilon_0 \left(1 - R^2 \exp\left[-\frac{2\beta L}{\epsilon_0}\right]\right)} \left(\exp\left[-\frac{\beta x}{\epsilon_0}\right] \left(R^2 \exp\left[-\frac{\beta(2L-\xi)}{\epsilon_0}\right] + \exp\left[-\frac{\beta(2L+\xi)}{\epsilon_0}\right] \right) \right.$$

$$\left. + \exp\left[\frac{\beta x}{\epsilon_0}\right] \left(\exp\left[-\frac{\beta(2L-\xi)}{\epsilon_0}\right] + R^2 \exp\left[-\frac{\beta(2L+\xi)}{\epsilon_0}\right] \right) \right) \qquad (3.28)$$

With these values of $\phi(x)$ and $\phi(x,\xi)$, one can differentiate the integral equation (3.21) twice with respect to x to eliminate the integrals, and obtain the following differential equation

$$\epsilon_0^2 \frac{d^2 E(x)}{dx^2} + (\epsilon^2 - \epsilon_p^2) E(x) = -\frac{\epsilon_1 I_1}{\epsilon_0} \qquad (3.29)$$

with the boundary conditions

$$E\left(-\frac{L}{2}\right) = \frac{I_1}{i\omega\epsilon_0} - \frac{v_0}{i\omega} \left(\frac{1-R}{1+R}\right) \left.\frac{dE(x)}{dx}\right|_{x=-\frac{L}{2}} \qquad (3.30)$$

and

$$E\left(\frac{L}{2}\right) = \frac{I_1}{i\omega\epsilon_0} - \frac{v_0}{i\omega} \left(\frac{1-R}{1+R}\right) \left.\frac{dE(x)}{dx}\right|_{x=\frac{L}{2}} \qquad (3.31)$$

where now ρ is replaced by z. The solution to Eq. (3.2) which satisfies Eqs. (3.2a) and (3.3) is given by

$$E'_x = \frac{I_1}{j\omega\varepsilon_0(1-\omega_p^2/\omega^2)}\left[1 - \frac{\omega_p^2/\omega^2 \cos\gamma z}{\cos\frac{\gamma l}{2} - j\frac{1-R}{1+R}\sqrt{1-\omega_p^2/\omega^2}\sin\frac{\gamma l}{2}}\right] \qquad (3.12)$$

where $\gamma = \omega\sqrt{\mu_0\varepsilon_0(\omega^2-\omega_p^2)}/\omega$. The field consists of a capacitive part and a space-varying part. When $\omega < \omega_p$, γ is real and the space-varying part varies sinusoidally in space.

The impedance of the dipole is obtained by integrating E_x.

$$Z(\omega) = -\frac{V}{I_1} = \int_{-l/2}^{l/2} \frac{E_x}{I_1}\,dz$$

$$= \frac{l}{j\omega\varepsilon_0(1-\omega_p^2/\omega^2)}\left[1 - \frac{\omega_p^2/\omega^2 \sin\frac{\gamma l}{2}}{\frac{\gamma l}{2}\left(\cos\frac{\gamma l}{2} - j\frac{1-R}{1+R}\sqrt{1-\omega_p^2/\omega^2}\sin\frac{\gamma l}{2}\right)}\right] \qquad (3.13)$$

For the special case of perfect reflection at the walls ($R = 1$) the impedance is given by

$$Z = \frac{l}{j\omega\varepsilon_0(1-\omega_p^2/\omega^2)}\left[1 - \frac{\omega_p^2}{\omega^2}\frac{\tan\frac{\gamma l}{2}}{\frac{\gamma l}{2}}\right] \qquad (3.14)$$

which is the result obtained by Hall.[6]

Shown in Figs. 3.5 and 3.6 are the real and imaginary parts of the impedance for different values of R. Note that, when R = 1, resonances occur whenever $\gamma l/2 = (2n+1)\pi/2$ where n is an integer. However, with R = 0 these resonances disappear except for the lowest order one. Since the spherical shell model does not exhibit Landau damping, the loss in this case can be attributed entirely to the end plate absorption, and the "Q" of the resonance is directly related to the reflection coefficient R.

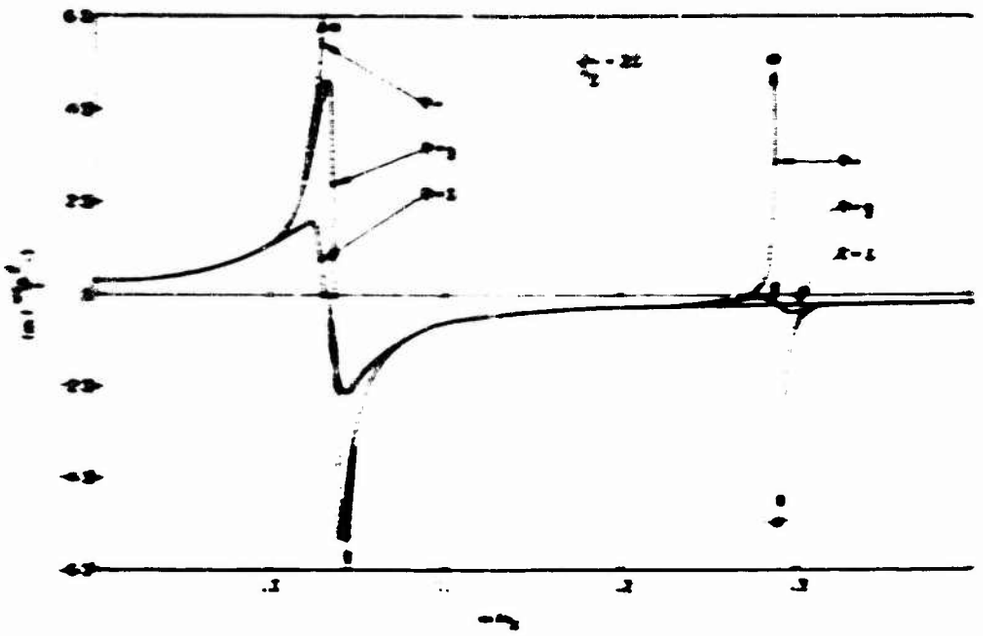

FIG. 3.4. THE IMAGINARY PART OF THE NORMALIZED DOUBLE IMPEDANCE VERSUS ω/ω_p. The parameter for the plots is the reflection coefficient Γ.

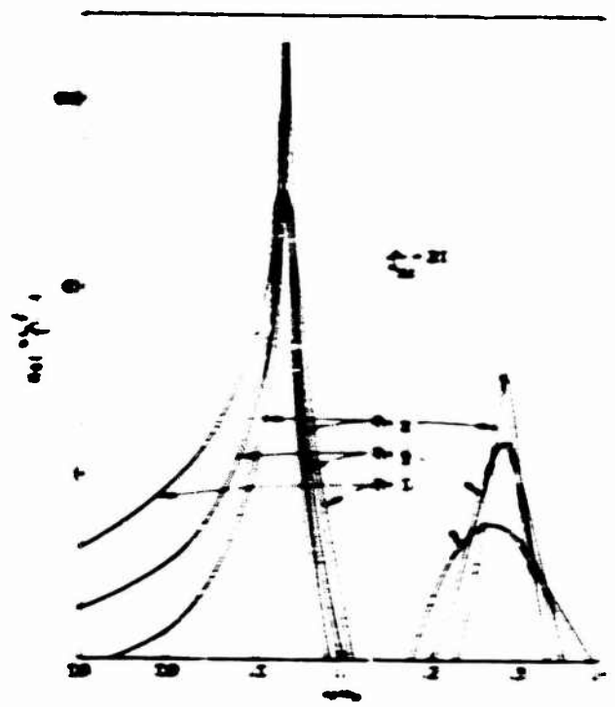

FIG. 3.5. THE REAL PART OF THE NORMALIZED DOUBLE IMPEDANCE VERSUS ω/ω_p.

It is of interest to compare the diode impedance with that of a somewhat similar system having a pair of parallel plane grids immersed in an infinite plasma. By assuming that the grids intercept field lines but not the particles, the impedance between the pair of grids can be obtained from the method described by Simmons.[4] For grids separated by a distance L and immersed in a plasma with a spherical shell velocity distribution, the impedance is found to be

$$Z_{pg} = \frac{L}{\omega\epsilon_0\sqrt{1-\omega_p^2/\omega^2}}\left[1 - \frac{\omega_p^2}{\omega^2}\cos\left(\frac{\omega L}{c}\sqrt{1-\frac{\omega_p^2}{\omega^2}}\right)\frac{\sin\frac{\omega L}{2c}}{\frac{\omega L}{2c}}\right] \qquad (3.34)$$

where ω_p is as defined previously. Shown in Fig. 3.7 is the impedance as a function of ω. The impedance of the parallel grids differs from

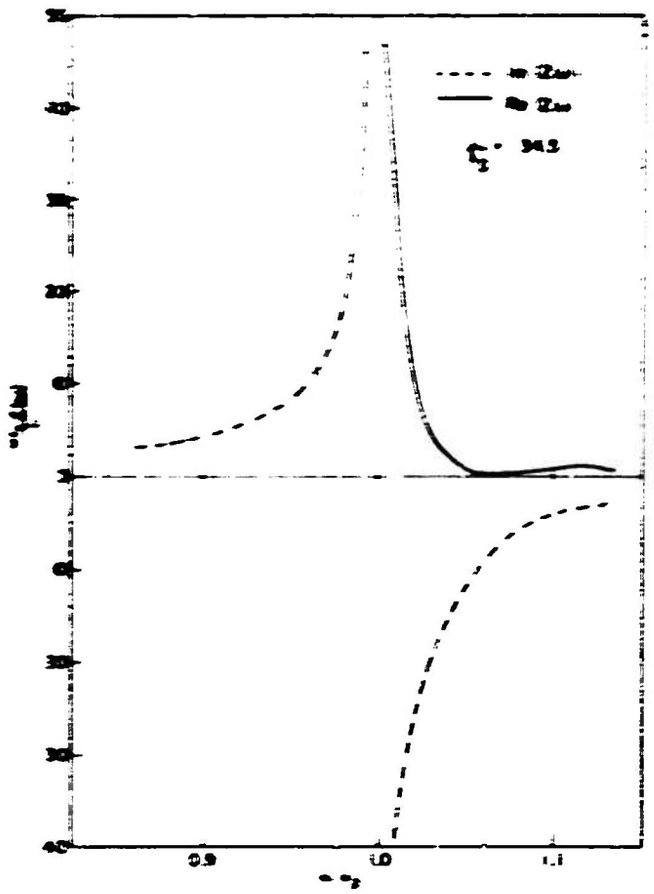

FIG. 3.7. NORMALIZED IMPEDANCE FOR A PAIR OF INFINITE GRIDS IMMERSED IN AN INFINITE PLASMA.

the diode impedance in several respects. First, the grid system exhibits resonance at the plasma frequency while the resonance for the diode is shifted above ω_p. Also, the grid impedance is infinite at $\omega = \omega_p$, while the diode impedance has poles along the real ω axis only when R = 1. Another difference is that the impedance of the grids is purely imaginary for frequencies below the plasma frequency while the diode impedance, except for the case of R = 1, is complex for all frequencies. The loss in the grid system is attributed to the energy carried away by the waves from the grid region to the external region.

C. CONCLUDING REMARKS

Electrostatic resonances in a nonuniform plasma diode are predicted by using the hydrodynamic model and a fictitious boundary condition. These resonances probably will be modified greatly when kinetic models are used to study the diode. The analysis of a uniform plasma diode using the spherical shell velocity distribution shows that wall absorption plays an important role in the determination of the diode impedance. In fact, when complete absorption occurs at the walls, the only resonance of significance occurs when the diode separation is exactly equal to a half-wavelength. Because of the absorption effect, resonances are not found when multiples of half-wavelength "fit" into the diode space. Thus, some of the resonances predicted by the hydro-dynamic model may not be observable, especially those found in the electron-rich diode where all of the electron trajectories hit the wall. (See the phase diagram of Fig. 2.2). However, the resonances predicted for the ion-rich case may be observable since most of the electrons in this case are trapped in the diode space and do not strike the wall.

Neither the hydrodynamic model nor the spherical shell model is capable of exhibiting the Landau damping effect. An analysis employing a more realistic gaussian velocity distribution will further modify the resonances and the impedances.

IV. DC THEORY OF CYLINDRICAL HOT MAGNETOPLASMA

In Chapter II we studied the dc properties of plasma confined between infinite planes. In a practical system the infinite system can only be approximated crudely. Most of the plasma devices which use the contact ionization process consist of circular emitters which face each other coaxially but are separated by a distance many times greater than the diameter of the emitters. The radial confinement of the plasma in such a system is achieved by the axial magnetic field. In this chapter we investigate the dc properties of a cylindrical column of magnetoplasma. First, a theoretical analysis will be given followed by some dc measurement results on the cylindrical column.

A CYLINDRICALLY SYMMETRIC SOLUTION TO THE BOLTZMANN EQUATION

The Boltzmann equation for the j^{th} species of the plasma in electric and magnetic fields is given by

$$\frac{\partial f_j}{\partial t} + \vec{v} \cdot \frac{\partial f_j}{\partial \vec{x}} + \frac{e_j}{m_j}\left(\vec{E} + \vec{v} \times \vec{B}\right) \cdot \frac{\partial f_j}{\partial \vec{v}} = \left(\frac{\partial f_j}{\partial t}\right)_{coll.} \qquad (4.1)$$

We seek a steady state solution $(\partial/\partial t = 0)$ to the Boltzmann equation under the assumption of negligibly small collision terms. In other words,

$$\vec{v} \cdot \frac{\partial f_j}{\partial \vec{x}} + \frac{e_j}{m_j}\left(\vec{E} + \vec{v} \times \vec{B}\right) \cdot \frac{\partial f_j}{\partial \vec{v}} = 0 \qquad (4.2)$$

We shall assume further that the plasma is cylindrically symmetric $(\partial/\partial\theta = 0)$ and uniform in the direction of the externally applied dc magnetic field $(\partial/\partial z = 0)$. Any function of the constants of the motion, such as the total energy, satisfies Eq. (4.2). One such solution is given by[3]

$$f_j(\vec{v},\vec{r}) = f_{oj}\left[-\frac{m_j}{2}\vec{v}\cdot\vec{v} - \vec{v}\cdot(\vec{r}_j \times \vec{B}) - \frac{e_j}{m_j}\vec{r}_j \times \vec{B}\cdot\vec{A}\cdot\vec{r} - \frac{e_j}{m_j}V\cdot\vec{r}\right] \qquad (4.3)$$

where $\vec{\omega}_j = \vec{i}_z \omega_j$ is a vector along the magnetic field, $\vec{r}$ is the coordinate vector perpendicular to the magnetic field, $\vec{A}(\vec{r})$ is the vector potential, and $V(\vec{r})$ is the scalar potential. As can be seen, Eq. (4.3) is given in terms of the total energy and the total angular momentum which are constants of motion. The electric and magnetic fields can be derived from $V(\vec{r})$ and $\vec{A}(\vec{r})$ by

$$\vec{B} = \nabla \times \vec{A}(\vec{r}) \; ;$$

$$\vec{E} = -\nabla V(\vec{r}) \; .$$

We shall prescribe the solution to have Maxwellian velocity distribution along the axis, and, hence,

$$f_j(\vec{v},\vec{r}) = A_j \exp\left[\frac{m_j}{\kappa T_j}\left(-\frac{\vec{v}^2}{2} + \vec{v} \cdot (\vec{\omega}_j \times \vec{r}) + \frac{e_j}{m_j}(\vec{\omega}_j \times \vec{r}) \cdot \vec{A}(\vec{r}) - \frac{e_j}{m_j} V(\vec{r})\right)\right] . \tag{4.4}$$

By assuming further that the diamagnetic field produced by the plasma rotation has negligible effect on the dc magnetic field, the vector potential becomes

$$\vec{A} = \vec{B}_o \times \vec{r}$$

and Eq. (4.4) can be reduced to

$$f_j(\vec{v},\vec{r}) = A_j \exp\left[\frac{m_j}{\kappa T_j}\left(-\frac{\vec{v}^2}{2} + \vec{v} \cdot (\vec{\omega}_j \times \vec{r}) + \frac{\omega_j \omega_{cj} r^2}{2} - \frac{e_j}{m_j} V(\vec{r})\right)\right] \tag{4.5}$$

where $\omega_{cj} = |e_j B_o|/m_j$ is the cyclotron frequency of the j^{th} species. Equation (4.5) can be rewritten as

$$f_j(\vec{v},\vec{r}) = A_j \exp\left[\frac{m_j}{\kappa T_j}\left(-\frac{[\vec{v} - \vec{\omega}_j \times \vec{r}]^2}{2} + \frac{[\omega_{cj}^2 + \omega_j \omega_{cj}]}{2} r^2 - \frac{e_j}{m_j} V(\vec{r})\right)\right] . \tag{4.6}$$

From Eq. (4.6) we can see that the whole species rotates as a solid body with rotational frequency ω_j.

When Eq. (4.6) is specialized for electrons and ions, we have

$$f_{oi}(\vec{v},\vec{r}) = A_i \exp\left[\frac{m_i}{\kappa T_i}\left(-\frac{[\vec{v} - \vec{\omega}_i \times \vec{r}]^2}{2} + \frac{[\omega_i^2 + \omega_i\omega_{ci}]}{2} r^2 - \frac{eV(r)}{m_i}\right)\right] \quad (4.7)$$

and

$$f_{oe}(\vec{v},\vec{r}) = A_e \exp\left[\frac{m_e}{\kappa T_e}\left(-\frac{[\vec{v} - \vec{\omega}_e \times \vec{r}]^2}{2} + \frac{[\omega_e^2 - \omega_e\omega_{ce}]}{2} r^2 + \frac{eV(r)}{m_e}\right)\right]. \quad (4.8)$$

The density profiles and the current densities can be obtained by performing the appropriate integration of Eqs. (4.7) and (4.8).

$$n_e(r) = n_e(0) \exp\left[\frac{m_e}{\kappa T_e}\left(\frac{[\omega_e^2 - \omega_e\omega_{ce}]}{2} r^2 + \frac{e}{m_e} V(r)\right)\right] , \quad (4.9)$$

$$n_i(r) = n_i(0) \exp\left[\frac{m_e}{\kappa T_i}\left(\frac{[\omega_i^2 + \omega_i\omega_{ci}]}{2} r^2 - \frac{e}{m_e} V(r)\right)\right] , \quad (4.10)$$

$$\vec{J}_e = - e(\vec{\omega}_e \times \vec{r})n_e(r) , \quad (4.11)$$

$$\vec{J}_i = e(\vec{\omega}_i \times \vec{r})n_i(r) . \quad (4.12)$$

For the special case of complete neutrality, the simple solution yields a gaussian density profile with mean squared radius

$$r_m^2 = - \frac{2\kappa T_i}{m_i(\omega_i^2 + \omega_i\omega_{ci})} = \frac{-2\kappa T_e}{m_e(\omega_e^2 - \omega_e\omega_{ce})} \quad (4.13)$$

and the electrons and ions each rotate as a solid body about the axis with frequencies ω_e and ω_i respectively. The following restrictions must be placed on ω_e and ω_i to avoid densities which rise with increasing r.

$$\omega_{ci} = \omega_i$$

$$\omega_e < \omega_{ce}$$

Since ω_{ci} and ω_{ce} are defined to be positive, the rotational vector $\bar{\omega}_i = \hat{z}\omega_i$ is anti-parallel to the magnetic field and $\bar{\omega}_e = \hat{z}\omega_e$ is parallel to the magnetic field. The above conditions restrict r_n^2 to

$$r_n^2 < \frac{2kT}{n_i m_i \omega_{ci}^2} \qquad (4.34)$$

By using Eq. (4.11), the rotational frequencies ω_e and ω_i can be obtained in terms of r_n^2 as follows

$$\omega_i = \frac{-\omega_{ci} + \sqrt{\omega_{ci}^2 + (4\pi n_i e^2/m_i) n_i r_n^2}}{2} \qquad (4.35)$$

$$\omega_e = \frac{\omega_{ce} - \sqrt{\omega_{ce}^2 - (4\pi n_e e^2/m_e) n_e r_n^2}}{2} \qquad (4.36)$$

There are two possible rotational frequencies for a given value of r_n^2 for each species.

Under the assumption of neutrality, the self-magnetic field can be computed from $\bar{J}_e$ and $\bar{J}_i$ by using Ampere's law. The density profile for the neutral case is given by $n_i r^2 = n_e r^2 = n_0 \exp(-r^2/r_n^2)$ and, hence, the total azimuthal current obtained from Eqs. (4.31) and (4.32) is

$$J_{total} = e n_0 (\omega_i - \omega_e) r_n^2 \exp(-r^2/r_n^2) \qquad (4.37)$$

From Ampere's law, the following relation is obtained for the z-component of the magnetic field

$$B_z(r) = e n_0 (\omega_i - \omega_e) \int_r^\infty \frac{r^2}{r} \exp\left(-\frac{r^2}{r_n^2}\right) dr$$

$$= \frac{e n_0 r_n^2 (\omega_i - \omega_e)}{2} \exp\left(-\frac{r^2}{r_n^2}\right) . \qquad (4.38)$$

Comparing this field with B_{z1} we have

$$\frac{-\omega B_z}{B_z} = \frac{\omega_{p1}^2 \omega_{p2}^2}{\omega_{c1}\omega_{c2}^2} \left(\omega_{c1} - \omega_{c2}\right) \exp\left(-\frac{r^2}{r_0^2}\right) \qquad (4.19)$$

where c is the speed of light. Thus, the self-magnetic field can be ignored if

$$\frac{\omega_{p1}^2 \omega_{p2}^2}{\omega_{c1}\omega_{c2}^2} \left(\omega_{c1} - \omega_{c2}\right) \ll 1 \qquad (4.20)$$

One way to minimize the left-hand side of (4.20) is to choose the smaller of the two possible rotational frequencies for each species given by Eqs. (4.17) and (4.18). In other words,

$$\omega_{c1} = \frac{\omega_{c1} - \sqrt{\omega_{c1}^2 - 4\omega_{p1}^2 \omega_{p2}^2 r_0^2}}{2} \qquad (4.21)$$

$$\omega_{c2} = \frac{\omega_{c2} - \sqrt{\omega_{c2}^2 - 4\omega_{p2}^2 \omega_{p1}^2 r_0^2}}{2} \qquad (4.22)$$

Later we shall assume that r_0 takes the minimum value allowed by the inequality of (4.20). For such a special case the inequality of (4.20) becomes

$$\frac{\omega_{p1}^2 \omega_{p2}^2}{\omega_{c1}\omega_{c2}^2} \left(\omega_{c1} - \omega_{c2}\right) \ll 1 \qquad (4.23)$$

where v_{t1} is the ion thermal speed. Many laboratory plasmas satisfy such an inequality.

The elementary solution obtained in this section can be used to construct more complicated solutions appropriate for a given plasma. In the following section we will consider some solutions synthesized from the elementary one.

B. SUPERPOSITION OF ROTATING CLOUDS

An example of a more complicated solution to the Boltzmann equation for the j^{th} species is

$$f_j(\vec{r},\vec{v}) = \int d\vec{\xi} F(\vec{\xi}) \exp\left[\frac{m_j}{\kappa T_j}\left(-\frac{[\vec{v} - \vec{\omega}_j \times (\vec{r} - \vec{\xi})]^2}{2} + \frac{\omega_j^2 + \omega_j \omega_{cj}}{2}(\vec{r}-\vec{\xi})^2 - \frac{e_j V(r)}{m_j}\right)\right]$$

(4.24)

which is a superposition of rotating clouds with different rotational frequencies. The most general valid solution is given by

$$f_j(\vec{r},\vec{v}) = \int d\vec{\xi} G(T) \exp\left[-\frac{m_j}{\kappa T}\left(-\frac{[\vec{v} - \vec{\omega}_j \times (\vec{r} - \vec{\xi})]^2}{2} + \frac{\omega_j^2 + \omega_j \omega_{cj}}{2} r^2 - \frac{e_j V(r)}{m_j}\right)\right] .$$

(4.25)

We have not found a practical system which can be described by Eqs. (4.24) and (4.25).

C. SUPERPOSITION OF DISPLACED ELEMENTARY SOLUTIONS

Under the assumption of complete neutrality, a more interesting type of solution is obtained. Such a solution is

$$f_i(\vec{r},\vec{v}) = A \int d\vec{\xi} F(\vec{\xi}) \exp\left[\frac{m_i}{\kappa T_i}\left(-\frac{[\vec{v} - \vec{\omega}_i \times (\vec{r} - \vec{\xi})]^2}{2} + \frac{\omega_i^2 + \omega_i \omega_{ci}}{2}(\vec{r}-\vec{\xi})^2\right)\right]$$

(4.26)

where $\vec{\xi}$ is a vector in the r, θ plane. Equation (4.26) is just the convolution of the elementary solution and the "displacement" function $F(\vec{\xi})$. Equation (4.26) satisfies the Boltzmann equation, but there is no way to handle the non-neutral cases in representation. The self-magnetic field will also spoil the solution. To insure neutrality the distribution function for the electrons must be of the form

$$f_e(\vec{r},\vec{v}) = A \int d\vec{\xi}\, F(\vec{\xi})\, \exp\left[\frac{m_e}{\kappa T_e}\left(-\frac{\left\{\vec{v} - \vec{\omega}_e \times (\vec{r} - \vec{\xi})\right\}^2}{2}\right.\right.$$

$$\left.\left. + \left\{\frac{\omega_e^2 - \omega_e\omega_{ce}}{2}\right\}\left\{\vec{r} - \vec{\xi}\right\}^2\right)\right] . \qquad (4.27)$$

where the rotational frequency ω_e is related to ω_i by Eq. (4.13).

An example of $F(\vec{\xi})$, which may be applicable to a practical situation, is

$$F(\vec{\xi}) = 1 \qquad \text{for} \quad 0 < |\vec{\xi}| < b_o$$

$$= 0 \qquad \text{for} \quad |\vec{\xi}| > b_o \quad . \qquad (4.28)$$

This is expected to give a solution which closely approximates a plasma produced between two circular diode plates of radius b_o and confined by an axial magnetic field. For ions the expressions for the density profile and the current density become

$$N_i(r) = \frac{2N_o}{\pi r_o^2 r_m^2} \int_0^{b_o} \xi\, I_o\left(\frac{2r\xi}{r_m^2}\right) \exp\left[-\frac{(r^2 + \xi^2)}{r_m^2}\right] d\xi \quad , \qquad (4.29)$$

$$J_{\theta i}(r) = \frac{2\omega_i N_o e}{\pi r_o^2 r_m^2} \int_0^{b_o} \left\{r\xi\, I_o\left(\frac{2r\xi}{r_m^2}\right) - \xi^2 I_1\left(\frac{2r\xi}{r_m^2}\right)\right\} \exp\left[-\frac{(r^2+\xi^2)}{r_m^2}\right] d\xi \qquad (4.30)$$

where $J_{\theta i}(r)$ is the θ component of the ion current density, I_o and I_1 are zero- and first-order modified Bessel functions of the first kind, N_o is the number of particles per unit length, and r_m is as defined in Eq. (4.13). From Eqs. (4.27) and (4.28), the electron density and current profiles can be obtained and are found to be related to $N_i(r)$ and $J_{\theta i}(r)$ in the following manner

$$N_e(r) = N_i(r) \qquad (4.31)$$

$$J_{\theta e}(r) = -\frac{\omega_e}{\omega_i} J_{\theta i}(r) \qquad (4.32)$$

Equations (4.29) and (4.30) can be integrated readily numerically, and the results for $\omega_i = -\omega_{ci}/2$ are shown in Figs. 4.1, 4.2, and 4.3. The rotational frequency ω_i is arbitrary, but the choice of $\omega_i = -\omega_{ci}/2$ gives a solution with best confinement (smallest mean radius). In the figures the parameter varied for the plots is

$$r_m = \sqrt{\frac{8\kappa T_i}{m_i \omega_{ci}^2}} \tag{4.33}$$

The graphs show what we expect of a magnetically confined plasma as the magnetic field is varied. The density profile becomes flat-topped as the magnetic field is increased and, at infinite magnetic field, the profile becomes perfectly flat-topped with a sharp boundary. In general, the density drop at the plasma edge occurs roughly within a distance of $2r_m$. The current density is highest where the density gradient is highest. The ion drift velocity is of the order of the ion thermal velocity at the plasma edge. Solving Eqs. (4.21) and (4.22) for ω_e under the condition of $T_i = T_e$ and $\omega_i = -\omega_{ci}/2$, we find $\omega_e \approx \omega_{ci}/4 = -\omega_i/2$.

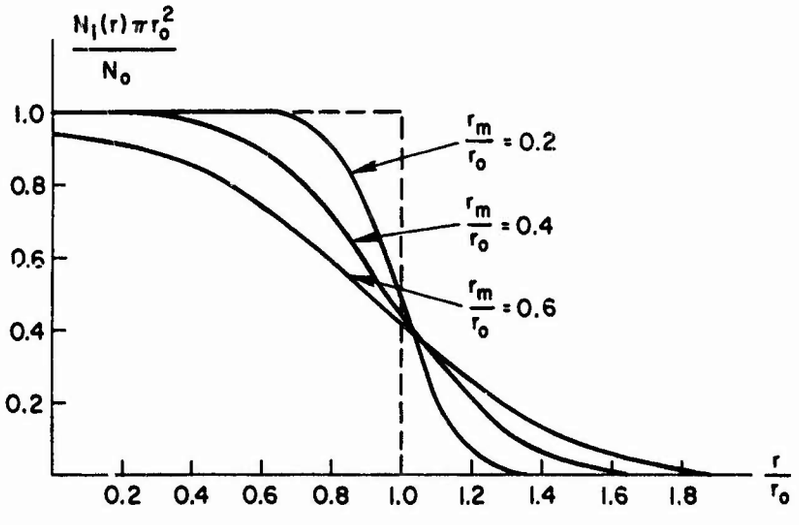

FIG. 4.1. DENSITY PROFILE. Normalized density is plotted versus normalized radius for different values of $r_m = \sqrt{8\kappa T_i/(m_i\omega_{ci}^2)}$.

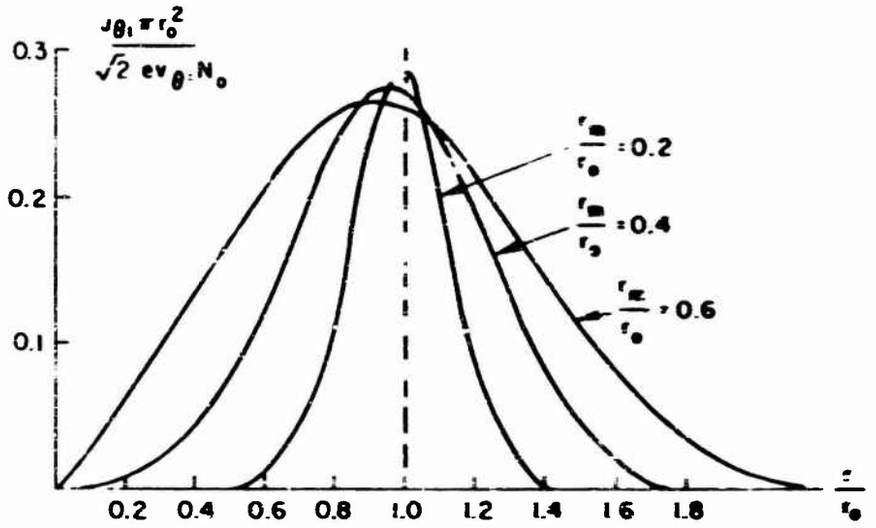

FIG. 2. ION CURRENT DENSITY. The $\hat{r}$ component of the ion current density is normalized to $\sqrt{2}\, v_{\theta i}\, e N_o \pi r_o^2$ and plotted vs r/r_o.

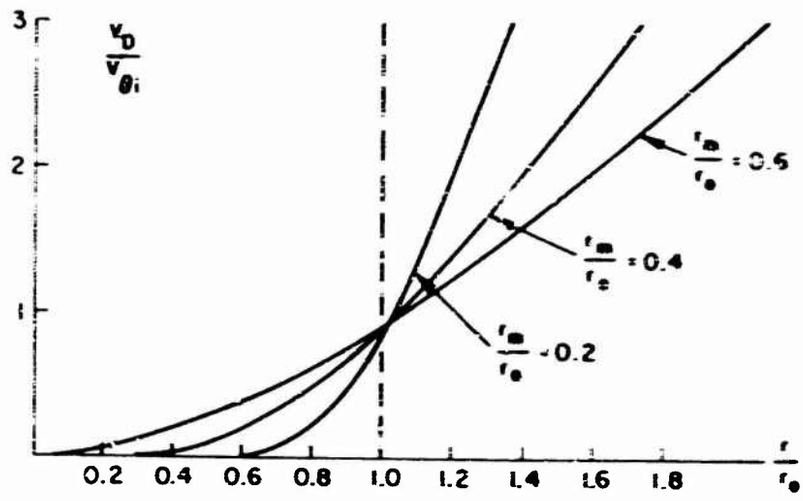

FIG. 3. NORMALIZED ION DRIFT VELOCITY VS r/r_o. The drift velocity is normalized to the ion thermal velocity $v_{\theta i}$.

Thus, the electron drift velocity is also of the order of the ion drift velocity, and, hence, negligibly small when compared to the electron thermal velocity.

W. H. Cutler[39] has derived an expression very similar to Eq. (-.29) but with an entirely different method. After approximation Cutler arbitrarily sets

$$r_n^2 = \frac{-4T_i}{n_1 \omega_{ci}^2}$$

This value does not satisfy the inequality (-.1-) for real ω_i and, hence, is disallowed in our theory.

D. EXPERIMENTAL MEASUREMENTS OF DC DENSITY AND DRIFT PROFILES

In the sodium plasma produced in the manner described in Chapter IIE, we attempted to measure the azimuthal electron drift and the density profile. For the measurement a modified Langmuir probe is used. The tip of this probe is shown in Fig. -.-. It can be rotated so that the dc density profile can be measured by facing the probe surface toward the buttons, while plasma rotation may be measured by facing the probe surface in the azimuthal direction. The detailed circuitry and the probe technique used to overcome various problems is discussed in Appendix A.

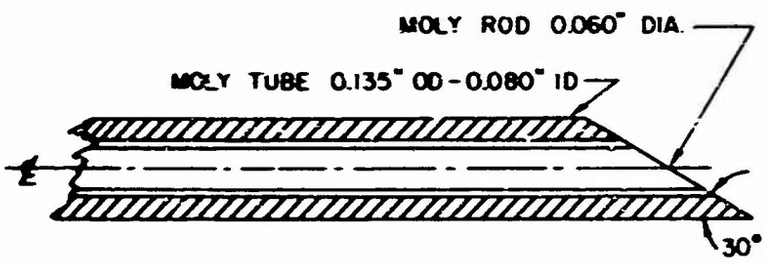

FIG. -.-. LANGMUIR PROBE

With the collecting surface facing the azimuthal direction, the probe curve is obtained first with the magnetic field directed one way and then with the magnetic field reversed. Presumably the azimuthal drift can be detected by noting the differences in the probe current for the two cases. Shown in Fig. 4.5 is a typical set of probe curves in the magnetic field. As the probe potential is increased from some negative value, the current rises exponentially and, at the plasma potential, breaks away from the exponential rise to form a "knee." We have plotted in Fig. 4.6 the current at the "knee" versus radius. There is a significant difference in the probe current when the magnetic field is reversed, indicating that an azimuthal drift is present. However, due to the lack of an appropriate probe theory, the measured result cannot be quantitatively related to the azimuthal drift. A similar measurement for ion drift is desirable, but considerable improvement on the probe circuits is required first since the ion currents are of the order of the leakage current or less.

At 180 gauss, the radius r_m as defined by Eq. (4.32) is 3 cm. This value is much too high to give current density profiles such as those of Fig. 4.6. Comparison of theoretical density profile was also made with the experimental density profile of a plasma produced in a similar manner by Cutler.[39] There again we found that invariably the experimental

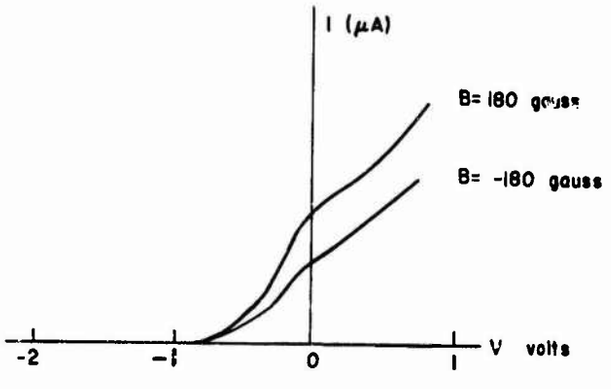

FIG. 4.5. TYPICAL SET OF PROBE CURVES. The two curves are obtained by keeping the probe in the identical position but by changing the direction of the magnetic field.

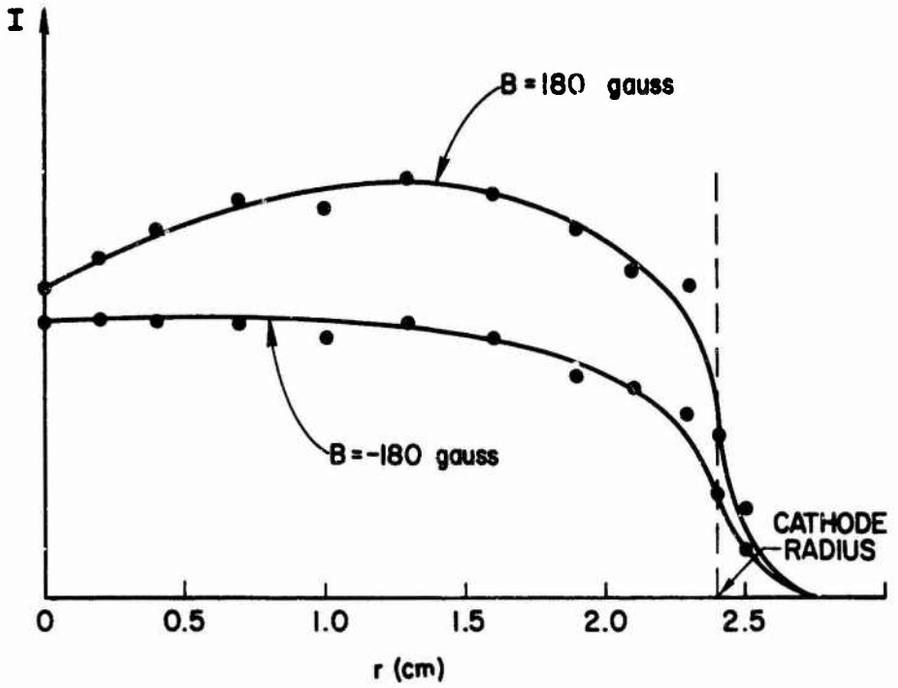

FIG. 4.6. AZIMUTHAL PROBE CURRENT VS RADIAL DISTANCE. The two curves are obtained with identical but oppositely directed magnetic fields. The parameters of the experimental plasma were: $T = 1800\ ^{o}K$; $n = 3 \times 10^{6}/cc$; $\lambda_o = 1.7$ mm.

density profile had a much sharper drop at the plasma edge than the theoretical profile. The discrepancy emphasizes the importance of the electric field which we have ignored in our theory. The electric field may be set up in the following manner. The primary electrons supplied within the solid cylinder, due to their small Larmor radii, have a sharper boundary than the ions. Hence, charge separation occurs and an electric field is set up which pulls the electrons outward and ions inward. Since the probe measures the electron current, it is not surprising that the profile is sharper than that predicted by a theory which assumes complete neutrality. Indeed, measurements show that there is an electric field present, though not concentrated near the plasma edge as might be expected. Shown in Fig. 4.7 is the potential profile of the column. An electric field of approximately 0.25 volts/cm is present.

For the study of waves along a plasma column undertaken in Chapter VI, we shall assume that the plasma column is uniform with a sharp

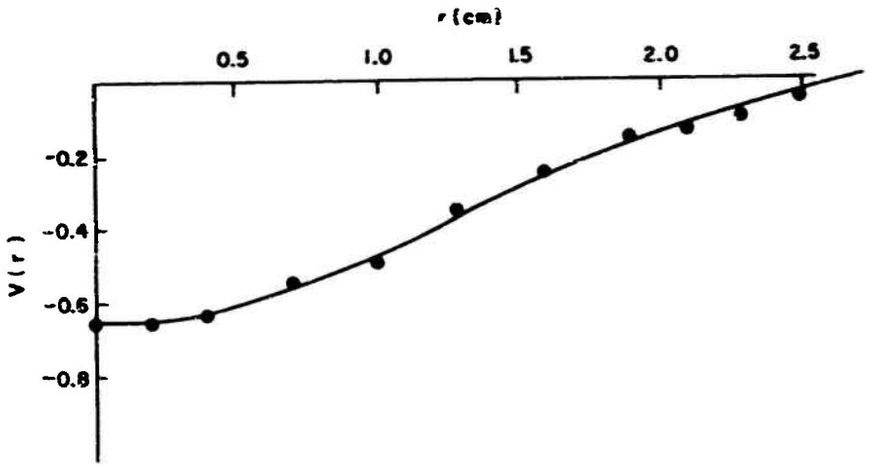

FIG. 4.7. POTENTIAL PROFILE.

boundary, and that there is no azimuthal drift. The results of this chapter serve to point out the range of validity of the dc model used in the rf analysis.

V. WAVES IN AN INFINITE MAGNETOPLASMA

In this chapter we investigate the waves in an infinite uniform hot magnetoplasma keeping in mind our final goal of obtaining results for a finite cylindrical plasma column. We are primarily concerned with the derivation of the dielectric tensors which describe the plasma behavior. We will demonstrate a new method to separate the plasma conduction current into polarization and magnetization currents. The separation is found to simplify the analysis considerably.

A. THE DIELECTRIC TENSOR IN A MAXWELLIAN ELECTRON PLASMA

Let us consider the linearized collisionless Boltzmann equation for the electrons. For the moment we shall assume that the ions are infinitely heavy. Then the zero and first order equations are given by

$$\left(\vec{v} \times \vec{B}_o\right) \cdot \frac{\partial f_o}{\partial \vec{v}} = 0 , \tag{5.1}$$

$$\frac{\partial f_1}{\partial t} + \vec{v} \cdot \frac{\partial f_1}{\partial \vec{x}} - \frac{e}{m} \left[\vec{v} \times \vec{B}_o\right] \cdot \frac{\partial f_1}{\partial \vec{v}} = \frac{e}{m} \left[\vec{E}_1(\vec{x},t) + \vec{v} \times \vec{B}_1(x,t)\right] \cdot \frac{\partial f_o}{\partial \vec{v}} \tag{5.2}$$

where $f_1 = f_1(t,\vec{x},\vec{v})$. By Fourier transforming in $\vec{x}$ and Laplace transforming in t, Eq. (5.2) is reduced to

$$(i\omega - i\vec{k} \cdot \vec{v}) f_1 - \frac{e}{m} \left[\vec{v} \times \vec{B}_o\right] \cdot \frac{\partial f_1}{\partial \vec{v}} = \frac{e}{m} \left(\vec{E} + \vec{v} \times \vec{B}\right) \cdot \frac{\partial f_o}{\partial \vec{v}} \tag{5.3}$$

where now $f_1 = f_1[\omega,\vec{k},\vec{v}]$. We introduce the following gyro-tensor

$$\vec{\vec{D}}(\varphi) = \vec{n},\vec{n} + (I - \vec{n},\vec{n})\cos\varphi - \vec{n} \times I \sin\varphi \tag{5.4}$$

and its integral

$$\begin{aligned} \vec{\vec{L}}(\varphi) &= \int_0^{\varphi} \vec{\vec{D}}(\varphi')\,d\varphi' \\ &= \vec{n},\vec{n}\,\varphi + (I - \vec{n},\vec{n}) \sin\varphi + \vec{n} \times I(\cos\varphi - 1) \end{aligned} \tag{5.5}$$

where $\vec{n}$ is a unit vector in the direction of the magnetic field and "I" is the unit tensor. The detailed derivation of the solution to Eq. (5.3) is given in Appendix B. The solution is found to be

$$f_1[\omega,\vec{k},\vec{v}] = \frac{e}{m\omega_c}\int_0^\infty \exp\left[\frac{i\omega\varphi}{\omega_c} + i\,\frac{\vec{k}\cdot\overleftrightarrow{L}\cdot\vec{v}}{\omega_c}\right]\vec{E}\cdot\overleftrightarrow{D}\cdot\frac{\partial f_o}{\partial\vec{v}}\,d\varphi\,. \qquad (5.6)$$

This solution can be verified by substituting it directly into Eq. (5.3).

The above solution agrees with those given by Fried[44] and Stix.[13] Through the use of the gyrotensors $\overleftrightarrow{D}(\varphi)$ and $\overleftrightarrow{L}(\varphi)$, our solution appears in a much simpler form than that given by Stix. The current density can be obtained by the integration

$$<\rho\vec{v}> = -\,e\int\vec{v}f_1[\omega,\vec{k},\vec{v}]d^3\vec{v}\,. \qquad (5.7)$$

In Appendix C we show that it is possible to separate the current density into polarization and magnetization currents, as suggested by Lorentz's electron theory of matter, i.e.

$$<\rho\vec{v}> = i\omega\,\vec{P} - i\vec{k}\times\vec{M} \qquad (5.8)$$

where $\vec{D} = \epsilon_o\vec{E} + \vec{P}$ and $\vec{B} = \mu_o(\vec{H} + \vec{M})$. For a Maxwellian plasma we obtain (see Appendices D and E),

$$\vec{P} = -\,\frac{\epsilon_o\omega_p^2}{\omega_c^2}\int_0^\infty \exp\left[-\,\frac{i\omega\varphi}{\omega_c} - \frac{v_\theta^2}{2\omega_c^2}\,(\vec{k}\cdot\overleftrightarrow{L})^2\right]\overleftrightarrow{L}(-\varphi)\cdot\vec{E}\,d\varphi \qquad (5.9)$$

and

$$\vec{M} = \frac{i\omega v_\theta^2}{\omega_c^3 c^2\mu_o}\int_0^\infty \overleftrightarrow{\mu}(\varphi)\cdot\vec{B}\exp\left[-\,\frac{i\omega\varphi}{\omega_c} - \frac{v_\theta^2}{2\omega_c^2}\,(\vec{k}\cdot\overleftrightarrow{L})^2\right]d\varphi \qquad (5.10)$$

where

$$\overleftrightarrow{\mu}(\varphi) = (I - \vec{n},\vec{n})\varphi\sin\varphi + (\vec{n}\times I)\varphi(1-\cos\varphi) + 2\vec{n},\vec{n}(1-\cos\varphi)$$

The importance of separating the current density into the two parts is realized when we deal with boundary conditions in a finite plasma. Without the vectors $\vec{P}$ and $\vec{E}_1$ it is necessary to work with surface charges and surface currents at the boundary. Such a task is very difficult, if not impossible, for a hot plasma boundary.

From Eq. (5.9) the electric susceptibility tensor $\bar{\chi}$, as well as the dielectric tensor $\bar{\epsilon}$, can be obtained from the following relation

$$\vec{D} = \epsilon_o \bar{\epsilon} \cdot \vec{E} = \epsilon_o \vec{E} + \vec{P} = \epsilon_o \bar{I} + \bar{\chi} \cdot \vec{E} .$$

We shall be concerned primarily with the dielectric properties of the plasma, since we are interested in electrostatic waves in which the magnetic energy is negligibly small. The dielectric tensor can be expressed in the following form

$$\bar{\epsilon} = \begin{bmatrix} \epsilon_{xx} & \epsilon_{xy} & \vdots \\ \epsilon_{yx} & \epsilon_{yy} & \vdots \\ \cdots & \cdots & \epsilon_{zz} \end{bmatrix}$$

with

$$\epsilon_{yy} = \epsilon_{xx} = 1 + \frac{\omega_p^2}{\omega_c^2} \int_0^\infty \sin \varphi \, e^{-u} \, d\varphi \qquad (5.11)$$

$$\epsilon_{zz} = 1 + \frac{\omega_p^2}{\omega_c^2} \int_0^\infty \varphi \, e^{-u} \, d\varphi \qquad (5.12)$$

$$\epsilon_{yx} = -\epsilon_{xy} = \frac{\omega_p^2}{\omega_c^2} \int_0^\infty (1 - \cos \varphi) e^{-u} \, d\varphi \qquad (5.13)$$

where

$$u = \frac{i\omega\varphi}{\omega_c} - \frac{v_\theta^2}{2\omega_c^2} (\vec{k} \cdot \vec{L})^2$$

$$= \frac{i\omega\varphi}{\omega_c} + \frac{k_\perp^2 v_\theta^2}{2\omega_c^2} \varphi^2 + \frac{k_\perp^2 v_\theta^2}{\omega_c^2} (1 - \cos \varphi) ,$$

$k_\perp$ and $k_\parallel$ are the wave numbers perpendicular and parallel to the magnetic field respectively. In Appendix D we show how to express Eqs. (5.11) to (5.13) in terms of the Hilbert transform of the gaussian as defined by Fried and Conte.[45] The result is

$$\epsilon_{xx} = \epsilon_{yy} = 1 + \frac{\omega_{p_o}^2 \zeta_o}{2\omega\omega_c} \exp\left[-\frac{\lambda^2}{2}\right] \sum_{-\infty}^{\infty} I_n (Z_{n+1} - Z_{n-1}) \qquad (5.14)$$

$$\epsilon_{zz} = 1 - \frac{\omega_p^2}{\omega^2} \zeta_o^2 \exp\left[-\frac{\lambda^2}{2}\right] \sum_{-\infty}^{\infty} I_n Z_n' \qquad (5.15)$$

$$\epsilon_{xy} = -\epsilon_{yx} = -\frac{i\omega_{p_o}^2 \zeta_o}{\omega_c \omega} \exp\left[-\frac{\lambda^2}{2}\right] \sum I_n \left(Z_n - \frac{Z_{n+1} + Z_{n-1}}{2}\right) \qquad (5.16)$$

where $I_n = I_n(\lambda^2/2)$ are modified Bessel functions,

$$\zeta_n = \frac{\omega - n\omega_c}{\sqrt{2}\, k_\parallel v_\theta},$$

$$\lambda = \frac{\sqrt{2}\, k_\perp v_\theta}{\omega_c},$$

and $Z_n = Z(\zeta_n)$ is the Hilbert transform of the gaussian, commonly called the Fried function, defined by

$$Z(\zeta_n) = \frac{1}{\sqrt{\pi}} \int_{-\infty}^{\infty} \frac{e^{-x^2}}{x - \zeta_n}\, dx \qquad \mathrm{Im}(\zeta_n) > 0 \,. \qquad (5.17)$$

Properties of this function are discussed in References 3 and 4, and a few simple relations involving $Z(\zeta)$ are given in Appendix D.

The dielectric tensor described by Eqs. (5.11) to (5.16) is much simpler than the "dielectric" tensor derived by earlier authors and described in the book by Stix.[13] In the representation given by Stix, the plasma conduction current is not divided into magnetization and polarization currents and hence the "dielectric" tensor is not truly the tensor

which relates the electric field to the displacement field. Even under quasi-static approximation, our results do not agree with that given by Stix.

B. THE DIELECTRIC TENSOR IN PLASMAS WITH TEMPERATURE ANISTROPY

The derivation of the dielectric tensors for plasmas with temperature anistropy is given in Appendix C. Equations (5.14), (5.15), and (5.16) remain unchanged, but some of the variables must be redefined as follows

$$\lambda^2 = \frac{2k_\perp^2 v_{\theta\perp}^2}{\omega_c^2}$$

and

$$\zeta_n = \frac{\omega - n\omega_c}{\sqrt{2}\, k_\parallel v_{\theta\parallel}}$$

where

$$v_{\theta\parallel} = \frac{\kappa T_\parallel}{m}$$

and

$$v_{\theta\perp}^2 = \frac{\kappa T_\perp}{m} \quad .$$

The limiting case of interest is $v_{\theta\perp} = 0$. In this limit the dielectric tensor elements become

$$\epsilon_{xx} = \epsilon_{yy} = 1 + \frac{\omega_p^2}{2\sqrt{2}\,\omega_c k_\parallel v_{\theta\parallel}} \left[Z\left(\frac{\omega-\omega_c}{\sqrt{2}\, k_\parallel v_{\theta\parallel}}\right) - Z\left(\frac{\omega+\omega_c}{\sqrt{2}\, k_\parallel v_{\theta\parallel}}\right)\right] \tag{5.18}$$

$$\epsilon_{zz} = 1 - \frac{\omega_p^2}{2k_\parallel^2 v_{\theta\parallel}^2} Z'\left(\frac{\omega}{\sqrt{2}\, k_\parallel v_{\theta\parallel}}\right) \tag{5.19}$$

and

$$\epsilon_{xy} = -\epsilon_{yx} = \frac{-i\omega_p^2}{2\sqrt{2}\,\omega_c k_\parallel v_{\theta\parallel}} \left[2Z\left(\frac{\omega}{\sqrt{2}\, k_\parallel v_{\theta\parallel}}\right) - Z\left(\frac{\omega-\omega_c}{\sqrt{2}\, k_\parallel v_{\theta\parallel}}\right) - Z\left(\frac{\omega+\omega_c}{\sqrt{2}\, k_\parallel v_{\theta\parallel}}\right)\right] . \tag{5.20}$$

These agree with the results obtained by Lichtenberg and Jayson.[9] Lichtenberg and Jayson derived the tensor by assuming that the plasma consisted of a continuum of streaming electrons with a gaussian velocity distribution along the magnetic field. They obtained the polarization tensor by integrating over the contribution from the continuum of electron streams. In Chapter VI the dispersion relation for the Lichtenberg-Jayson model is compared with that of a fully thermal plasma model.

The cold plasma dielectric tensor is recovered by letting $v_{\theta_\parallel}$ approach zero in Eqs. (5.18) to (5.20).

C. DIELECTRIC TENSOR FOR A MULTI-COMPONENT PLASMA

The polarization vector for a multi-component plasma is given by the sum of the polarization in each of the components. Thus, the dielectric tensor is given by

$$\vec{\epsilon} = I + \sum_j \vec{\pi}_j$$

where $\vec{\pi}_j$ is the electric susceptibility tensor for the j^{th} species. The elements of π_j are given by

$$\pi_{zzj} = -\frac{\omega_{pj}^2}{\omega^2}\zeta_{oj}^2 \exp\left[-\frac{\lambda_j^2}{2}\right] \sum_{-\infty}^{\infty} I_n Z_n' \qquad (5.21)$$

$$\pi_{xyj} = -\pi_{yxj} = -\frac{i\omega_{pj}^2\zeta_{oj}}{\omega_{cj}\omega} \exp\left[-\frac{\lambda_j^2}{2}\right] \sum_{-\infty}^{\infty} I_n\left(Z_n - \frac{Z_{n+1}+Z_{n-1}}{2}\right) \qquad (5.22)$$

and

$$\pi_{xxj} = \pi_{yyj} = \frac{\omega_{pj}^2\zeta_{oj}}{2\omega_{cj}\omega} \exp\left[-\frac{\lambda_j^2}{2}\right] \sum_{-\infty}^{\infty} I_n(Z_{n+1} - Z_{n-1}) \qquad (5.23)$$

where

$$I_n = I_n\left(\frac{\lambda_j^2}{2}\right) ,$$

$$Z_n = Z(\zeta_{nj}) ,$$

$$\zeta_{nj} = \frac{\omega - n\omega_{cj}}{\sqrt{2}\, k_{\parallel} v_{\theta j}} ,$$

$$\lambda_j = \frac{\sqrt{2}\, k_{\perp} v_{\theta j}}{\omega_{cj}} .$$

D. THE QUASI-STATIC DISPERSION RELATION FOR THE INFINITE PLASMA

Having obtained the dielectric tensors, we can now derive the dispersion relation for the plane electrostatic waves in the magnetoplasma. The distinguishing feature of electrostatic waves is that the electric field is derivable from a scalar potential

$$\vec{E}_1(\vec{x},t) = - \nabla \phi(x,t) , \qquad (5.24)$$

and, hence,

$$\nabla \times \vec{E}_1(\vec{x},t) = 0 .$$

This approximation, commonly called the quasi-static approximation, is valid whenever the phase velocities of the waves are much less than the speed of light. Using this analysis and assuming plane wave propagation of the form $\exp[i\omega t - i\vec{k} \cdot \vec{x}]$, we obtain the following result, relating the potential and the electric field.

$$\vec{E}[\omega,\vec{k}] = i\vec{k}\, \phi[\omega,\vec{k}] . \qquad (5.25)$$

From the second Maxwell equation we get

$$\nabla \cdot \vec{D}(t,\vec{x}) = -i\vec{k} \cdot \vec{D}_{\omega,\vec{k}} \exp[i\omega t - i\vec{k} \cdot \vec{x}]$$

$$= -i\vec{k} \cdot \vec{\epsilon} \cdot \vec{E}_{\omega,\vec{k}} \exp[i\omega t - i\vec{k} \cdot \vec{x}]$$

$$= 0 \qquad (5.26)$$

Direct substitution of Eq. (5.25) into Eq. (5.26) yields the following relation

$$\left(\epsilon_{xx} k_x^2 + \epsilon_{xx} k_y^2 + \epsilon_{zz} k_z^2\right) \mathcal{E}(k_x, k_y, k_z, \omega) = 0 \qquad (5.27)$$

which in turn yields the dispersion relation

$$\epsilon_{xx} k_\perp^2 + \epsilon_{zz} k_z^2 = 0 \qquad (5.28)$$

where $k_\perp^2 = k_x^2 + k_y^2$ is the square of the wave number perpendicular to the magnetic field. As expected, the dispersion relation is independent of the angle between the perpendicular component of $\vec{k}$ and the x axis. This dispersion relation, though it appears to be different, is identical to the result obtained by Stix.[13]

In an electron plasma the dispersion relation can be given in terms of one integral or one series as follows

$$k_\perp^2 + k_z^2 + \left(\frac{\omega_p}{v_t}\right)^2 \left[1 - \frac{k\omega}{\omega_c} S_1\right] = 0 \qquad (5.29)$$

where

$$S_1 = \int_0^\infty \exp\left[-\frac{k\omega}{\omega_c} t - \frac{k_\perp^2 v_t^2}{2\omega_c^2} t^2 - \frac{k_z^2}{2} [1 - \cos t]\right] dt$$

$$= \exp\left[-\frac{k_z^2}{2}\right] \sum_{n=-\infty}^{\infty} \frac{k\omega_c}{\sqrt{2}\, k_\perp v_t} I_n Z_n$$

and k, I_n and Z_n are as defined in Section VA.

The special case of purely perpendicular propagation ($k_{\parallel} = 0$) has been studied by Bernstein.[46] For this case we have from Eq. (5.28)

$$\epsilon_{xx} = 0 \tag{5.30}$$

as the dispersion relation. By using Eq. (5.29) and the asymptotic relation for Z_a given in Appendix D, we obtain the following dispersion relation for the "Bernstein" modes.

$$1 - \frac{2\omega_p^2}{k^2 v_c^2} \exp\left[-\frac{k^2}{2}\right] \sum_{-\infty}^{\infty} \frac{n I_n(k^2/2)}{\omega - n\omega_c} = 0 \ . \tag{5.31}$$

This dispersion predicts resonances near the harmonics of the cyclotron frequency. Several papers on the experimental observations of such resonances have been published.[47,48] A novel method of summing the series of Eq. (5.31) in terms of Nielson's cylinder function has been given by Barfler.[49] A computer program based on this result is used in obtaining the electric susceptibility tensor for the ions.

E. CYLINDRICAL WAVES

In this section we illustrate a method of synthesizing cylindrical waves from the plane waves. The rf potential for a plane wave may be expressed as follows

$$\phi(\omega,\vec{x}) = \phi(\omega,\vec{k}) e^{-i\vec{k}\cdot\vec{x}} \ . \tag{5.32}$$

From the potential the electric field and the displacement vectors can be obtained

$$\vec{E}(\omega,\vec{x}) = -\nabla \phi(\omega,\vec{x}) = i\vec{k}\, \phi(\omega,\vec{k}) e^{-i\vec{k}\cdot\vec{x}} \tag{5.33}$$

$$\vec{D}(\omega,\vec{x}) = \vec{\epsilon} \cdot \vec{k}\, \phi(\omega,\vec{k}) e^{-i\vec{k}\cdot\vec{x}} \ . \tag{5.34}$$

In the cylindrical coordinate system we let

$$k_x = k_\perp \cos \varphi$$

$$k_y = k_\perp \sin \varphi$$

$$x = r \cos \theta$$

$$y = r \sin \theta$$

where φ is the angle between the x axis and the plane containing the z axis and $\vec{k}$. The potential can now be expressed in the following manner

$$\phi[\omega,r,\theta,z) = \phi[\omega,k_\perp,k_\parallel,\varphi]\exp[-ik_\parallel z - ik_\perp r \cos(\theta-\varphi)] \quad . \quad (5.35)$$

The cylindrical wave is synthesized by taking these waves with identical amplitude, $k_\perp$ and $k_\parallel$ but with phase variation of the form

$$\phi[\omega,k_\perp,k_\parallel,\varphi] = \frac{\phi_o}{2\pi} e^{im\varphi}$$

where m is an integer. Synthesis of such plane waves yields [50]

$$\phi[\omega,r,\theta,z) = \frac{\phi_o}{2\pi} \int_{\theta-\pi}^{\theta+\pi} e^{im\varphi} \exp[-ik_\parallel z - ik_\perp r \cos(\theta-\varphi)]d\varphi$$

$$= \phi_o e^{im\theta} e^{-ik_\parallel z} J_m(k_\perp r) \quad (5.36)$$

where $J_m(k_\perp r)$ is the Bessel function of the order m. Similar integrations for the electric and displacement fields yield

$$E_z[\omega,r,\theta,z) = -ik_\parallel \phi_o \exp[im\theta - ik_\parallel z]J_m(k_\perp r) \quad (5.37)$$

$$E_\theta[\omega,r,\theta,z) = \phi_o \frac{im}{r} \exp[im\theta - ik_\parallel z]J_m(k_\perp r) \quad (5.38)$$

$$E_r[\omega,r,\theta,z) = k_\perp \phi_o \exp[im\theta - ik_\parallel z]J'_m(k_\perp r) \quad (5.39)$$

$$D_z[\omega,r,\theta,z) = -i\epsilon_{zz}k_z \phi_o \exp[im\theta - ik_{\parallel}z]J_m(k_{\perp}r) \tag{5.40}$$

$$D_r[\omega,r,\theta,z) = \phi_o \exp[im\theta - ik_{\parallel}z]\left[\frac{im\,\epsilon_{xy}}{r} J_m(k_{\perp}r) + k_{\perp}\epsilon_{xx}J'_m(k_{\perp}r)\right] \tag{5.41}$$

$$D_\theta[\omega,r,\theta,z) = \phi_o \exp[im\theta - ik_{\parallel}z]\left[\frac{im\,\epsilon_{xx}}{r} J_m(k_{\perp}r) - k_{\perp}\epsilon_{xy}J'_m(k_{\perp}r)\right]. \tag{5.42}$$

This technique of cylindrical wave synthesis has been employed by others in the past. In our representation $\overleftrightarrow{\epsilon}$ is independent of φ, the integration variable. In Stix' representation the dielectric tensor is a function of φ, and the integrals for the displacement vector is somewhat more difficult to evaluate then in our case.

The solution obtained above is valid for an infinite plasma. Our ultimate goal is to find the solution for a finite plasma, particularly a cylindrical column of plasma. In a finite plasma the most difficult task is the treatment of the boundary. To make the problem manageable, we must assume that the plasma column is uniform with a sharp boundary. In reality, a sharp boundary cannot occur because of thermal motion, though such a model may approximate the plasma column, as suggested by the theory and, in particular, the measurements discussed in Chapter IV. In Chapter VI we shall use the fields given by Eqs. (5.37) to (5.42) as the solution within the cylindrical plasma column and match them to the fields outside the plasma.

VI. ELECTROSTATIC WAVES IN A CYLINDRICAL COLUMN OF MAGNETOPLASMA

In this chapter we investigate the dispersion relation for electrostatic waves propagating along a column of cylindrical, collisionless magnetoplasma. The geometry we consider is that of an infinitely long, uniform, cylindrical plasma enclosed within a cylindrical waveguide as shown in Fig. 1.1. First, the dispersion relation for the electrostatic waves is derived. Some numerical solutions to the dispersion relation for a Maxwellian electron plasma are presented and compared with the dispersion relations based on other plasma models. Our results are also compared with the available experimental dispersion relations. At low magnetic fields, the surface wave is found to be unstable, and the instability character is investigated. The unstable ion surface wave is also studied.

A. QUASI-STATIC DISPERSION RELATION

Since there are two distinct regions within the waveguide, we need two sets of solutions, one valid within the plasma and the other valid in the free space region between the plasma and the conducting wall. For the plasma region we shall use the quasi-static solution, obtained in the previous chapter and given by

$$E_z[\omega,r,\theta,z) = -ik_{\parallel} \phi_o \exp[im\theta - ik_{\parallel} z]J_m(k_{\perp} r) \ , \tag{5.37}$$

$$E_\theta[\omega,r,\theta,z) = \frac{im\,\phi_o}{r} \exp[im\theta - ik_{\parallel} z]J_m(k_{\perp} r) \ , \tag{5.38}$$

$$E_r[\omega,r,\theta,z) = k_{\perp} \phi_o \exp[im\theta - ik_{\parallel} z]J'_m(k_{\perp} r) \ , \tag{5.39}$$

$$D_z[\omega,r,\theta,z) = -ik_{\parallel} \epsilon_{zz} \phi_o \exp[im\theta - ik_{\parallel} z]J_m(k_{\perp} r) \ , \tag{5.40}$$

$$D_r[\omega,r,\theta,z) = \phi_o \exp[im\theta - ik_{\parallel} z]\left[\frac{im\,\epsilon_{xy}}{r} J_m(k_{\perp} r) + k_{\perp} \epsilon_{xx} J'_m(k_{\perp} r)\right], \tag{5.41}$$

$$D_\theta[\omega,r,\theta,z) = \phi_o \exp[im\theta - ik_{\parallel} z]\left[\frac{im\,\epsilon_{xx}}{r} J_m(k_{\perp} r) - k_{\perp} \epsilon_{xy} J'_m(k_{\perp} r)\right] . \tag{5.42}$$

In the free space region, $b < r < a$, the solution to the equation $\nabla^2\phi = 0$ with the requirement of $\phi(a,\theta,z) = 0$ is given by

$$\phi(r,\theta,z) = A_o[J_m(ik_\parallel r)H_m(ik_\parallel a) - J_m(ik_\parallel a)H_m(ik_\parallel r)]e^{im\theta - ik_\parallel z} \qquad (6.1)$$

where $J_m(ik_\parallel r)$ and $H_m(ik_\parallel r)$ are Bessel and Hankel functions of order m. The components of the electric field are then obtained from Eq. (6.1) by $\bar{E} = -\nabla\phi$. At the free space plasma boundary, the tangential component of the electric field and the normal component of the displacement vector are matched. This yields the following dispersion relation for the waves

$$k_\perp b\epsilon_{xx}\frac{J_m'(k_\perp b)}{J_m(k_\perp b)} + im\epsilon_{xy} = \frac{ik_\parallel b[J_m'(ik_\parallel b)H_m(ik_\parallel a) - J_m(ik_\parallel a)H_m'(ik_\parallel b)]}{J_m(ik_\parallel b)H_m(ik_\parallel a) - J_m(ik_\parallel a)H_m'(ik_\parallel b)} \qquad (6.2)$$

with

$$k_\perp^2 + k_\parallel^2\frac{\epsilon_{zz}}{\epsilon_{xx}} = 0$$

and the dielectric tensor elements are as described in Chapter VC. The dispersion relation of Eq. (6.2), in appearance, is very familiar. In the cold plasma model[7] and in the Lichtenberg-Jayson ($T_\perp = 0$) model,[9] the dispersion relation is identical to Eq. (6.2). The only difference, though by no means small, is in the dielectric tensor elements.

To solve the dispersion equation in the form given by Eq. (6.2) is a formidable task. For example, the computation of the dielectric tensors above involves infinite summations of products of the Bessel and Fried functions. Only under certain conditions do these summations converge rapidly enough for computer analysis. In restricting our study to the cylindrically symmetric modes ($m=0$), we have

$$k_\perp b\epsilon_{xx}\frac{J_1(k_\perp b)}{J_o(k_\perp b)} = \frac{ik_\parallel[J_1(ik_\parallel b)H_o(ik_\parallel a) - J_o(ik_\parallel a)H_1(ik_\parallel b)]}{[J_o(ik_\parallel b)H_o(ik_\parallel a) - J_o(ik_\parallel a)H_o(ik_\parallel)]} \; . \qquad (6.3)$$

Even for this case, a thorough analysis of all the modes is formidable.

B. THE CASE OF HIGH MAGNETIC FIELD ($\omega_{ce} > \omega_{pe}$) WITH STATIONARY IONS

1. Comparison of the Dispersion Relations for Several Different Plasma Models

The dispersion relation for the electrostatic waves in a cold plasma column was first derived by Trivelpiece[7] and its solutions are commonly called the Trivelpiece modes. The hydrodynamic model, obtained by taking the moments of the Boltzmann equation, was used by Agdur and Weissglas[8] to study the temperature effects on the Trivelpiece modes. Unfortunately, the hydrodynamic model does not account properly for the temperature effects. In this section we present the dispersion relation for waves in a Maxwellian plasma column and compare it with the dispersion relations derived by using other models. We shall assume that the ions are infinitely heavy.

Equation (6.3) is solved numerically for the Maxwellian electron plasma by assuming real ω and seeking complex k_z. The computation procedure is described in Appendix E. The result for the lowest order mode is shown in Fig. 6.1. Also shown on the same graph are the dispersion relations for waves in a cold plasma column, in a "hydrodynamic" plasma, and in an infinite Maxwellian plasma. For the infinite hot plasma, the dispersion relation presented is the lowest order Landau mode as defined by Simonen.[42]

At low values of ω, the three models yield identical dispersion relations, but, at high values of ω, the dispersion relation for the Maxwellian plasma column merges smoothly into the hot infinite plasma dispersion relation, while the dispersion relation for the hydrodynamic model approaches the thermal speed of the one dimensional adiabatic Bohm and Gross[51] waves. As we can see, the wave in the column of the Maxwellian plasma is Landau damped.

The dispersion relation for the zero transverse temperature model ($T_\perp = 0$) was also computed, but, at the high magnetic field considered above, the results for $T_\perp = 0$ and $T_\perp = T_\parallel$ are identical. This is not surprising since, at high magnetic fields, the transverse motion of the electrons is inhibited.

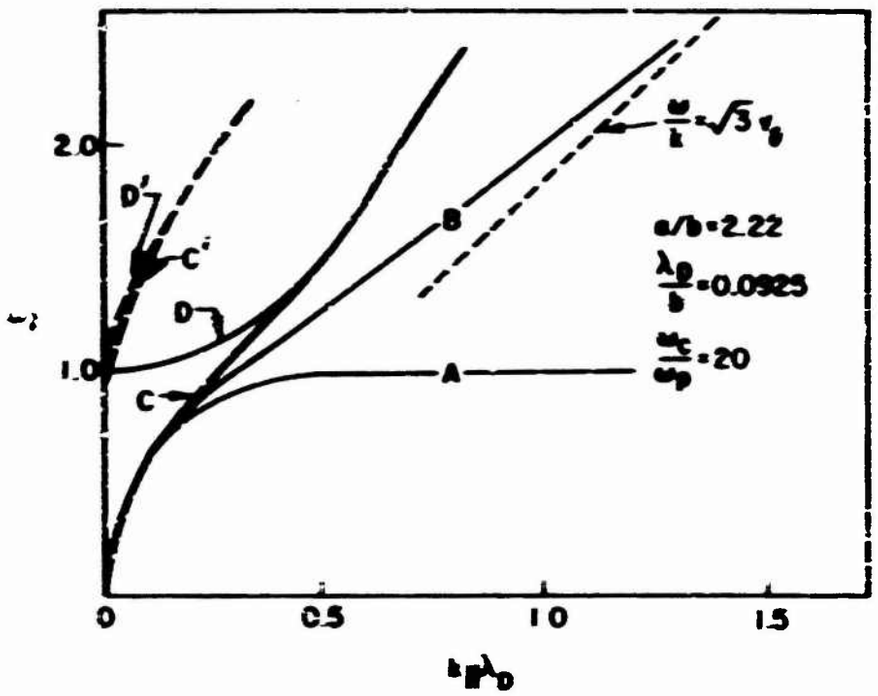

A = normalized frequency versus normalized wave number for a wave in a cylindrical column of cold plasma ($T = 0$)

B = normalized frequency versus normalized wave number for a wave in a cylindrical column of hydrodynamic plasma ($P_1 = \beta n_1 T$)

C = real part of $k_1 \lambda_D$ versus ω/ω_p for a cylindrical column of Maxwellian plasma

C' = damping decrement $\ln(k_1 \lambda_D)$ versus ω/ω_p for a cylindrical column of Maxwellian plasma

D = real part of $k_1 \lambda_D$ versus ω/ω_p for an infinite Maxwellian plasma

D' = damping decrement $\ln(k_1 \lambda_D)$ versus ω/ω_p for an infinite Maxwellian plasma

FIG. 3.1. DISPERSION RELATIONS FOR VARIOUS PLASMA MODELS.

2. Comparison with Available Experimental Observations

Using the model with $T = 0$, we also compute dispersion curves, which can be compared with the experimental observations of Malmberg and Wharton.[12] Malmberg and Wharton measured the propagation constant and the damping rate at frequencies near the electron plasma frequency.

Their experiment was conducted in a duoplasmatron type hydrogen arc source, which produced a plasma with high longitudinal temperature. Because of the high longitudinal temperature, the model with $T_\perp = 0$ is well-suited for the analysis. The experimental density profile given by Malmberg and Wharton is highly nonuniform as shown in Fig. 6.2. For computational purposes the plasma is approximated by a uniform, cylindrical plasma column as shown in curves A and B in Fig. 6.2. For the uniform column, the density is assumed to be $1.6 \times 10^8/cm^3$, which matches the asymptotic behavior of the theoretical result to that of the experimental curve. The radius for column A is chosen so that the total number of electrons in the column equals the total number in the nonuniform plasma. Since Malmberg and Wharton report that the absolute value of

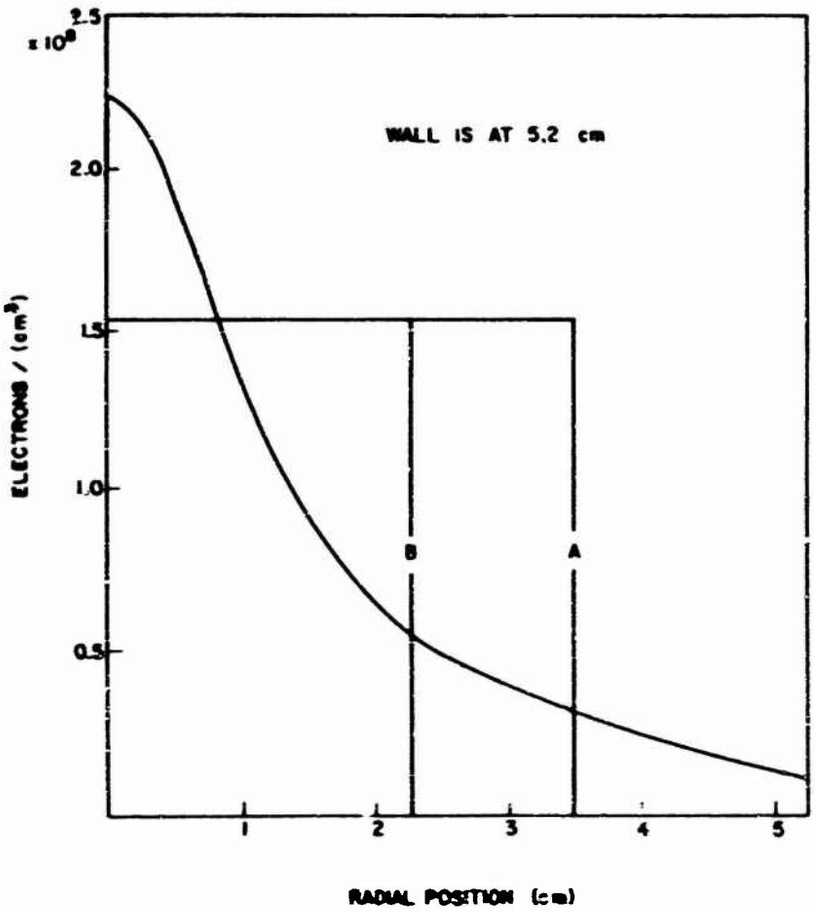

FIG. 6.2. DENSITY PROFILE FOR MALMBERG AND WHARTON EXPERIMENT.

the density profile may not be accurate, the procedure used to obtain the equivalent radius may not be valid. In fact, better agreement with the experimental dispersion relation is obtained when the column is assumed to be 2.25 cm in radius as shown in curve B. From the data supplied by Malmberg and Wharton, we find $\lambda_D = 0.19$ cm and $\omega_c/\omega_p = 4.0$. The real part of $k_{\parallel}$ obtained via the dispersion relation is compared with the experimental result in Fig. 6.3. The curves marked A' and B' are

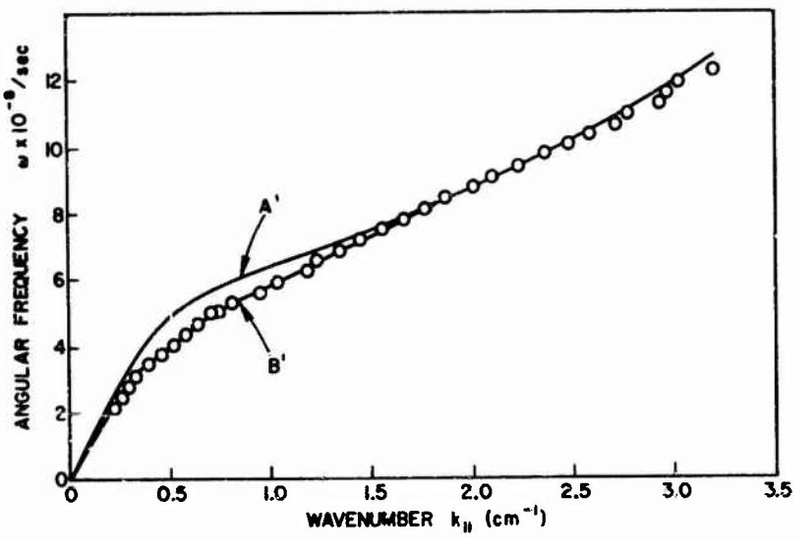

A' = plasma radius b = 3.5 cm

B' = plasma radius b = 2.25 cm

FIG. 6.3. ANGULAR FREQUENCY VERSUS WAVE NUMBER. Experimental data obtained by Malmberg and Wharton is compared with theoretical results.

the theoretical results for plasmas represented by curves A and B of Fig. 6.2. In Fig. 6.4 we have a graph of $\mathrm{Im}(k_{\parallel})/\mathrm{Re}(k_{\parallel})$ versus v_p/v_θ, where $v_p = \omega/\mathrm{Re}(k_{\parallel})$ is the phase velocity. The theoretical curve is computed by using B of Fig. 6.2. The agreement between the theory and experimental points is good, despite the approximate nature of the model.

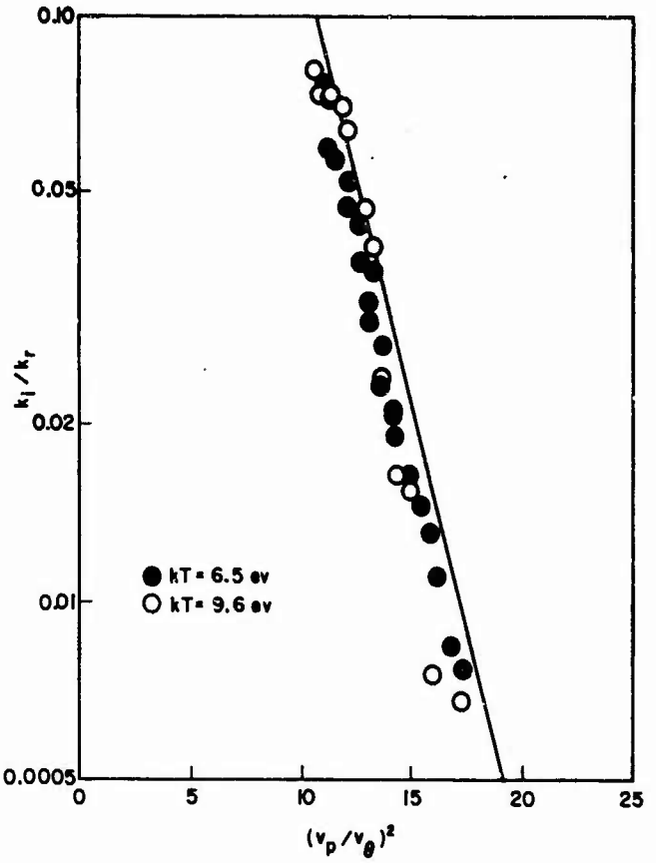

FIG. 6.4. k_i/k_r VERSUS $(v_p/v_\theta)^2$ FOR MALMBERG AND WHARTON EXPERIMENT.

C. SURFACE WAVE INSTABILITY IN ELECTRON PLASMAS AT LOW MAGNETIC FIELDS

When $\omega_c < \omega_p$, the lowest order mode in a cold electron plasma column is a surface wave in the range $\omega_c < \omega < \omega_H$, where $\omega_H = \sqrt{(\omega_p^2 + \omega_c^2)/2}$ (see Fig. 1.2). When the dispersion relation [Eq. (6.2)] was first solved in this region for real ω, instability was indicated. In this section we establish the presence of unstable surface waves and study the character of the instability.

One way to determine the presence of an instability is to map the negative real $k_\parallel$ axis into the complex ω plane and see if the roots fall into the lower half plane. Such a mapping for a typical surface mode is shown in Fig. 6.5. Instability is indicated since the roots fall below the real ω axis for a range of $k_\parallel b$.

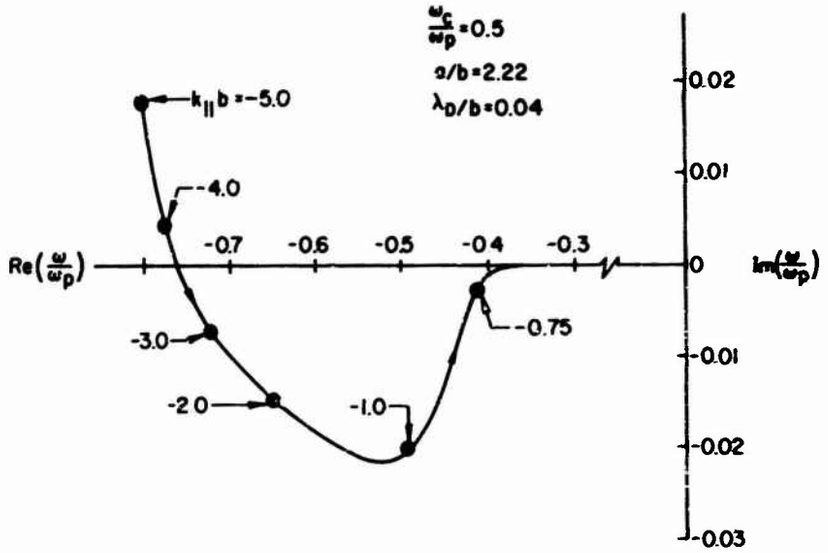

FIG. 6 5. NEGATIVE REAL $k_{||}b$ AXIS MAPPED INTO THE COMPLEX ω/ω_p PLANE VIA THE DISPERSION RELATION, SHOWING UNSTABLE ROOT.

All instabilities can be classified into two types, convective and nonconvective (absolute) instabilities. A nonconvective instability grows with time until limited by nonlinear effects, while the convective instability is one in which a perturbation is amplified in space. We have established that an instability is present, but, as yet, we have not determined whether it is convective or nonconvective.

Derfler[14,15] developed two methods of classifying instabilities. The first method is to map the complex ω plane into the complex $k_{||}$ plane through the "positive frequency part" of the dispersion relation and study the saddle-points $(d\omega/dk = 0)$, which are caused by the merging of the two roots of the dispersion relation. The way in which the roots merge, as the imaginary part of the frequency is changed, is intimately related to the classification of the instability. Nonconvective instability occurs if and only if the two roots merge across the negative real $k_{||}$ axis with frequencies in the lower half plane. This criterion is more difficult to use than the second one which is described below.

The saddle-points when mapped into the complex ω plane through the dispersion relation become branch points. If the branch point, associated with the instability, falls in the lower half plane, the instability

is nonconvective. Otherwise, the instability is convective. Briller pointed out a method of locating the branch point, and his method is incorporated in Figs. 6.6 and 6.7. First, the negative real $k_i b$ axis is mapped into the complex ω plane. One then chooses a point A near the most unstable frequency and maps the line AB, i.e., $\mathrm{Re}(k_i b)$ = constant, into the frequency plane. This line will bend around the branch point as shown in Fig. 6.7. Now we take a point C on this line and map the line CD of Fig. 6.6 into the frequency plane. These mappings make a noose in the complex ω plane. The branch point must be inside the noose, and, by repeating the mapping procedure, the noose

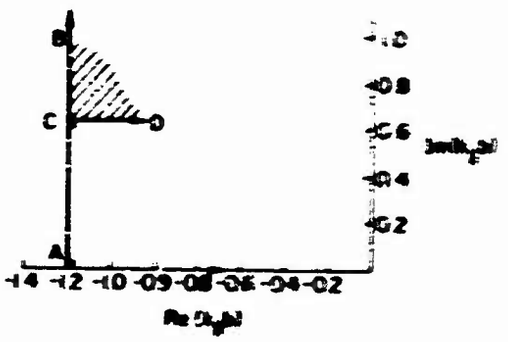

FIG. 6.6. COMPLEX $k_i b$ PLANE. The saddle point, $\partial\omega/\partial k_i = 0$, must be inside the shaded area (see Fig. 6.7).

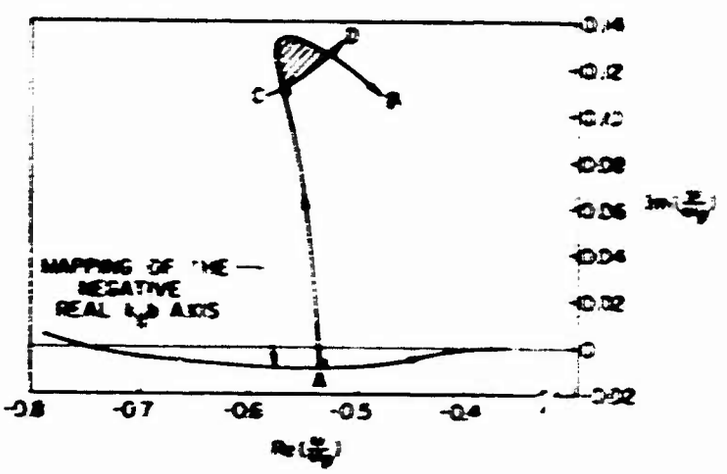

FIG. 6.7. COMPLEX FREQUENCY PLANE. The lines shown in Fig. 6.6 are mapped into complex $\omega = \omega_r + i\omega_i$ plane via the dispersion relation. The branch point, $\partial\omega/\partial k_i = 0$, must be inside the shaded area.

can be tightened to exactly locate the branch point. In our case, the branch point is in the upper half plane, and, hence, we have a convective instability.

The instability investigated above is a relatively mild case compared to those at lower magnetic fields. Attempts were made to apply the stability criterion at lower magnetic fields, but we were unable to locate the branch point due to computational difficulties. Thus, whether the instability remains convective or not for all values of the magnetic field is still an open question.

We now study the behavior of the instability as a function of the various parameters. Shown in Fig. [illegible] are mappings of the negative real

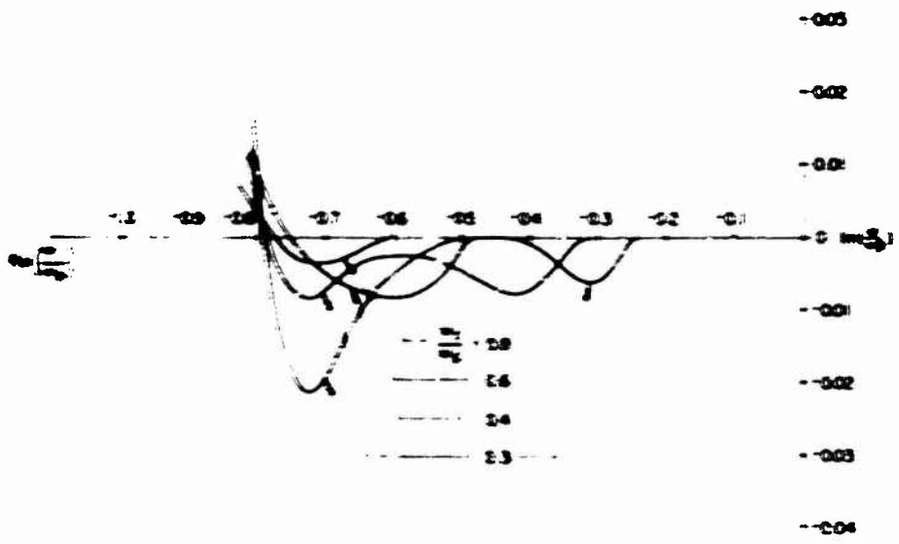

FIG. [illegible]. REAL WAVE NUMBERS AS MAPPED INTO THE COMPLEX FREQUENCY PLANE VIA THE DISPERSION RELATION. On the range of parameters shown, the solution represents surface waves. $a_D b = 2.22$, $\omega_{pi}/\omega_{ce} b = 0.14$.

wave numbers, $k_z b$, into the complex ω plane for the lowest order mode with ω_{ci}/ω_{pi} as a parameter. The instability is strong near the cyclotron frequency and at the hybrid frequency. Also, whenever the cyclotron harmonics are below $\omega_H = \sqrt{\omega_{pi}^2 + \omega_{ce}^2}$, the instability is enhanced at these harmonics as seen in Fig. [illegible]. At large negative

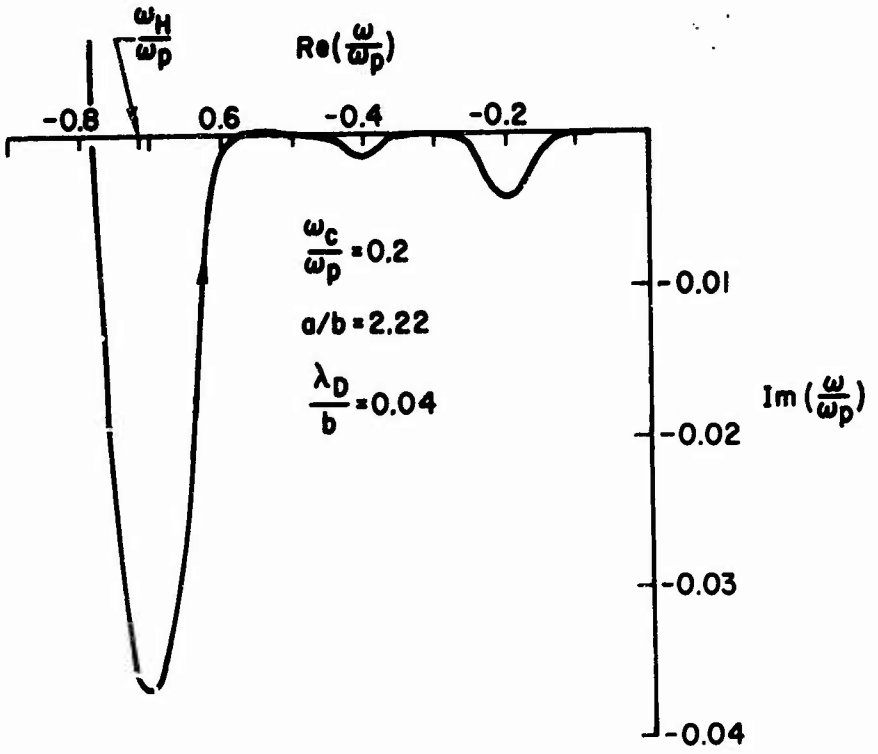

FIG. 6.9. MAPPING OF THE NEGATIVE REAL $(k_{\parallel}b)$ AXIS INTO THE COMPLEX ω/ω_p PLANE VIA THE DISPERSION RELATION FOR $\omega_c/\omega_p = 0.2$.

values of $k_{\parallel}b$, Landau damping sets in and makes the waves stable. Shown in Figs. 6.10 and 6.11 are the real and imaginary parts of the frequencies versus $k_{\parallel}b$ with ω_c/ω_p as a parameter. Unlike the surface wave in a cold plasma column for which the dispersion relation goes asymptotically to $\omega = \omega_H$, the real part of ω goes above ω_H as $k_{\parallel}b$ is increased indefinitely. The magnitudes of the electrostatic potential profiles are shown in Fig. 6.12 for $\omega_c/\omega_p = 0.3$. Note that the fields concentrate near the edge of the plasma as the frequency is raised above ω_c.

The curves of Fig. 6.8 seem to indicate that the plasma is more unstable at lower magnetic fields. However, the solution at $\omega_c = 0$ is known to reduce to the cold plasma case and, hence, is stable. Figure 6.13 shows the imaginary part of the most unstable frequency versus ω_c/ω_p. There are two curves, one for the instability at the cyclotron frequency and the other at the hybrid frequency ω_H. The portion of the curve shown by the dotted line was not computed. Although the instability

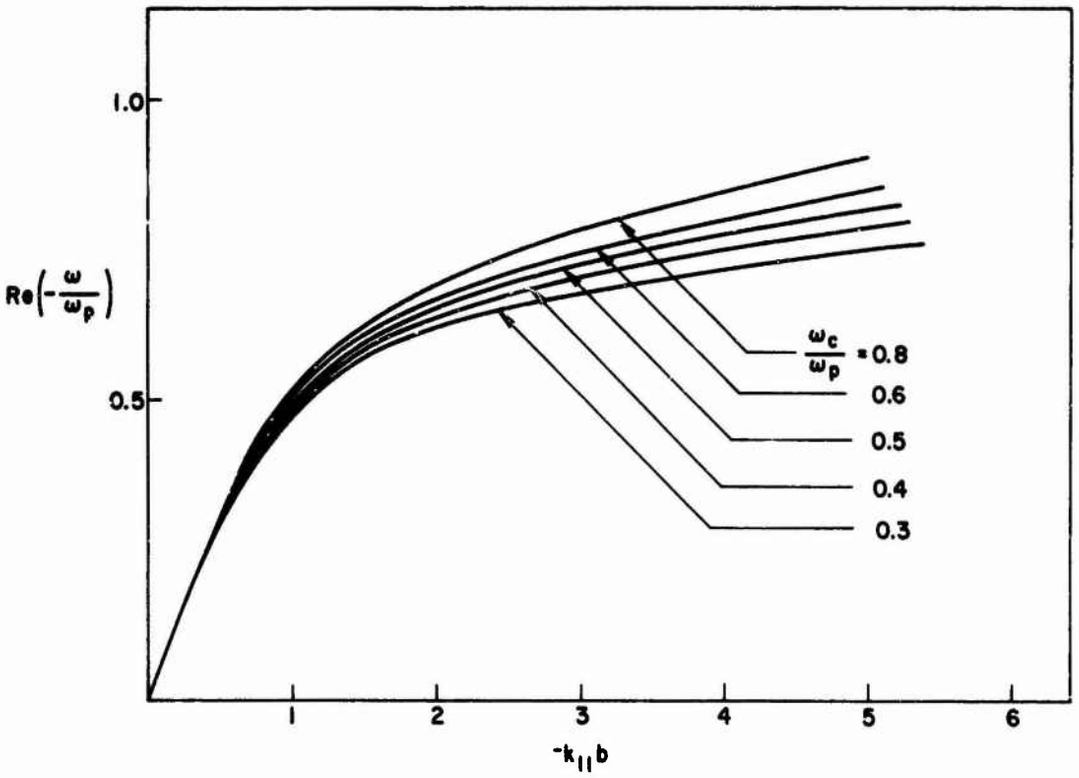

FIG. 6.10. DISPERSION DIAGRAMS FOR THE SURFACE WAVES SHOWING THE REAL PART OF ω/ω_p VERSUS WAVE NUMBER $k_{\|}b$.

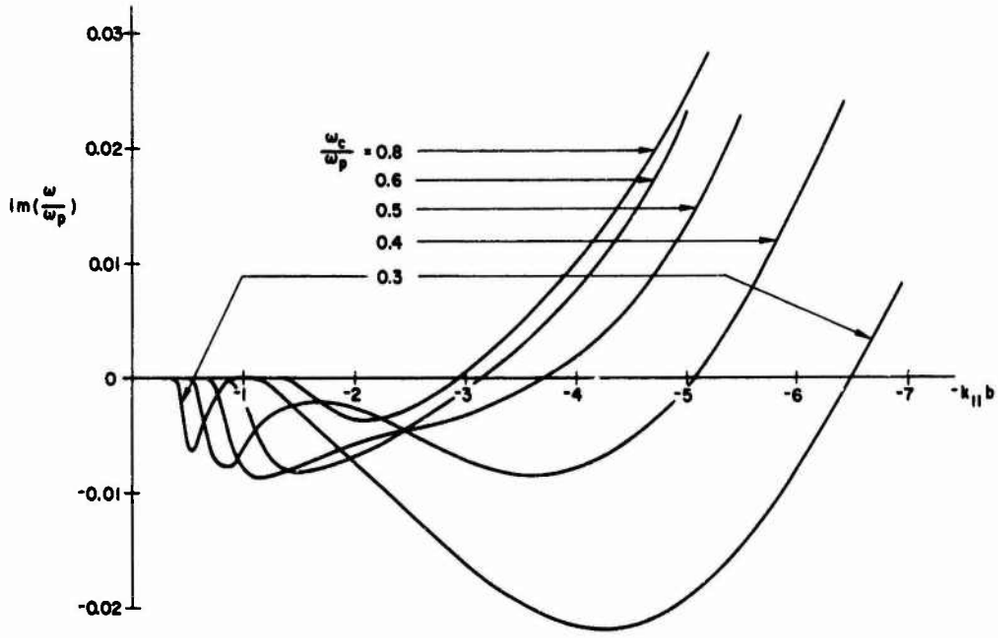

FIG. 6.11. DISPERSION DIAGRAMS FOR THE SURFACE WAVES SHOWING THE IMAGINARY PART OF ω/ω_p VERSUS WAVE NUMBER $k_{\|}b$.

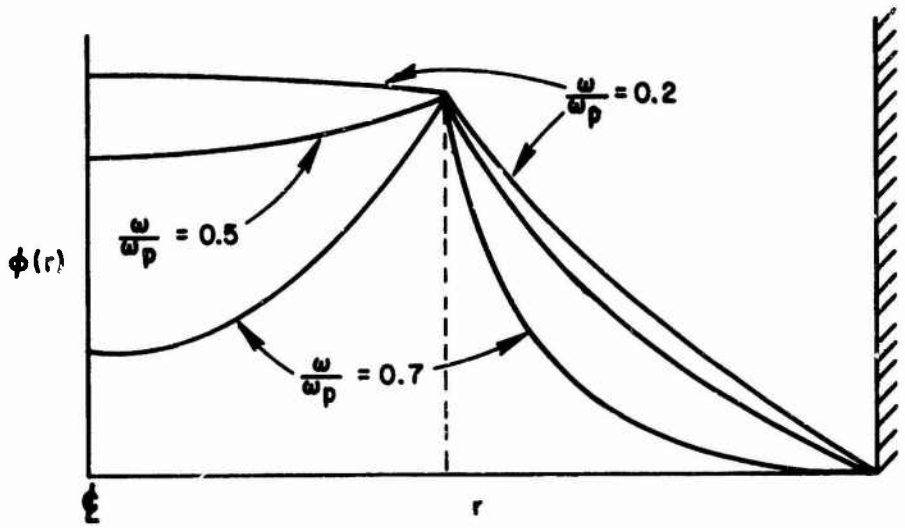

FIG. 6.12. RF POTENTIAL PROFILES AT SEVERAL FREQUENCIES WITH $\omega_c/\omega_p = 0.3$.

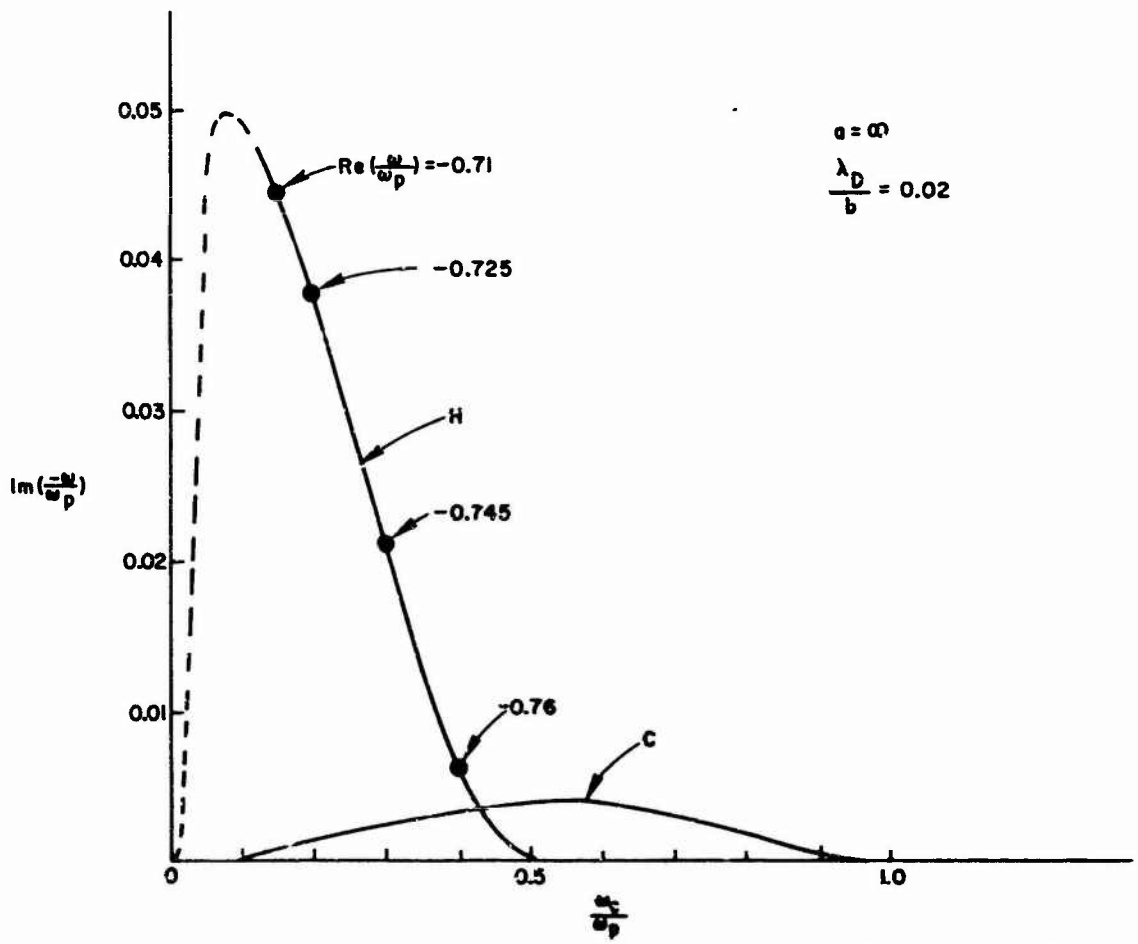

FIG. 6.13. THE IMAGINARY PART OF THE MOST UNSTABLE FREQUENCY VERSUS ω_c/ω_p.

appears to increase as ω_c is decreased, the solution at $\omega_c = 0$ is known to be stable, and thus a transition curve, such as the one shown by the dotted line, must exist. With cyclotron frequencies below $\omega_c = 0.1\ \omega_p$, the summations in the dielectric tensor converge too slowly and accuracy is lost. Consequently, we were unable to cover this range.

The effects of other parameters on the instability are shown in Figs. 6.14 and 6.15. In Fig. 6.14 we show the effect of temperature anistropy. The roots of the dispersion relation are plotted with $T_\perp/T_\parallel$

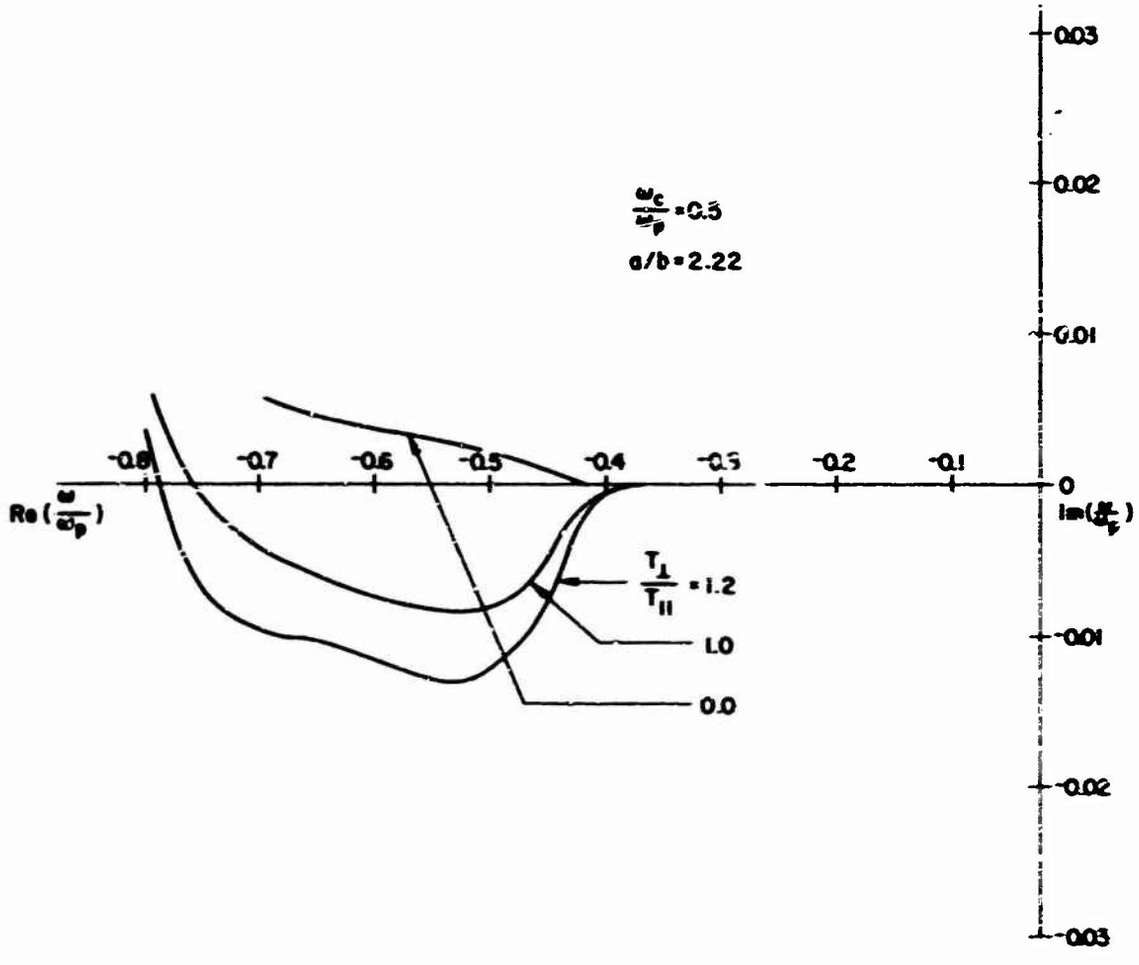

FIG. 6.14. REAL WAVE NUMBER AS MAPPED INTO THE COMPLEX ω/ω_p PLANE VIA THE DISPERSION RELATION. The locus diagram illustrates the effect of the transverse temperature on the surface wave. ω_c/ω_p = 0.5, a/b = 2.22 and $\lambda_D/b = 0.04$.

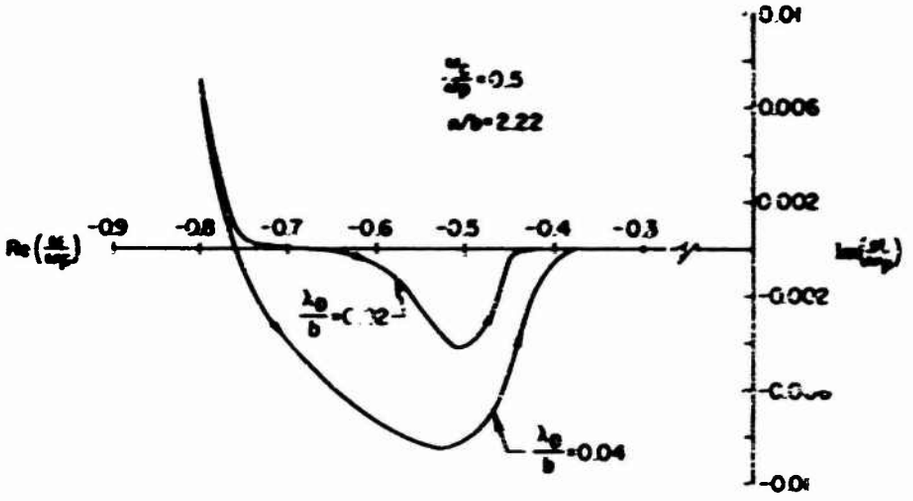

FIG. 6.15. MAPPINGS OF THE NEGATIVE $k_\perp b$ AXIS INTO THE COMPLEX ω/ω_p PLANE WITH λ_D/b AS A PARAMETER.

as a parameter. The plasma is stable when $T_\perp = 0$, and the instability, in its nonlinear limit, may provide a mechanism to convert transverse into longitudinal temperature. Shown in Fig. 6.15 are the roots of the dispersion relation with λ_D/b as a parameter. Since we keep ω_p and b constant, a change in λ_D/b is equivalent to a change in the overall temperature. We see that the higher the ratio λ_D/b (hence, higher the temperature), the greater the instability. These graphs indicate that the instability is due to finite Larmor radii effects.

No conclusive experimental evidence of the surface wave instability has been found. There is, however, a report of surface wave self oscillations with zero magnetic field in a plasma column.[53] Our theory predicts strong instability at low magnetic field, but the instability should disappear at zero magnetic field. Since we are unable to compute the dispersion relation in the very low magnetic field region, we cannot relate the observed oscillation to our instability. Also at large Larmor radii, our dc model with sharp boundary breaks down.

[illegible]

In the analysis of parts 3 and 4 we considered only the electron motion and completely ignored the ion motion. In this section we include the ion motion and investigate the dispersion relation near the ion plasma and ion cyclotron frequencies.

In a cold plasma consisting of electrons and ions the longitudinal wave becomes a surface wave [illegible] in the region [illegible] where

$$\frac{1}{\omega_{pe}^2} + \frac{1}{\omega_{ce}^2 + \omega_{pi}^2} = \frac{1}{\omega_{pi}^2}$$

provided $\omega_{ce} \gg \omega_{pi}$. The cold plasma dispersion relation near the ion plasma frequency is shown in Fig. [illegible]. When the ion plasma medium is moved, the surface wave is again found to be unstable. The computation for the plasma with ions and a neutral gas present is more complicated than that for the electron plasma. In calculating the computation, a finite ion-neutral collision frequency of [illegible] is used. Further simplification is achieved in assuming that the transverse temperature of the electrons is zero. Shown in Fig. [illegible] is the coupling of the negative ion mode [illegible] with the [illegible] mode in Fig. [illegible]. The real and imaginary

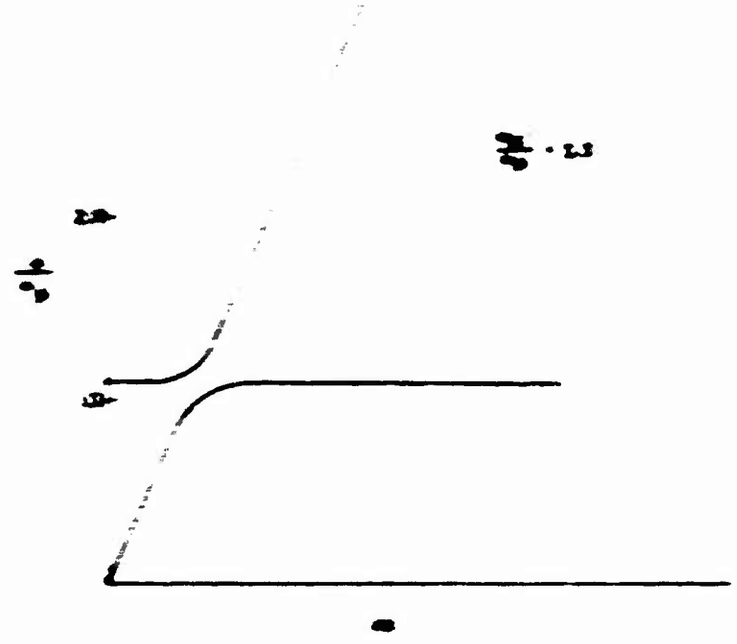

FIG. [illegible] COLD PLASMA DISPERSION RELATION NEAR THE ION PLASMA FREQUENCY

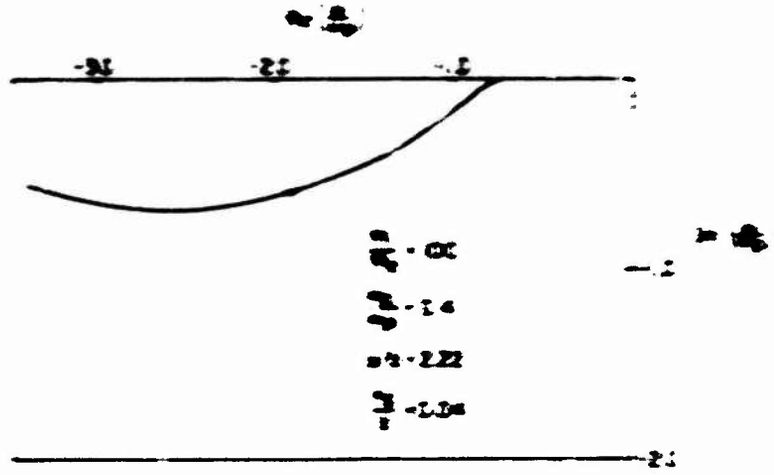

FIG [illegible] MAPPING OF THE REACTIVE REGION AND AREA INTO THE COMPLEX [illegible] PLANE

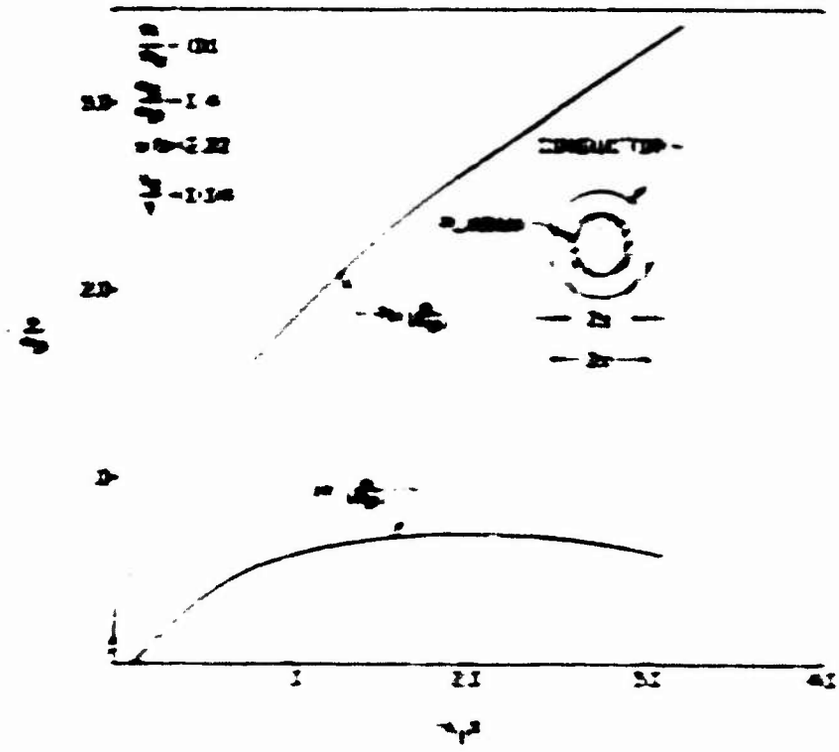

FIG [illegible] TIME REGION AND DOMINANCE POINTS OF [illegible] KERNELS [illegible]

parts of [illegible] versus [illegible]. The instability appears to be very strong since the ratio of the imaginary part of the frequency to the real part can be of the order of 1/2. We should keep in mind, however, that the model used in this computation is collisionless. In the range of our investigation the longitudinal dielectric tensor element ϵ_{zz} is predominantly electronic. Since the operating frequency is very much lower than the electron plasma frequency, a small number of electron-neutral or electron-ion collisions may alter the result. A further investigation of the ion surface wave instability should, therefore, include the electron-ion collision effects. Also these ion surface waves for practical ion-electron mass ratios have very long wavelengths. Often the wavelengths will exceed the length of the practical plasma column and end effects, such as line tying, may determine whether this instability occurs or not.

I. HIGHER ORDER MODES

Due to the tremendous complexity involved in solving the dispersion relation, very little was done to investigate the higher order modes. The azimuthally varying modes are completely ignored, and some of these modes may be even more unstable than the symmetric mode [illegible]. We paid little attention to the mode commonly called the upper hybrid mode, which appears in the cold plasma column (see Fig. [illegible]). The graph in Fig. [illegible] shows the dispersion relation for the hybrid mode in a hot electron plasma with ω_c [illegible] ω_p. The mode is heavily damped which may explain the inability of the experimenters to observe this mode. In addition to this hybrid mode, there is an infinite number of the hybrid modes in a hot plasma, each associated with one of the Bernstein modes. We did not investigate these modes.

We also did not undertake the study of higher order radial modes, since they are probably not as interesting as the azimuthal modes or hybrid modes. Our investigation treats only a small portion of a vast problem.

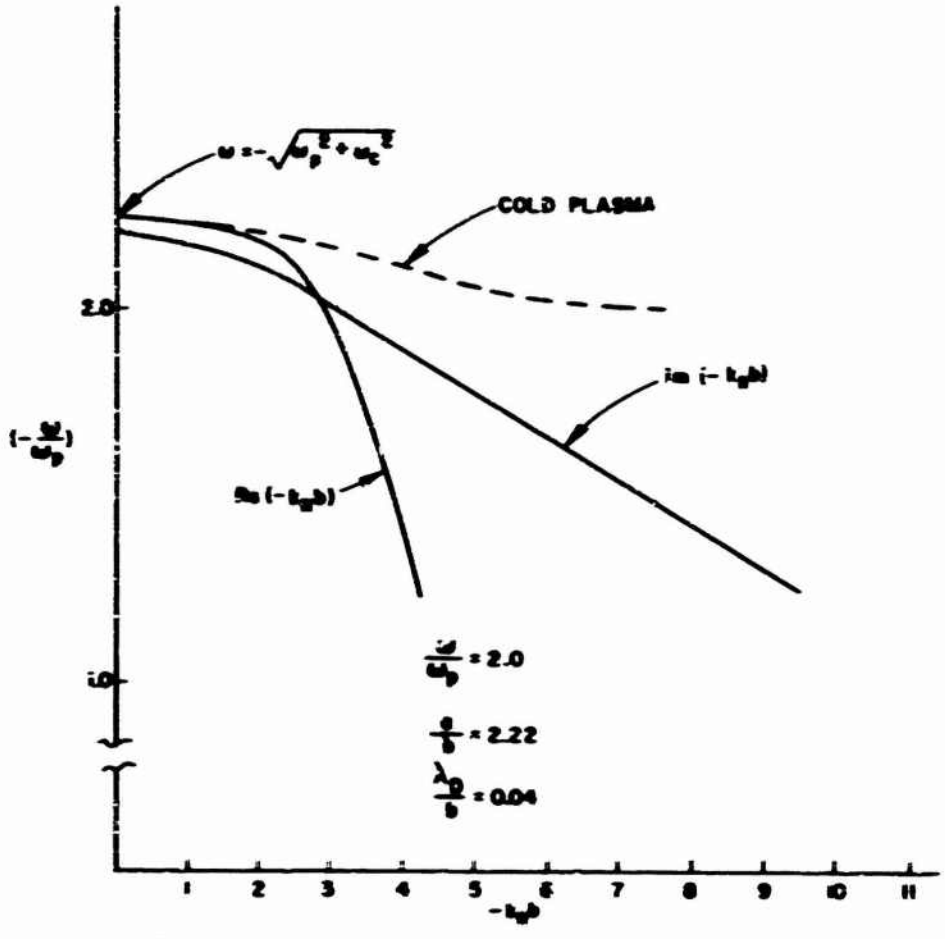

FIG. 6.19. DISPERSION RELATION FOR THE HYBRID MODE.

VII. CONCLUSION

In our study of electrostatic waves we emphasized the effects due to the finite boundary as well as the effects of magnetic fields and plasma temperature. The first part of this report treated plasma diodes in the absence of a magnetic field. A dc study of the equilibrium plasma diode was undertaken to provide a basis for the rf analysis. The dc analysis yielded some interesting results regarding the possibility of plasma formation within a diode. It was found that under equilibrium conditions plasma is formed even when the generation rate of one of the charged species at the walls is orders of magnitude lower than that of the other. The formation of plasma due to the trapping of rare species in the coulomb field of the abundant species was demonstrated in the case of metal emitters where the emission rate of the ions was very much lower than that of the electrons.

An rf analysis using the hydrodynamic model for the nonuniform plasma revealed the existence of a series of electrostatic resonances in the diode. However, an analysis of a uniform plasma diode using a kinetic plasma model showed that the end plate loss, due to absorption of the electrons at the walls, introduces a large loss mechanism. The loss may make some of the resonances predicted from the hydrodynamic model unobservable. Since this loss mechanism is related to the process which causes end plate diffusion in devices such as the Q-machine, the rf measurements of the electrostatic fields may yield information regarding the end plate diffusion coefficient.

The second part of this report dealt with the study of electrostatic wave propagation along a cylindrical column of Maxwellian plasma. First, a dc study of the density profile and azimuthal current in a cylindrical column was conducted. The theoretical analysis of the column under the assumption of complete neutrality showed that at high magnetic fields when the ion Larmor radii became much smaller than the plasma radius, the density drop was confined to the small region at the plasma edge. Experimental measurements indicated that the density drop at the plasma edge is in fact much sharper than that predicted from our theory. For the purpose of rf studies, we assumed that the plasma was uniform with

as infinitely sharp boundary since we were not interested in azimuthal instabilities, but in surface waves.

To obtain the solution for waves in the hot plasma column, we first derived the dielectric tensor appropriate for plane waves in an infinite plasma. Solutions for waves in a plasma column and the dispersion relation for these waves were obtained through plane wave synthesis. The numerical solution of the dispersion relation revealed that the electrostatic surface waves propagating along the column were unstable.

When only the electrons were assumed to respond to the rf fields, the electron surface waves which occur when $\omega_c < \omega_p$ were found to be unstable. Since the surface wave became stable when $T_e = 0$, we conclude that the instability was due to finite Larmor radii effects. We were able to classify the instability only in the mildly unstable case $\omega_c = 0.1\ \omega_p$, in which the instability was found to be convective. Such an instability can most likely be suppressed by collisions or by external agents causing Landau damping effects. For more severely unstable cases at low magnetic fields, the application of the stability criterion was hampered by numerical difficulties. In fact, it was not possible to compute the dispersion relation in the range $0 < \omega_r < 0.1\ \omega_p$ with our program. Our study was also confined to relatively symmetric modes.

When the ion motion was included in the analysis, the surface wave which occurs when $\omega_{ci} < \omega_{pi}$ was also found to be unstable. The unstable ion surface waves are of great interest since the instability appears to be very strong. Also, while the electron surface wave is easily stabilized by raising the cyclotron frequency above the plasma frequency ($\omega_c > \omega_p$), the stabilizing condition for the ion surface wave ($\omega_{ci} > \omega_{pi}$) may be difficult to attain in high density plasmas such as those in fusion devices. The numerical analysis was exceedingly difficult for the ion surface waves and we were unable to do a more thorough analysis.

Despite the simplifications made by assuming that the plasma column was uniform with a sharp boundary, the computation of the dispersion relation on the whole was extremely time consuming. A considerable improvement of the computer program is needed before a more exhaustive analysis can be made. A future analysis should include the azimuthally varying waves. Such a study may yield modes which are more unstable than the

cylindrically symmetric modes. A study of azimuthally varying ion waves should prove to be very interesting since many of the observed low frequency instabilities are associated with azimuthally varying waves.[5] A wave addition undertaking should take into account the nonuniformity of the plasma column. In such a column other instabilities such as the universal instability may occur in addition to the surface wave instability discussed in this paper.

APPENDIX A. LOW DENSITY PROBE MEASUREMENT

In this appendix we show some of the difficulties encountered in probing a low density plasma and the ways in which these problems are overcome. In our sodium plasma the typical density is of the order of 2×10^7/cc, which is lower than most of the laboratory plasmas. In the probe measurements of a low density plasma, the smallness of the probe current is the biggest problem. The probe size can be increased to increase the total current, but beyond a certain size the probe disturbs the plasma too much. Also, the probe should be as small as possible to make local measurements.

To obtain accurate probe measurements it is necessary to have the "knee" of the probe curve show clearly. This can be attained by a guard-ring arrangement of the probe. The above consideration is taken into account in the design of the co-axial probe shown in Fig. 4.4. Normally the stem of the guard-ring probe is insulated so that the current is drawn only through the probe surface and the co-planar guard-ring surface. However, since a film of sodium would quickly form on an insulated surface, causing leakage current, we decided not to coat the stem. Instead we made the whole probe as small as possible. The size of the probe is such that the total current drawn to the whole probe at the plasma potential is less than 1 percent of the total electron current from the emitters under normal operating conditions.

Maneuverability is another desirable feature of a probe. The details of the probe driving mechanism is described by Simonen.[42] The probe moves in and out as well as rotates so that the probe surface can be made to face either in the azimuthal or axial direction. When an axial magnetic field is applied, the density can be measured by facing the probe in the axial direction, while azimuthal drift can be studied by facing the probe in the azimuthal direction.

Typical probe currents are of the order of a few microamperes. This is a level where leakage currents from various sources begin to interfere with the probe curve, particularly leakage between the guard ring and the probe. Moreover, a dc amplifier is required to amplify the voltage across the current pick-up resistor to drive the XY recorder.

A schematic drawing of the probe circuit is shown in Fig. A.1. The amplifier is a Keithley 604 electrometer amplifier, which has the desired characteristic of high input impedance, low noise and drift. However, it is necessary to keep the electrometer terminals near the ground as shown in Fig. A.1. Since a terminal of the amplifier needs to be grounded, we are forced to use two sweep circuits instead of one to keep the guard ring voltage equal to the probe voltage. The sweep circuit is shown in Fig. A.2. Two such circuits with matched characteristics but insulated from each other were constructed and placed in a metal box. When a master switch is turned on, the two circuits simultaneously sweep out a single identical saw-tooth wave form. The time constant of the sweep is variable from 1 to [illegible] seconds and the amplitude is variable from [illegible] to 2[illegible] volts.

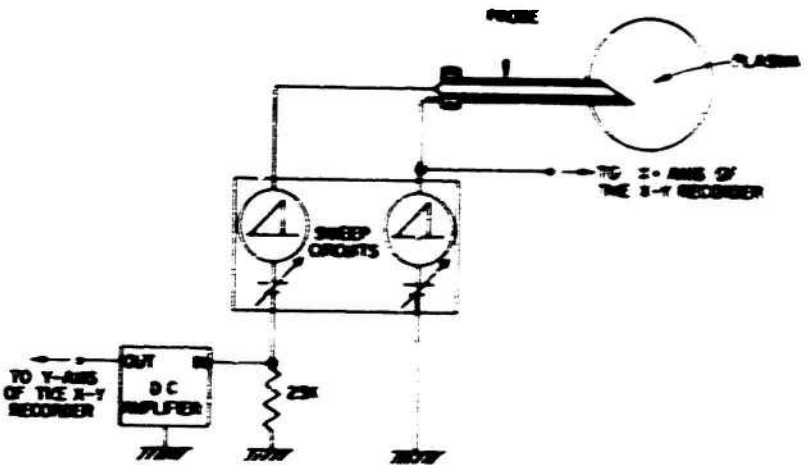

FIG. A.1. PROBE CIRCUIT

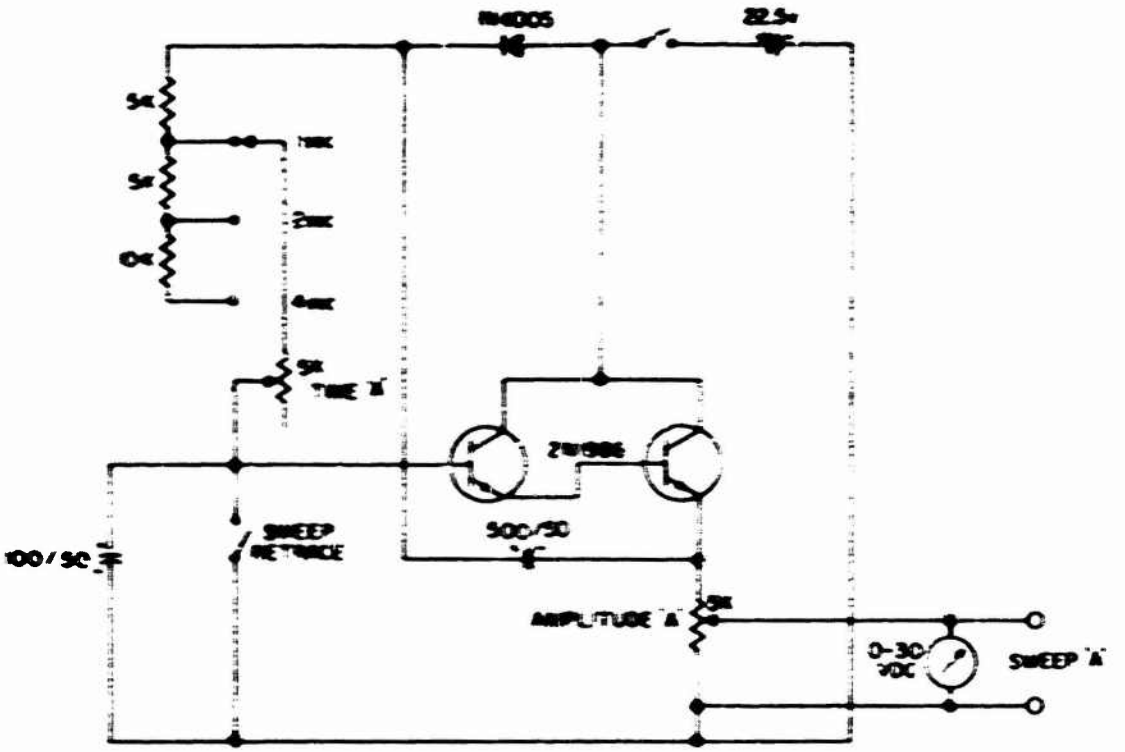

FIG. A.2. SWEEP CIRCUIT.

APPENDIX B. SOLUTION OF THE LINEARIZED BOLTZMANN EQUATION

In this appendix we obtain a solution of the linearized Boltzmann equation for a uniform plasma in a magnetic field. The solution has been derived by others using several different approaches, but we present a derivation here for the sake of completeness. The analysis can be generalized to any species of the plasma, but to avoid extra subscript we shall apply the analysis to electrons only. We shall assume that the plasma is collisionless and that there is no dc electric field. Then the zeroth and the first order Boltzmann equations are given by

$$(\vec{v} \times \vec{B}_o) \cdot \frac{\partial f_o(\vec{v})}{\partial \vec{v}} = 0 \qquad \text{(B.1)}$$

$$\frac{\partial f_1(t,\vec{x},\vec{v})}{\partial t} + \vec{v} \cdot \frac{\partial f_1(t,\vec{x},\vec{v})}{\partial \vec{x}} - \frac{e}{m}(\vec{v} \times \vec{B}_o) \cdot \frac{\partial f_1(t,\vec{x},\vec{v})}{\partial \vec{v}} = \frac{e}{m}\left(\vec{E}_1(t,\vec{x}) + \vec{v} \times \vec{B}_1(t,\vec{x})\right) \cdot \frac{\partial f_o(\vec{v})}{\partial \vec{v}} \qquad \text{(B.2)}$$

Let us make the following definition

$$\frac{e\,\vec{B}_o}{m} = \vec{\omega}_c = \vec{n}\,\omega_c$$

where $\vec{n}$ is a unit vector in the direction of the magnetic field. We Fourier analyze the linearized equation in space $(\mathrm{Im}\,(\vec{k}) = 0)$ and Laplace analyze in time $(\mathrm{Im}\,(\omega) < 0$ on L.I.P.$)$ to get

$$i(\omega - \vec{k} \cdot \vec{v})\, f_1[\omega,\vec{k},\vec{v}] + \omega_c(\vec{n} \times \vec{v}) \cdot \frac{\partial}{\partial \vec{v}} f_1[\omega,\vec{k},\vec{v}]$$

$$= \frac{e}{m}\left(\vec{E}[\omega,\vec{k}] + \vec{v} \times \vec{B}[\omega,\vec{k}]\right) \cdot \frac{\partial f_o(\vec{v})}{\partial \vec{v}} + f_1(0,\vec{k},\vec{v}] \qquad \text{(B.3)}$$

where $f_1(0,\vec{k},\vec{v}]$ is the initial value of $f_1(t,\vec{k},\vec{v}]$. Equation (B.3) can be solved by the method of characteristics.[56] By introducing a parameter t so that $\vec{v} = \vec{v}(t)$, the characteristics of Eq. (B.3) become

$$\dot{\vec{v}} = \omega_c(\vec{n} \times \vec{v}) \tag{B.4}$$

and

$$f_1[\omega,\vec{k},\vec{v}] + i(\omega - \vec{k}\cdot\vec{v})f_1[\omega,\vec{k},\vec{v}] = g[\vec{v}] \tag{B.5}$$

where the dot represents the derivstive with respect to the parameter t and

$$g[\vec{v}] = \frac{e}{m}\left(\vec{E}[\omega,\vec{k}] + \vec{v} \times \vec{B}[\omega,\vec{k}]\right) \cdot \frac{\partial f_o}{\partial \vec{v}} + f_1(0,\vec{k},\vec{v}] \quad . \tag{B.6}$$

Note that t is not the "time" which has been taken out of the problem by Laplace analysis. Equation (B.4) is solved by introducing the gyro-tensor defined by

$$\vec{\vec{D}}(\varphi) = \vec{n},\vec{n} + (I - \vec{n},\vec{n})\cos\varphi - \vec{n} \times I \sin\varphi \tag{B.7}$$

or, in tensor notation, by

$$D_{ij}(\varphi) = n_i n_j + (\delta_{ij} - n_i n_j)\cos\varphi - \epsilon_{ijk}\, n_k \sin\varphi \quad . \tag{B.8}$$

Then

$$\vec{v}(t) = \vec{\vec{D}}(-\omega_c t + \omega_c t') \cdot \vec{v}(t') \tag{B.9}$$

satisfies Eq. (B.4), as can be seen by inspection. The homogeneous part of Eq. (B.5) gives

$$\frac{d\,\ell n\, f_H}{dt} = -i(\omega - \vec{k}\cdot\vec{v}) \quad . \tag{B.10}$$

Thus

$$\ell n\, f_H = -i\omega t + i\int^t \vec{k}\cdot\vec{v}(t')dt' + \text{constant}$$

or

$$f_H = C\exp\left[-i\omega t + i\int^t \vec{k}\cdot\vec{v}(t')dt'\right] \tag{B.11}$$

where [illegible] is given by Eq. B.4). We solve the [illegible] equation by the method of variation of constant. Substituting

$$[\text{illegible}] \quad (B.5)$$

into Eq. B.3) one obtains

$$[\text{illegible}] \quad (B.6)$$

From Eq. B.6) we get

$$[\text{illegible}] \quad (B.7)$$

Therefore,

$$[\text{illegible}] \quad (B.8)$$

Solving for [illegible] we have

$$[\text{illegible}] \quad (B.9)$$

Thus,

$$[\text{illegible}] \quad (B.10)$$

or

$$[\text{illegible}] \quad (B.11)$$

Then

$$\vec{\nabla}\vec{\nabla} \cdot \vec{r} = \vec{\nabla}\left(\frac{\partial}{\partial x}\hat{i} + \frac{\partial}{\partial y}\hat{j} + \frac{\partial}{\partial z}\hat{k}\right) \cdot \left(x\hat{i} + y\hat{j} + z\hat{k}\right)$$

but

$$\hat{i} \cdot \hat{i} = 1$$

Therefore

$$\vec{\nabla}\vec{\nabla} \cdot \vec{r} = \vec{\nabla}\left(\frac{\partial x}{\partial x} + \frac{\partial y}{\partial y} + \frac{\partial z}{\partial z}\right)$$

$$= \vec{\nabla} \cdot \frac{m_1 \vec{r}}{m_1}$$

Since the operation $\vec{\nabla} \cdot$ applies to everything on the right, we have

$$\vec{\nabla}\vec{\nabla} \cdot \vec{r} = \vec{\nabla} \cdot \vec{\nabla}(\cdots) = \vec{\nabla} \cdot \vec{\nabla} \cdot \vec{\nabla}(\cdots) = \vec{\nabla} \cdot \frac{m_1 \vec{r}}{m_1}$$

and hence

$$\vec{\nabla}(\cdots) = \frac{1}{m_1}\int \cdots \frac{m_1 \vec{r}}{m_1} \cdot \frac{m_1 \vec{r}}{m_1} \vec{\nabla}(\cdots) = \vec{\nabla}(\cdots)$$

$$= \frac{m_1 \vec{r}}{m_1}$$

APPENDIX C. POLARIZATION AND MAGNETIZATION CURRENTS

The first order current and charge density in a hot electron plasma can be obtained from the relation

$$\bar{J}^{(1)} = -e\int \bar{v}\, f^{(1)}(\bar{r},\bar{v},t)\, d^3v \qquad (C.1)$$

and

$$\rho^{(1)} = -e\int f^{(1)}(\bar{r},\bar{v},t)\, d^3v \qquad (C.2)$$

where $f^{(1)}(\bar{r},\bar{v},t)$ is as defined in Eq. 3.14. In this appendix we exhibit in the plasma current $\bar{J}^{(1)}$ the polarization and magnetization currents

$$\bar{J}^{(1)} = \frac{\partial \bar{P}}{\partial t} + \nabla\times\bar{M} + \bar{J}_0 \qquad (C.3)$$

so that the plasma can be characterized completely in the polarization $\bar{P}$ and the magnetization $\bar{M}$ without distinguishing free charges and free currents. In subsection (a) below we derive a few useful tensor relations in Section A. In Section B we separate the plasma current into the two parts for the case of an isotropic zero order velocity distribution function. A result for the anisotropic distribution function is given in Section C.

A. Tensor Relations

We shall first derive a few general tensor relations. Let $\bar{A}$, $\bar{B}$, $\bar{C}$ and $\bar{D}$ be arbitrary vectors. Then we have

$$\bar{C}\times(\bar{A}\times\bar{B}) = \bar{B}(\bar{C}\cdot\bar{A}) - \bar{A}(\bar{C}\cdot\bar{B}) \qquad (C.4)$$

Let $\bar{T}$ be an arbitrary tensor. Then $\bar{A}\cdot\bar{B}-\bar{T}$ is a vector and from Eq. (C.4) we have

$$\bar{B}\cdot\bar{T}\times\bar{C} = \bar{C}\cdot\bar{B}\,\bar{T} - \bar{C}\cdot\bar{T}\,\bar{B} \qquad (C.5)$$

By omitting the redundant brackets, we obtain

$$\bar{B} \cdot \bar{\nabla} \cdot \bar{C} \cdot \bar{I} \cdot \bar{B} \cdot \bar{\nabla} \cdot \bar{C} \cdot \bar{B} \qquad (C.5$$

Since $\bar{B}$ is arbitrary, Eq. (C.5) yields

$$\bar{\nabla} \cdot \bar{C} \cdot \bar{I} \cdot \bar{\nabla} \cdot \bar{C} \cdot \bar{I} \qquad (C.$$

By taking $\bar{A} \cdot \bar{\nabla} \cdot \bar{B}$ and performing a similar analysis, we obtain

$$\bar{C} \cdot \bar{B} \cdot \bar{\nabla} \cdot \bar{I} \cdot \bar{B} \cdot \bar{\nabla} \qquad (C.$$

We now derive a few special relations for the spatial tensors we use in the subsequent analysis. Let $\bar{A}$ and $\bar{B}$ be arbitrary vectors and $\bar{I}$ the unit tensor. Then

$$\bar{A} \cdot \bar{I} \cdot \bar{A} \cdot \bar{B} \cdot \bar{A} \cdot \bar{I} \cdot \bar{A} \cdot \bar{B} \cdot \bar{A} \cdot \bar{I}$$
$$\cdot \bar{A} \cdot \bar{I} \cdot \bar{B}$$
$$\cdot \bar{A} \cdot \bar{I} \cdot \bar{I} \cdot \bar{B} \qquad (C.9$$

Since $\bar{A}$ and $\bar{B}$ are arbitrary vectors,

$$\cdot \cdot \bar{I} \cdot \bar{I} \cdot \bar{I} \qquad (C.$$

Similarly, we can show that the unit tensor is given by

$$\bar{A} \cdot \bar{I} \cdot \bar{I} \cdot \bar{A} \cdot \bar{I} \cdot \bar{I} \cdot \bar{I} \cdot \bar{A}$$
$$\cdot \bar{A} \cdot \bar{I} \cdot \bar{I} \cdot \bar{I} \cdot \bar{A}$$
$$\cdot \bar{A} \cdot \bar{I} \cdot \bar{I} \cdot \bar{I} \cdot \bar{I} \cdot \bar{A}$$
$$\cdot \bar{A} \cdot \bar{I} \cdot \bar{I} \cdot \bar{I} \cdot \bar{I} \cdot \bar{I} \cdot \bar{A}$$
$$\cdot \bar{A} \cdot \bar{I} \cdot \bar{I} \cdot \bar{I} \cdot \bar{I} \cdot \bar{I} \cdot \bar{I} \cdot \bar{A} \qquad (C.$$

Thus

$$\bar{\bar{\alpha}} \cdot \bar{\bar{\alpha}} + \bar{\bar{\beta}} \cdot \bar{\bar{\beta}} = \bar{\bar{I}} \quad (3.12)$$

By using Eqs. (3.11) and (3.12), we get

$$\bar{\bar{D}}(\xi) = \bar{\bar{\alpha}} \cdot \bar{\bar{\alpha}} + \bar{\bar{I}} \cos\xi - \bar{\bar{I}} - \bar{\bar{\alpha}}\bar{\bar{\alpha}} \sin\xi \quad (3.13)$$

where $\bar{\bar{D}}(\xi)$ is as defined by Eq. (3.7). We also have

$$\frac{d\bar{\bar{D}}(\xi)}{d\xi} \cdot \bar{\bar{D}} = -\bar{\bar{\alpha}} \cdot \bar{\bar{\alpha}} + \bar{\bar{I}} \cos\xi - \bar{\bar{I}} - \bar{\bar{\alpha}}\bar{\bar{\alpha}} \sin\xi \quad (3.14)$$

Thus, from Eqs. (3.13) and (3.14) we get

$$\bar{\bar{D}}' = -\bar{\bar{I}} + \bar{\bar{\alpha}} \quad (3.15)$$

Equation (3.9) can be expressed in terms of $\bar{\bar{\alpha}}$ as

$$\bar{\bar{D}}' = -\bar{\bar{I}} + \bar{\bar{\alpha}} \cdot \bar{\bar{\alpha}} \quad (3.16)$$

By a direct dyadic multiplication of Eq. (3.15) with $\bar{\bar{\alpha}}$, we get the following two relations

$$\bar{\bar{\alpha}} \cdot \bar{\bar{\alpha}} \cdot \bar{\bar{I}} = -\bar{\bar{\alpha}} \quad (3.17)$$

$$\bar{\bar{\alpha}} \cdot \bar{\bar{\alpha}} \cdot \bar{\bar{\alpha}} = -\bar{\bar{\alpha}} \quad (3.18)$$

3. Isotropic Velocity Distribution Functions

In this section we shall consider a completely symmetric zero order velocity distribution $f_0(\bar{v}) = f_0(-\bar{v})$. In this case the perturbed velocity distribution function [Eq. (3.5)] becomes

$$f_1(\bar{r},\bar{v},t) = \frac{e}{m_i}\int_{-\infty}^{t} e^{\bar{\bar{\alpha}}\cdot\bar{\bar{I}}_1 - \bar{\bar{D}}(\xi)} \cdot \frac{\partial f_0}{\partial \bar{v}}\, d\xi \quad (3.19)$$

where

$$\ell = -\frac{kc}{\omega_c} z + \frac{\vec{k}\cdot\vec{x} - \vec{k}\cdot\vec{x}_0(z) - \omega t}{\omega_c}$$

The charge density can be obtained by integration of (C.19).

$$\langle \delta \rangle = -\frac{e^2}{m\omega_c} \int_0^\infty dz \int e^{i\ell} \vec{E}\cdot\vec{\delta} \cdot \frac{\partial f_0}{\partial \vec{v}} e^{-i\omega t} \qquad (C.21)$$

By partial integration in $\vec{v}$, we obtain

$$= -\frac{e^2}{m\omega_c} \int_0^\infty dz \int \frac{1}{k_z} \vec{k}\cdot\vec{E}\cdot\vec{\delta} \cdot \frac{\partial f_0}{\partial \vec{v}} e^{-i\omega t}$$

$$= \frac{e^2}{m\omega_c} \int_0^\infty dz \int e^{i\ell} \frac{1}{k_z} \vec{k}\cdot\vec{E}\cdot\vec{E}\cdot\vec{E} \cdot \frac{\partial f_0}{\partial \vec{v}} e^{-i\omega t} \qquad (C.22)$$

The polarization charge associated with a plane wave is given by

$$\delta_p = i\vec{k}\cdot\vec{P} \qquad (C.23)$$

We now identify the total charge δ with δ_p and identify $\vec{P}$ from Eq. (C.23) with

$$\vec{P} = \frac{e^2}{m\omega_c} \int_0^\infty dz \int e^{i\ell} \frac{1}{k_z} \vec{E}\cdot\vec{E}\cdot\vec{E} \cdot \frac{\partial f_0}{\partial \vec{v}} e^{-i\omega t} \qquad (C.24)$$

The first order plasma current can be obtained by the following integration

$$\langle \vec{J}^{(1)} \rangle = -e \int \vec{v} \, \delta^{(1)} \, d^3v$$

$$= -\frac{e^2}{m\omega_c} \int_0^\infty dz \int \frac{\partial f_0}{\partial \vec{v}} e^{-i\omega t} e^{i\ell} \left[\vec{E}\cdot\vec{E} - \frac{\omega_c \vec{E}}{k_z} \right] \qquad (C.25)$$

remaining after $i\vec{k} \times \vec{M}$ is subtracted from Eq. (C.26), vanish. We show that this is indeed the case. Let

$$\vec{A} = i\omega\vec{P} - \langle \rho\vec{v} \rangle - i\vec{k} \times \vec{M} \ .$$

Then

$$\vec{A} = \frac{e^2}{m\omega_c} \int_0^\infty dx \int e^{\frac{i\omega}{v}x} e^{\ell} f_0(\vec{v}) \left[\frac{\omega\vec{L}}{v_c} - I - \frac{i(\vec{k}\cdot I\cdot\vec{v})}{\omega_c} \vec{L} \right] \cdot (\vec{E} - \vec{D}) \quad (C.30)$$

Since $I = \vec{L}\vec{L} + \vec{L} \times \vec{n}$ from (C.1), we have

$$\vec{A} = \frac{e^2}{m\omega_c} \int_0^\infty dx \int e^{\frac{i\omega}{v}x} e^{\ell} f_0(\vec{v}) \left[\frac{\omega\vec{L}}{v_c} - I - \frac{i(\vec{k}\cdot\vec{L}\vec{L}\cdot\vec{v})}{\omega_c} \vec{L} - \frac{i\vec{k}\cdot(\vec{L}\times\vec{n})\cdot\vec{v}}{\omega_c} \vec{L} \right] \cdot \vec{E}\cdot\vec{D}$$

$$= \frac{e^2}{m\omega_c} \int_0^\infty dx \int e^{\frac{i\omega}{v}x} f_0(\vec{v}) \left[\frac{\partial e^{\ell}}{\partial \ell} \vec{L} + Ie^{\ell} + e^{\ell} \frac{i\vec{k}\cdot(\vec{L}\times\vec{n})\cdot\vec{v}}{\omega_c} \vec{L} \right] \cdot \vec{E}\cdot\vec{D} \ . \quad (C.31)$$

Partial integration in ℓ of the first term yields

$$\vec{A} = \frac{e^2}{m\omega_c} \int_0^\infty dx \int e^{\frac{i\omega}{v}x} e^{\ell} f_0(\vec{v}) \left[-\vec{L}\cdot(\vec{E}\vec{L}) - \vec{L}\cdot(\vec{E}\vec{L}) + \vec{E}\cdot\vec{L} \right.$$

$$\left. + \left\{ \frac{i\vec{k}\cdot(\vec{L}\times\vec{n})\cdot\vec{v}}{\omega_c} \right\} \vec{L}\cdot(\vec{E}\vec{L}) \right] \ . \quad (C.32)$$

Let the first three terms of the integrand be $-\vec{C}$. Then

$$\vec{C} = f_0 e^{\ell} \left[\vec{L}\cdot(\vec{E}\vec{L}) + (\vec{L}\vec{L})\cdot\vec{E} \right] \ . \quad (C.33)$$

By using Eqs. (C.1), (C.7), and (C.16), we get

$$\vec{C} = f_0 e^{\ell} \left[\vec{L}\cdot(\vec{E}\vec{L}) - (\vec{L}\times\vec{n})\cdot\vec{E}\cdot\vec{L} \right]$$

$$= f_0 e^{\ell} \left[\vec{L}\cdot(\vec{E}\vec{L}) - \vec{L}\cdot(\vec{n}\times\vec{E})\cdot\vec{L} \right]$$

$$= f_0 e^{\ell} \left[\vec{L}\cdot(\vec{E}\vec{L}) + \vec{L}\cdot(\vec{E} - \vec{L}\vec{L})\cdot\vec{L} \right]$$

$$= 0 \ .$$

a subdivision as simple as that described in (2) cannot be accomplished. However, if we ignore forces of the order $\vec{v} \times \vec{B}$ as compared with $\vec{E}$ then the problem simplifies, and in fact the procedure to separate the currents is identical to that followed in Section (2). The result is again given by Eqs (C.24) and (C.27) where now $f_0(\vec{r})$ is as defined in (C.35). For electrostatic terms the approximation $\vec{v} \times \vec{B} = 0$ should be very good.

APPENDIX D. THE DIELECTRIC SUSCEPTIBILITY TENSOR FOR MAXWELLIAN ELECTRON PLASMAS

In this appendix we evaluate the dielectric susceptibility tensor appropriate for Maxwellian electron plasmas. In particular, we express the tensor elements in terms of the Hilbert transform of the gaussian as tabulated by Fried and Conte. The susceptibility tensor for the case of isotropic temperature is given in Section 7.1. The case of anisotropic temperature can be handled by a slight modification of the procedure followed for the isotropic case. In Section D.2 the result for the anisotropic case is given without derivation. Some useful properties of the Hilbert transform of the gaussian are given in Section D.3.

D.1 Isotropic Maxwellian Velocity Distribution

From Eq. X.2 we have

$$\bar{\bar{\chi}} = \frac{\omega_p^2}{n_0 c} \int_0^\infty d\omega' \int d^3v \, \exp\left[i\left(\frac{\omega' t}{c} - \frac{\vec{k}\cdot\vec{v}t}{c}\right)\right] \vec{v}\vec{v} \cdot \frac{\partial f_0}{\partial \vec{v}} \qquad D.1$$

The distribution function and the normalization condition are given by

$$f_0(\vec{v}) = A \exp\left[-\frac{m v^2}{2kT}\right] . \qquad D.2$$

$$\int f_0(\vec{v}) \, d^3v = n_0 . \qquad D.3$$

Substituting D.2 into D.1 we obtain

$$\bar{\bar{\chi}} = \frac{\omega_p^2 m}{n_0 kT} \int_0^\infty d\omega' \, e^{i\omega' t} \int d^3v \, \vec{v}\vec{v} \exp\left[i\frac{\omega' t}{c}\right] \exp\left[-\frac{v^2}{2v_0^2} - \frac{i\vec{k}\cdot\vec{v}t}{c}\right] . \qquad D.4$$

The velocity integral of Eq. D.4 can be performed and the result is given by

$$\bar{\bar{\chi}} = \frac{\omega_p^2}{\omega^2} \int_0^\infty d\omega' \, e^{i\omega' t} \, \bar{\bar{\Gamma}} \exp\left[-\frac{\omega' t}{c} - \frac{k^2 v_0^2}{2\omega'^2} t^2\right] . \qquad D.5$$

A direct substitution of $\bar{\bar{L}}$ and $\bar{\bar{L}}^{-}$ gives

$$\bar{\bar{L}} \cdot (\bar{k} - \bar{L}) = \bar{k}(\bar{k}\cdot\bar{L}) - \cos\theta] + \bar{L}\cos\theta + \bar{k}\times\bar{L}\,[1 - \cos\theta]$$
$$= -\bar{L}(-\theta) - \bar{L} \,. \qquad (D.6)$$

In terms of Cartesian coordinates we obtain

$$\bar{L} \cdot (\bar{k}\times\bar{L}) = \bar{i}_x k_x k_y + \bar{i}_y k_y k_x \cos\theta - k_y(1 - \cos\theta)]$$
$$+ \bar{i}_y k_y k_y \cos\theta + k_x(1 - \cos\theta)] \qquad (D.7)$$

where $\bar{i}_x$, $\bar{i}_y$ and $\bar{i}_z$ are unit vectors along x, y and z axis respectively with the dc magnetic field directed along the z axis. The electric susceptibility tensor defined by

$$\bar{P} = \epsilon_0 \bar{\chi} \cdot \bar{E} \qquad (D.8)$$

yields

$$\bar{\chi} = \begin{bmatrix} \chi_{xx} & \chi_{xy} & \vdots \\ \chi_{yx} & \chi_{yy} & \vdots \\ \cdots & \cdots & \chi_{zz} \end{bmatrix}$$

with

$$\chi_{xx} = \chi_{yy} = \frac{\omega_p^2}{2\omega_c^2}\int_0^\infty \sin x\, e^{-\alpha x}\, dx \qquad (D.9)$$

$$\chi_{zz} = \frac{\omega_p^2}{\omega_c^2}\int_0^\infty x\, e^{-\alpha x}\, dx \qquad (D.10)$$

$$\chi_{xy} = -\chi_{yx} = -\frac{\omega_p^2}{2\omega_c^2}\int_0^\infty (1 - \cos x)e^{-\alpha x}\, dx \,. \qquad (D.11)$$

where

$$\alpha = \frac{\omega\xi}{v_c} - \frac{v_\theta^2}{2v_c^2}(k-\bar{k})^2$$

$$= \frac{\omega\xi}{v_c} + \frac{k_\perp^2 v_\theta^2}{2v_c^2}\xi^2 + \frac{k^2 v_\theta^2}{v_c^2}(1-\cos\varphi) \quad .$$

There are four types of integrals to be evaluated

$$S_1(k_\perp, k_\parallel, \omega\xi) = \int_0^\infty e^{-\alpha}\, d\alpha \qquad (D.12)$$

$$S_2(k_\perp, k_\parallel, \omega\xi) = \int_0^\infty \alpha\, e^{-\alpha}\, d\alpha \qquad (D.13)$$

$$S_3(k_\perp, k_\parallel, \omega\xi) = \int_0^\infty \sin\alpha\, e^{-\alpha}\, d\alpha \qquad (D.14)$$

$$S_4(k_\perp, k_\parallel, \omega\xi) = \int_0^\infty \cos\alpha\, e^{-\alpha}\, d\alpha \; . \qquad (D.15)$$

However, all of the integrals can be obtained from one integral S_1 due to the following relations:

$$S_3(k_\perp, k_\parallel, \omega\xi) = \frac{S_1(k_\perp, k_\parallel, \omega\xi - v_c) - S_1(k_\perp, k_\parallel, \omega\xi + v_c)}{2i} \qquad (D.16)$$

$$S_4(k_\perp, k_\parallel, \omega\xi) = \frac{S_1(k_\perp, k_\parallel, \omega\xi - v_c) + S_1(k_\perp, k_\parallel, \omega\xi + v_c)}{2} \quad , \qquad (D.17)$$

and by partial integration of the following integral

$$\int_0^\infty \left(\frac{k\omega}{v_c} + \frac{k_\perp^2 v_\theta^2}{v_c^2}\, t + \frac{k^2 v_\theta^2}{v_c^2} \sin t \right) e^{-\alpha} d\alpha$$

one obtains

$$\chi = -\frac{\omega_p}{\omega_c} S_1(k_\parallel, k_\perp, \omega) - \frac{k_\parallel^2 v_{te}^2}{\omega_c^2} S_2(k_\parallel, k_\perp, \omega) - \frac{k_\perp^2 v_{te}^2}{\omega_c^2} S_3(k_\parallel, k_\perp, \omega) . \quad \text{(D.14)}$$

In addition the following relation is also true.

$$S_2(k_\parallel, k_\perp, \omega) = -\frac{\omega_c}{\omega} \frac{k_\parallel}{k_\perp} S_1(k_\parallel, k_\perp, \omega) . \quad \text{(D.15)}$$

Thus the only integral needed is S_1, which we shall evaluate now. Let us first introduce the variables

$$\frac{\lambda^2}{2} = \frac{k_\perp^2 v_{te}^2}{\omega_c^2}$$

$$\alpha^2 = \frac{k_\parallel^2 v_{te}^2}{2\omega_c^2}, \qquad \alpha = \frac{k_\parallel v_{te}}{\sqrt{2}\,\omega_c}$$

and

$$p_n = \frac{\omega}{\sqrt{2}\,\omega_c} - n$$

and use the well-known expansion

$$\exp\left[-\frac{\lambda^2}{2}\cos\varphi\right] = \sum_{-\infty}^{\infty} I_n\left(\frac{\lambda^2}{2}\right) e^{in\varphi} \quad \text{(D.16)}$$

where I_n are the modified Bessel functions. Then S_1 becomes

$$S_1 = \sum_{-\infty}^{\infty} \exp\left[-\frac{\lambda^2}{2}\right] I_n\left(\frac{\lambda^2}{2}\right) \int_0^\infty d\varphi\, e^{-\alpha^2\varphi^2 - p_n\varphi} \quad \text{(D.17)}$$

We now change the integration variable to $s = \pm\alpha\varphi$, where the sign is fixed such that $s > 0$ for $\varphi > 0$, and obtain

$$S_1 = \sum_{-\infty}^{\infty} \exp\left[-\frac{\lambda^2}{2}\right] I_n\left(\frac{\lambda^2}{2}\right) \int_{\zeta} \frac{d\omega}{(2\pi)} \exp\left[-s^2 - \left(\frac{\omega}{2\pi}\right) s\right] \qquad (D.22)$$

The integral can be expressed in terms of the confluent hypergeometric function, $\Psi[a,b;c]$, first introduced by Tricomi.[37]

$$S_1 = \sum_{-\infty}^{\infty} \exp\left[-\frac{\lambda^2}{2}\right] I_n\left(\frac{\lambda^2}{2}\right) \left[\frac{1}{(2\pi)}\right] \Psi\left[\frac{1}{2}, \frac{1}{2}; \left(\frac{\omega}{2\pi}\right)^2\right] . \qquad (D.23)$$

With these particular parameters, Ψ can also be expressed in terms of the Hilbert transform of the gaussian as defined by Fried and Conte.[45]

$$Z(\zeta) = e^{-1/2} \int_{-\infty}^{\infty} \frac{e^{-x^2}\, dx}{x - \zeta} \qquad \text{Im}\,\zeta > 0 . \qquad (D.24)$$

Let us define a new variable

$$\zeta_n = \frac{\omega - n\omega_c}{\sqrt{2}\, k_\parallel v_\theta} . \qquad (D.25)$$

Then $\Psi\left[\frac{1}{2}, \frac{1}{2}; -\zeta^2\right] = Z(\zeta)$ as can be shown by comparing the power series expansions of $Z(\zeta)$ and $\Psi\left[\frac{1}{2}, \frac{1}{2}; -\zeta^2\right]$. The function $Z(\zeta)$ is defined such that it is regular for $\text{Im}\,\zeta > 0$, in other words, when

$$\text{Im}\left(\frac{\omega - n\omega_c}{\sqrt{2}\, k_\parallel v_\theta}\right) > 0 . \qquad (D.26)$$

Since on a Laplace integral path $\text{Im}\,\omega < 0$, the inequality of (D.26) requires that $k_\parallel < 0$, which makes $\alpha < 0$. Thus the negative sign in front of α must be selected in order to keep $s > 0$ in (D.22), and so

$$S_1(k_\parallel, k_\perp, \omega) = \frac{-\sqrt{2}\,\omega_c}{k_\parallel v_\theta} \sum_{-\infty}^{\infty} \exp\left[-\frac{\lambda^2}{2}\right] I_n\left(\frac{\lambda^2}{2}\right) Z(\zeta_n) . \qquad (D.27)$$

When (D.27) is introduced into Eqs. (D.15) through (D.19), the elements of the dielectric susceptibility tensor become

$$\chi_{xx} = \chi_{yy} = \frac{\omega_p^2}{2k_z v_{th}} \exp\left[-\frac{\lambda^2}{2}\right] \sum_{n=-\infty}^{\infty} I_n\left(\frac{\lambda^2}{2}\right)\left[Z_{n+1} - Z_{n-1}\right] , \qquad (D.28)$$

$$\chi_{zz} = -\frac{\omega_p^2}{k_z^2 v_{th}^2} \exp\left[-\frac{\lambda^2}{2}\right] \sum_{n=-\infty}^{\infty} I_n\left(\frac{\lambda^2}{2}\right) \zeta_n Z_n , \qquad (D.29)$$

$$\chi_{xy} = -\chi_{yx} = -\frac{i\omega_p^2 \zeta_n}{k_z v_{th}} \exp\left[-\frac{\lambda^2}{2}\right] \sum_{n=-\infty}^{\infty} I_n\left(\frac{\lambda^2}{2}\right)\left[Z_n - \frac{Z_{n+1}+Z_{n-1}}{2}\right] \qquad (D.30)$$

where $Z_n = Z(\zeta_n)$.

c. Anistropic Maxwellian Velocity Distribution with Drift

By assuming the forces of the order $\vec{v} \times \vec{B}$ to be negligible as compared to E, the polarization vector is again given by Eq. (D.1), where now for the anistropic drifting Maxwellian velocity distribution we have

$$f_0(\vec{v}) = A \exp\left[-\frac{m}{2kT_{\parallel}}(v_{\parallel} - u_0)^2 - \frac{m}{2kT_{\perp}} v_{\perp}^2\right] . \qquad (D.31)$$

With (D.31) the velocity integral in (D.1) can be performed to give

$$\vec{P} = \frac{\epsilon_0 \omega_p^2}{k_z^2 v_{th\parallel}^2} \int_0^{\infty} d\tau \; \vec{L} \cdot (\vec{E}\vec{L}^*) \exp\left[-\frac{i(\omega - k_{\parallel} u_0)}{k_z v_{th\parallel}} \tau - \frac{k_{\perp}^2 v_{th\perp}^2}{2\omega_c^2} \tau^2 - \frac{k_{\perp}^2 v_{th\perp}^2}{\omega_c^2}(1 - \cos\omega_c\tau)\right]$$

(D.32)

where

$$v_{th\parallel}^2 = \frac{kT_{\parallel}}{m}$$

and

$$v_{th\perp}^2 = \frac{kT_{\perp}}{m} .$$

In terms of the Hilbert transform of the gaussian, we have

$$\chi_{xx} = \chi_{yy} = \frac{\omega_p^2}{2\sqrt{2}\,\omega_c k_\parallel v_{\theta_i}} \exp\left[-\frac{\lambda^2}{2}\right] \sum_{-\infty}^{\infty} I_n\left(\frac{\lambda^2}{2}\right) \left[Z_{n+1} - Z_{n-1}\right] \qquad (D.33)$$

$$\chi_{zz} = -\frac{\omega_p^2}{2k_\parallel^2 v_{\theta_i}^2} \exp\left[-\frac{\lambda^2}{2}\right] \sum_{-\infty}^{\infty} I_n\left(\frac{\lambda^2}{2}\right) Z_n' \qquad (D.34)$$

$$\chi_{xy} = -\chi_{yx} = \frac{-i\omega_p^2}{\sqrt{2}\,\omega_c k_\parallel v_{\theta_i}} \exp\left[-\frac{\lambda^2}{2}\right] \sum_{-\infty}^{\infty} I_n\left(\frac{\lambda^2}{2}\right) \left[Z_n' - \frac{Z_{n+1} + Z_{n-1}}{2}\right] \qquad (D.35)$$

where

$$Z_n = Z(\zeta_n) \,,$$

$$\zeta_n = \frac{\omega - k_\parallel v_\theta - n\omega_c}{\sqrt{2}\,k_\parallel v_{\theta_i}} \,,$$

$$\frac{\lambda^2}{2} = \frac{k_\perp^2 v_{\theta_i}^2}{2\omega_c^2} \,.$$

3. Properties of $Z(\zeta)$

The function $Z(\zeta)$ is defined by the integral of Eq. (D.24) when $\mathrm{Im}\,\zeta > 0$. In the lower ζ plane $Z(\zeta)$ and its n^{th} derivative $Z^n(\zeta)$ are given by their analytic continuation

$$Z^{(n)}(\zeta) = [Z^n(\zeta^*)]^* + 2i\sqrt{\pi}\,(-1)^n\, h_n(\zeta)\exp(-\zeta^2) \qquad (D.36)$$

where $h_n(\zeta)$ are the Hermite polynomials[58] satisfying the recurrence relation

$$h_n(\zeta) = -2\zeta h_{n-1}(\zeta) - h_{n-1}'(\zeta) \qquad \text{with} \quad h_0(\zeta) = 1 \,.$$

The function $Z(\zeta)$ satisfies the following differential equation

$$Z'(\zeta) + 2\zeta Z(\zeta) + 2 = 0 \qquad (D.37)$$

and the symmetry relation

$$z^{(n)}(-\zeta^*) = (-1)^{n+1}[z^{(n)}(\zeta)]^* . \tag{D.38}$$

$z(\zeta)$ can be expanded in terms of the power series

$$z(\zeta) = i\sqrt{\pi}\, e^{-\zeta^2} - 2\zeta\left[1 - \frac{2}{3}\zeta^2 + \frac{4}{15}\zeta^4 - \cdots + \frac{(-\zeta^2)^n \sqrt{\pi}}{2(n + 1/2)!} + \cdots\right] \tag{D.39}$$

and the asymptotic expansion

$$z(\zeta) \sim i\sqrt{\pi}\, A\, e^{-\zeta^2} - \frac{1}{\zeta} - \frac{1}{2\zeta^3} - \cdots - \frac{(n - 1/2)!}{\sqrt{\pi}\,\zeta^{2n+1}} \tag{D.40}$$

where

$$A = \begin{cases} 0 & \text{Im } \zeta > 0 \\ 1 & \text{Im } \zeta = 0 \\ 2 & \text{Im } \zeta < 0 \end{cases} .$$

For computational purposes, two continued fraction expansions are useful:[42] if $|\zeta|$ is small,

$$z'(\zeta) = i2\sqrt{\pi}\,\zeta\, e^{-\zeta^2} - 2\left[\frac{1}{1} + \frac{\zeta^2}{1/2} - \cdots \frac{n\zeta^2}{2n - 1/2} + \frac{(n - 1/2)\zeta^2}{2n + 1/2} - \cdots\right] \quad n \geq 1 \tag{D.41}$$

or if $|\zeta|$ is large,

$$z'(\zeta) = \frac{1}{-\zeta^2 + 3/2 + \cdots \dfrac{-(1 - 1/2n)}{2 - \zeta^2/n - 1/2n + \cdots}} \qquad \begin{matrix} \text{Im } \zeta > 0 \\ n \geq 2 \end{matrix} \tag{D.42}$$

To obtain the relation equivalent to Eq. (D.42) for $\text{Im } \zeta < 0$, we use Eq. (D.36). Continued fraction expansions are useful in the intermediate range of $|\zeta|$, i.e., $2 < |\zeta| < 8$, where neither the power series expansion nor the asymptotic expansion are satisfactory.

APPENDIX E. RELATION BETWEEN $\vec{B}$ AND $\vec{M}$ FOR A MAXWELLIAN PLASMA

For a plasma with isotropic temperature, the magnetization vector as defined by Eq. (C.24) can be expressed in terms of the magnetic induction $\vec{B}$. Equation (C.24) is given by

$$\vec{M} = -\frac{e^2}{m\omega_c^2}\int_0^\infty d\varphi \int e^{i\vec{k}\cdot\vec{v}} \times \vec{L}\cdot(\vec{E}\cdot\vec{L}')]f_o(\vec{v})d^3\vec{v} \qquad (C.24)$$

For a Maxwellian distribution we have

$$\vec{v}\, f_o(\vec{v}) = -v_\theta^2 \frac{\partial f_o(\vec{v})}{\partial \vec{v}} . \qquad (E.1)$$

By introducing (E.1) into (C.24) we obtain

$$\vec{M} = -\frac{e^2 v_\theta^2}{m\omega_c^2}\int_0^\infty d\varphi \int e^{i\vec{k}}\left[\frac{\partial f_o(\vec{v})}{\partial \vec{v}} \times \vec{L}\cdot(\vec{E}\cdot\vec{L}')\right]d^3\vec{v} . \qquad (E.2)$$

Partial integration in $\vec{v}$ yields

$$\vec{M} = -\frac{e^2 v_\theta^2}{m\omega_c^2}\int_0^\infty d\varphi \int d^3\vec{v}\, f_o(\vec{v})e^{i\vec{k}}[i\vec{k}\cdot\vec{L}\times\vec{L}\cdot(\vec{E}\cdot\vec{L}')] . \qquad (E.3)$$

The velocity integrals can be performed with the result

$$\vec{M} = -\frac{e^2 v_\theta^2}{m\omega_c^2}\int_0^\infty d\varphi\; i\vec{k}\cdot\vec{L}\times\vec{L}\cdot(\vec{E}\cdot\vec{L}')\exp\left[-\frac{i\omega\varphi}{\omega_c} - \frac{v_\theta^2\varphi^2}{2\omega_c^2}(\vec{k}\cdot\vec{L})^2\right] . \qquad (E.4)$$

From Eq. (D.6) we have

$$\vec{k}\cdot\vec{L}\times\vec{L}\cdot(\vec{E}\cdot\vec{L}') = -\vec{k}\cdot\vec{L}(\varphi)\times\vec{L}(-\varphi)\cdot\vec{E} . \qquad (E.5)$$

By directly substituting the definition of $\tilde{L}(\varphi)$ into (E.5), one obtains the relation

$$i\vec{k} \cdot \tilde{L}(\varphi) \times \tilde{L}(-\varphi) \cdot \vec{E} = \tilde{\mu}(\varphi) \cdot i\vec{k} \times \vec{E} \qquad (E.6)$$

where

$$\tilde{\mu}(\varphi) = \vec{n}\vec{n}(1 - \cos\varphi) + (I - \vec{n}\vec{n})\varphi \sin\varphi + (\vec{n} \times I)\varphi(1 - \cos\varphi) \; . \qquad (E.7)$$

Maxwell's equation gives

$$\vec{k} \times \vec{E} = \omega \vec{B}$$

Hence,

$$\vec{H} = \frac{i\omega^2 v_{\theta_0}^2 n_0}{\omega_c^3} \int_0^\infty \tilde{\mu}(\varphi) \cdot \vec{B} \exp\left[-\frac{i\omega\varphi}{\omega_c} - \frac{v_\theta^2}{2\omega_c^2}(\vec{k} \cdot \vec{L})\right] d\varphi$$

$$= \frac{i\omega}{\omega_c^3} \frac{\omega_p^2 v_\theta^2}{c^2 \mu_0} \int_0^\infty \tilde{\mu}(\varphi) \cdot \vec{B} \exp\left[-\frac{i\omega\varphi}{\omega_c} - \frac{v_\theta^2}{2\omega_c^2}(\vec{k} \cdot \vec{L})\right] d\varphi \; . \qquad (E.8)$$

Thus for a Maxwellian plasma with isotropic temperature, the magnetization vector can be expressed in terms of $\vec{B}$.

APPENDIX B. COMPUTER PROGRAM FOR SOLVING THE DISPERSION RELATION

1. The Root Finding Procedure

The computer program used to solve the dispersion relation, Eq. (4.2), is briefly described in this section. Let us define

$$\text{Det}\,[A_{ij}] = \frac{J_1(k_1 a)}{J_0(k_1 a)} - \frac{\text{[illegible]}}{\text{[illegible]}} \qquad (B.1)$$

$$\text{Det}\,[A_{ij}] = a_{11}^2 - a_{12}^2 \qquad (B.2)$$

The solutions of the dispersion relation are chosen to the simultaneous conditions, $k = \ldots$ and $\ldots$ are known [illegible] and $\ldots$.

Based on the fact that a_{11} and a_{12} for a fixed $\ldots$ are slowly varying functions of $\ldots$ most of the time, we apply Muller's procedure[4] to find $\ldots$ as a function of $\ldots$ from $\ldots$. The Muller method's procedure produces the root $\ldots$ from a trial value $\ldots$ by the equation

$$\ldots = \ldots - \frac{\text{Det}\,[A_{ij}]}{\ldots} \qquad (B.3)$$

where $\ldots$. Once $\ldots$ is found, we substitute this value into Eq. (B.2), making k a function of $\ldots$ and $\ldots$ only. Then Muller's root finding procedure is used to solve $k = \ldots$ in order to find $\ldots$ as a function of $\ldots$.

The steps in the root finding procedure are explained in the two flow diagrams of Figs. B.1 and B.2. Figure B.1 shows how $\ldots$ is obtained by means of Muller's procedure and Fig. B.2 describes Muller's procedure to find $\ldots$. For a fixed $\ldots$ Muller's method requires three trial values $\ldots$, $\ldots$ and $\ldots$ with the corresponding $k = \ldots$, $k = \ldots$ and $k = \ldots$. The program $\ldots$ is not a satisfactory root, it is used as a trial value to produce a more satisfactory root. The process is repeated until the root is found to a desired degree of accuracy.

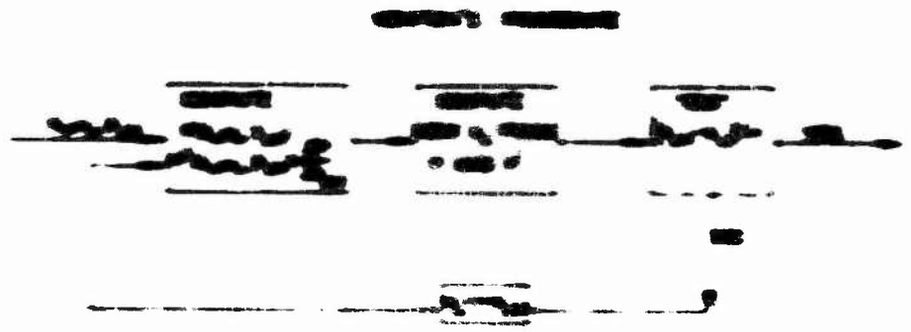

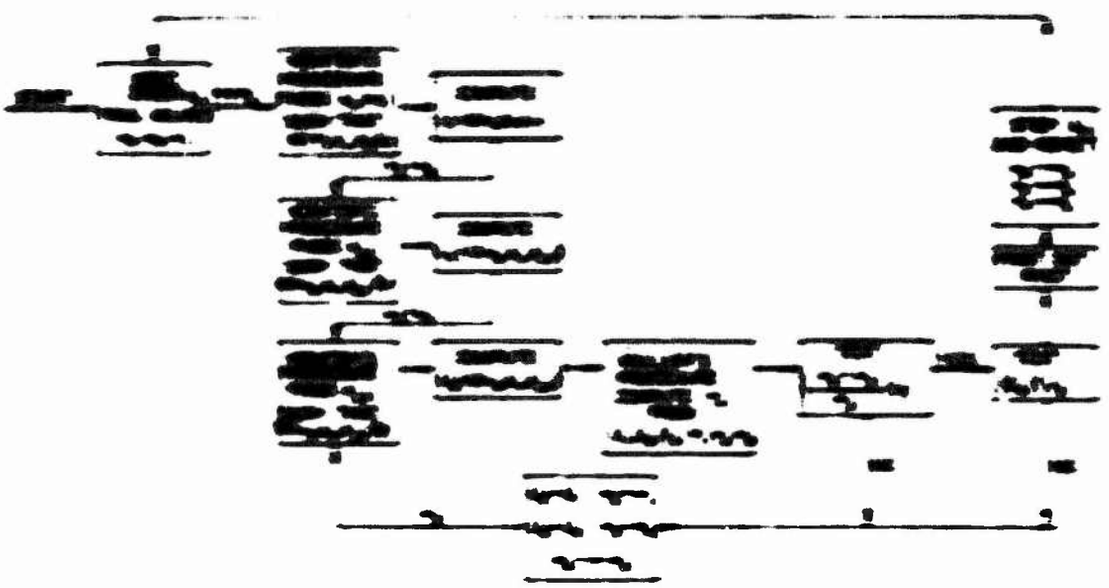

The root finding procedure works only if the trial values are near a root. Thus the program is started at a point where the root is either known or can be guessed easily so that the very initial trial values α_x, α_y and α_z are not far from a root. Once the root is found, k_0 is changed by a small increment and α_x, α_y and α_z are changed in the manner described in the flow diagram. By this means the roots can be tracked into points where they are not easily obtained or known.

F. Functions Used in the Program for Dielectric Planes

In Section E we discussed the overall procedure to find the roots of the dispersion relation. In this section we describe the manner in which the various [illegible] are computed.

a. Eulerian Constant of the gamma function, γ

A short program developed by Shaffer and Simmons[42] is used to compute γ.

b. Modified Bessel Functions, $I_0(k^2/2)$

The series expansion of I_0 is used. The argument of the functions $k^2/2$ is small enough in our calculations to enable us to use the power series expansion.

c. The ratio of the Bessel functions $J_1(k_- b)/J_0(k_- b)$

A continued fraction expansion[43] given by

$$\frac{J_1(k_-)}{J_0(k_-)} = \frac{x}{2} - \frac{x^2}{4} - \frac{x^2}{6} - \cdots \frac{x^2}{2n} - \cdots \qquad (F.4)$$

is used to compute the ratio for $0 < |k_- b| < 1$. For $|k_- b| \geq 1$, asymptotic series are used to compute $J_1(k_- b)$ and $J_0(k_- b)$.

d. Hankel functions H_0 and H_1

For the cases with finite waveguide radius, a program based on power series and asymptotic expansions written by J. Simpson[66] is used. For $a = \infty$, Eq. (E.1) reduces to

$$S = k_\perp \epsilon_{xx} \frac{J_1(k_\perp b)}{J_0(k_\perp b)} - ik_t \frac{H_1^{(1)}(ik_t b)}{H_0^{(1)}(ik_t b)} \quad . \qquad (F.5)$$

For this case a continued fraction expansion for H_0/H_1 developed by Barfler is used in the range $|jk_t b| \geq 1.5$. The continued fraction is given by

$$-ix \frac{H_n^{(1)}(ix)}{H_{n-1}^{(1)}(ix)} = x \frac{K_n(x)}{K_{n-1}(x)} = (2x-2n-1) + \frac{(1+2n)(3/2 + n)(1/2)}{1 + x}$$

$$- \frac{(1/2 - n)(5/2 - n)1/4}{2 + x} - \frac{(3/2 - n)(7/2 + n)1/4}{3 + x} - \cdots$$

(F.6)

For smaller values of $|x|$, power series representations for H_1 and H_0 are used.

3. Functions Used in the Program for Ions

For waves near the ion cyclotron and ion plasma frequencies, the wave numbers $k_\parallel$ are very small as compared to $|k_\perp|$, making the wave propagation almost perpendicular to the column. In a certain range of small $k_\parallel$, $|k_\perp|$ becomes so large that a prohibitive number of terms has to be taken in the series representation of the ions susceptibility.

We saw in Appendix D that only one integration is needed to evaluate the susceptibility tensor elements, i.e.,

$$S_{ii} = \int_0^\infty d\varphi \exp\left[-\frac{i\omega\varphi}{\omega_{ci}} - \frac{k_\parallel^2 v_{\theta i}^2 \varphi^2}{2\omega_{ci}^2} - \frac{k_\perp^2 v_{\theta i}^2}{\omega_{ci}^2} (1 - \cos\varphi) \right] \quad . \quad (F.7)$$

This integral represents a Laplace transform of a product of two functions,

$$q_1(\varphi) = \exp\left[-\frac{k_\parallel^2 v_{\theta i}^2}{2\omega_{ci}^2} \varphi^2 \right] \qquad (F.8)$$

$$q_2(\varphi) = \exp\left[-\frac{k_\perp^2 v_{\theta i}^2}{\omega_{ci}^2}(1 - \cos\varphi)\right] \qquad \text{(F.9)}$$

and, hence, the convolution theorem can be used in its evaluation. The result of this procedure is given by

$$S_{1i} = \int_{-\infty}^{\infty} \frac{\exp\left[-(w/x_i)^2\right]}{x_i\sqrt{\pi}} J_\perp\left(\nu - w, \frac{\lambda^2}{2}\right) dw \qquad \text{(F.10)}$$

where

$$x_i^2 = \frac{2k_\parallel^2 v_{\theta i}^2}{\omega_{ci}^2}$$

$$\frac{\lambda_i^2}{2} = \frac{k_\perp^2 v_{\theta i}^2}{\omega_{ci}^2}$$

$$\nu = \frac{\omega}{\omega_{ci}}$$

and

$$J_\perp\left(\nu, \frac{\lambda^2}{2}\right) = \int_0^\infty \exp\left[i\nu\varphi - \frac{\lambda_i^2}{2}(1 - \cos\varphi)\right] d\varphi \,. \qquad \text{(F.11)}$$

The integral for purely transverse propagation $J_\perp[\nu,(\lambda^2/2)]$ has been evaluated by Derfler[49] in terms of Nielson's cylinder function.[63] A fast computer program based on this result is used to find $J_\perp[\nu,(\lambda^2/2)]$. The integral of Eq. (F.10) is then evaluated by the Gauss-Hermite quadrature formula.[64] This technique is particularly good when the quantity x_i is very small in which case $\exp[-(\nu/x_i)^2]/(\sqrt{\pi}\, x_i)$ approximates a Dirac delta function.

The entire program was written in SUBALGOL which is the Stanford version of ALGOL 60.

REFERENCES

1. W. B. Nottingham, "Thermionic Emission," Encyclopedia of Physics, Vol. XXI, S. Flugge, Ed. (Apringer-Verlag, Berlin, 1956).

2. P. Weissglas, "Resonance Oscillations in a Hot Non-Uniform Plasma," Phys. Rev. Letters, 10, 206 (1963).

3. J. V. Parker, "Resonance Oscillations in a Hot Non-Uniform Plasma," TR No. 20, Calif, Inst. of Tech., Pasadena, Calif., May 1963.

4. A. Dattner, "A Study of Plasma Resonances," Ericsson Technics, 2, 309 (1957); "Resonance Densities in a Cylindrical Plasma Column," Phys. Rev. Letters, 10, 205 (1963).

5. S. V. Goeler, "Influence of Ion Loss on Diffusion of Cesium Plasma in the Q Machine," Phys. Fluids, 7, 463 (1964).

6. B. Hall, "Parallel-Plate Plasma Problem," American J. Phys. 31, 696 (1963).

7. A. W. Trivelpiece and R. W. Gould, "Space Charge Waves in Cylindrical Plasma Columns," J. Appl. Phys., 30, 1784 (1959).

8. B. Agdur and P. Weissglas, "Waves in Hot, Anisotropic Electron Plasmas," Ericsson Technics, 20, 267 (1964).

9. A. J. Lichtenberg and J. S. Jayson, "Propagation and Instabilities of Waves in Bounded Finite Temperature Plasma," J. Appl. Phys., 36, 449 (1965).

10. H. H. Kuehl, G. E. Stewart, and C. Yeh, "Wave Propagation in Hot Plasma Waveguides with Infinite Magnetostatic Fields," Phys. Fluids, 8, 723 (1965).

11. J. E. Drummond, "Basic Microwave Properties of Hot Magnetoplasmas," Phys. Rev., 110, 293 (1958).

12. K. N. Stepanov, "Kinetic Theory of Magnetohydrodynamic Waves," Soviet Physics JETP, 7, 892 (1958).

13. T. H. Stix, The Theory of Plasma Waves, (McGraw Hill Book Co., New York, 1962).

14. H. Derfler, "Theory of R-F Probe Measurements in a Fully Ionized Plasma," Proc. 5th Inter. Conf. Ionization Phenomena in Gases (North-Holland Pub. Co., Amsterdam, 1961) Vol. 2, p. 1423.

15. H. Derfler, "Growing Wave and Instability Criteria for Hot Plasmas," 8th Inter. Conf. on Phenomena in Ionized Gases, Vienna, Austria 1967 (to be published).

16. B. B. Kadomtsev and A. V. Nedospasov, "Instability of the Positive Column in a Magnetic Field and the 'Anomalous' Diffusion Effect," J. Nucl. Energy, C1, 230 (1960).

17. S. Chandrasekhar, Hydrodynamic and Hydromagnetic Stability, (Clarendon Press, Oxford, England 1961) p. 485.

18. O. Buneman, "Dissipation of Currents in Ionized Media," Phys. Rev., 115. 503 (1959).

19. F. W. Crawford and J. A. Tataronis, "Absolute Instabilities of Perpendicularly Propagating Cyclotron Harmonic Plasma Waves," J. Appl. Phys., 36, 2930 (1965).

20. L. I. Rudakov and R. Z. Sagdeev, "Oscillations of an Inhomogeneous Plasma in a Magnetic Field," Soviet Physics JETP, 37(10), 952 (1960).

21. N. A. Krall and M. N. Rosenbluth, "Stability of Slightly Inhomogeneous Plasma," Phys. of Fluids, 4, 163 (1961).

22. N. A. Krall and M. N. Rosenbluth, "Trapping Instabilities in a Slightly Inhomogeneous Plasma," Phys. of Fluids, 5, 1435 (1962).

23. A. B. Mikhailovskii and A. V. Timofeev, "Theory of Cyclotron Instability in a Non-Uniform Plasma," Soviet Physics JETP, 17, 626 (1963).

24. R. F. Post and M. N. Rosenbluth, "Electrostatic Instabilities in Finite Mirror-Confined Plasmas," Phys. of Fluids, 9, 730 (1966).

25. A. L. Eichenbaum and K. G. Hernquist, "Space Charge Instabilities in Synthesized Plasmas," J. Appl. Phys., 32, 16 (1961).

26. I. Langmuir, "The Nature of Adsorbed Films of Caesium on Tungsten Part 1," Phys. Rev., 43, 224 (1933).

27. L. M. Milue-Thomson, Jacobian Elliptic Function Tables, (Dover Publications, Inc., New York, 1950).

28. H. Hancock, Elliptic Integrals, (Dover Publications, Inc., New York, 1958).

29. R. W. Wright, "Positive and Negative Thermionic Emission from Molybdenum," Phys. Rev., 60, 465 (1941).

30. R. E. Honig, "Vapor Pressure Data for the More Common Elements," RCA Review, 13, 195 (1957).

31. L. P. Smith, "Thermionic Emission," Handbook of Physics, E. U. Condon and H. Odishaw, Eds. (McGraw-Hill, New York, 1958) Part 8, ch. 6.

32. H. Derfler and H. Omura, Quarterly Research Review No. 10, Stanford Electronics Laboratories, Stanford University, Stanford, California 1964, p. I-99.

33. A. N. Nesmeyanov, Vapor Pressure of the Elements, (Academic Press, New York, 1961).

34. I. Langmuir and K. H. Kingdon, "Thermionic Effects Caused by Vapors of Alkali Metals," Proc. Roy. Soc. (London), 107A, 61 (1925).

35. E. P. Gyftopoulos and J. D. Levine, "Work Function Variation of Metals Coated by Metallic Films," J. Appl. Phys., 33, 67 (1962).

36. J. D. Levine and E. P. Gyftopoulos, "Adsorption Physics of Metallic Surfaces Partially Covered by Metallic Particles. I," Surface Science, I, 171 (1964).

37. J. D. Levine and E. P. Gyftopoulos, " Adsorption Physics of Metallic Surfaces Partially Covered by Metallic Particles. II," Surface Science, I, 225 (1964).

38. H. Derfler and T. C. Simonen, "Landau Waves: An Experimental Fact," Phys. Rev. Letters, 17, 172 (1966).

39. W. H. Cutler, "Thermal Cesium Plasma," Microwave Laboratory Report No. 1326, Stanford University (1965).

40. D. J. Rose and M. Clark, Plasmas and Controlled Fusion, (The M.I.T. Press and John Wiley and Sons, Inc., 1961).

41. D. R. Dobrott, "On the One-Dimensional Plasma-Conductivity Kernel in the Space-Frequency and Space-Time Domains," Technical Report No. 0256-2, Electron Devices Lab., Stanford Electronics Laboratories, Stanford, Calif., 1963.

42. T. C. Simonen, "Landau Waves," Report SUIPR No. 100, Institute for Plasma Research, Stanford, Calif., 1966.

43. O. Buneman, Plasma Dynamics, (Class notes for a graduate course [EE 292K] at Stanford University), Chapter 15.

44. B. D. Fried, Future Foundation of Electronics, (McGraw-Hill Book Co., New York, 1966), Chapter 9.

45. B. D. Fried and S. D. Conte, The Plasma Dispersion Function (Academic Press, N.Y., 1961).

46. I. B. Bernstein, "Waves in a Plasma in a Magnetic Field," Phys. Rev., 109, 10 (1958).

47. F. W. Crawford, G. S. Kino, H. H. Weiss, "Excitation of Cyclotron Harmonic Resonances in a Mercury-Vapor Discharge," Phys. Rev. Letts., 13, 229 (1964).

48. H. Okegamic, "Microwave Emission at Electron Cyclotron Harmonics," SUIPR Report No. 29, Institute for Plasma Research, Stanford Electronics Laboratories, Stanford, Calif., 1965.

49. H. Derfler, to be published.

50. E. Jahnke and F. Ende, Tables of Functions, (Dover Publications, New York, 1945), Chatper 8.

51. D. Bohm and E. D. Gross, "Theory of Plasma Oscillations," Phys. Rev., 74, 1951 (1945).

52. J. H. Malmberg and C. B. Wharton, "Dispersion of Electron Plasma Waves," Phys. Rev. Letts. 17, 175 (1966).

53. J. M. Jones, "Self-Excited Plasma Surface-Waves," Physics Letts., 5, 324 (1963).

54. J. E. Simpson, "An Instability of a Beam-Generated Plasma in a Uniform Magnetic Field," Report SUIPR No. 38, Plasma Physics Lab., Stanford Electrics Laboratories, Stanford, Calif., 1965, p. 43.

55. K. I. Thomassen, "Turbulent Diffusion in a Penning-Type Discharge," Phys. Fluids 9, 1836 (1966).

56. E. Kamke, Differentialgleichungen, Vol. II, (Akademische Verlagsgesellschaft Becker und Erler Kom.-Ges., Leipzig 1944), p. 31.

57. A. Erdelyi, et al, Higher Transcendental Functions, (McGraw-Hill Book Co., New York, 1953) Vol. II, Chapter VI.

58. P. M. Morse and H. Feshbach, Methods of Theoretical Physics (McGraw-Hill Book Co., N.Y., 1953) Vol. 1.

59. G. H. Hardy, A Course of Pure Mathematics (Cambridge University Press, Cambridge, England, 1960), p. 288.

60. D. Muller, "A Method for Solving Algebraic Equations Using an Automatic Computer," Mathematical Tables and Other Aids to Computation, 10, 208 (1956).

61. A. N. Khovanskii, The Application of Continued Fractions and Their Generalization to Problems in Approximation Theory (P. Noordhoff, The Netherlands, 1963).

62. Reference 54, Appendix B.

63. N. Nielsen, Handbuch der Theorie der Cylinderfunktionen (Druck und Verlag von B. G. Teubner, Leipzig, 1904).

64. Z. Kopal, Numerical Analysis (John Wiley and Sons, Inc., 1961), Appendix IV.

UNCLASSIFIED
Security Classification

DOCUMENT CONTROL DATA - R&D

(Security classification of title, body of abstract and indexing annotation must be entered when the overall report is classified)

1. ORIGINATING ACTIVITY (Corporate author)
The Board of Trustees of the Leland
Stanford Junior University
Stanford, California

2a. REPORT SECURITY CLASSIFICATION
UNCLASSIFIED

2b. GROUP
NA

3. REPORT TITLE
ELECTROSTATIE WAVES IN BOUNDED HOT PLASMAS

4. DESCRIPTIVE NOTES (Type of report and inclusive dates)
Technical Report

5. AUTHOR(S) (Last name, first name, initial)
Masayuki Omura

6. REPORT DATE	7a. TOTAL NO. OF PAGES	7b. NO. OF REFS
June 1967	128	64

8a. CONTRACT OR GRANT NO.	9a. ORIGINATOR'S REPORT NUMBER(S)
DA 28-043 AMC-00482(E)	SUIPR REPORT NO. 156
b. PROJECT NO. 1G-22001-A-055-04-09	
c.	9b. OTHER REPORT NO(S) (Any other numbers that may be assigned this report) ECOM-00482-11
d.	

AVAILABILITY/LIMITATION NOTICES
This document is subject to specisl export controls snd each transmittal to foreign governments or foreign nstionsls may be made only with prior approval of CG, USAECOM, AMSEL-KL-TG, Ft. Monmouth, N.J. 00703

11. SUPPLEMENTARY NOTES	12. SPONSORING MILITARY ACTIVITY
	U.S. Army Electronics Command Ft. Monmouth, N.J. AMSEL-KL-TG

13. ABSTRACT This report desls with the study of electrostatic waves in bounded hot plssmss snd, except for s few dc messurements, is theoretical.

The study is brosdly divided into two psrts. The first section investigates wsves in s diode system with no dc msgnetic field applied. A dc snalysis of the equilibrium plssms produced within s thermionic diode is undertsken to provide s basis for the rf analysis, snd expected plssms densities in the diode are computed for s vsriety of prscticsl situations. Electrostatic wave resonances in the diode are predicted by using the hydrodynsmic model for the nonuniform plssms. The impedsnce of s uniform plssms diode is obtsined by using s kinetic model of the plssms. This model enables us to tske into sccount the end plste electron sbsorption loss, s process similsr to thst which csuses end plate diffusion in the Q-mschine. The sbsorption loss is found to have s large effect on the impedsnce of the diode.

The second psrt of the report desls with the study of guided wsves slong s cylindricsl column of Msxwellisn plssms in s magnetic field. A dc study of the plssms column is first conducted. Theoretical density snd current profiles are obtsined snd sre compsred with the messured results. Since sn rf snalysis using s self-consistent dc solution is quite involved, the plssms column is approximated by s uniform plssms with s shsrp boundsry snd no drift. To obtsin the rf fields in such s column, s plsne-wsve solution for sn infinite Msxwellisn plssms in sn spplied msgnetic field is first obtsined. By superimposing infinitely nsny plsne wsvez, the fields within the column are constructed, snd by matching the sppropriste fields st the boundsry, s dispersion relstion is derived.

DD FORM 1 JAN 64 1473

UNCLASSIFIED
Security Classification

DD Form 1473
ELECTROSTATIC WAVES IN BOUNDED HOT PLASMAS
Abstract - Page 2

The solutions to the dispersion relation reveal the existence of a new type of unstable wave. When only the electrons are assumed to respond to the electric field, the surface waves which propagate when $\omega_{ce} < \omega_{pe}$ are found to be unstable. When the ion motion is included, additional unstable surface waves are obtained whenever $\omega_{ci} < \omega_{pi}$. A study of the instability shows that it is due to finite Larmor radii effects and is driven by the transverse energy of the particles.

While the "electron" surface wave instability is relatively weak and can easily be stabilized by making $\omega_{ce} > \omega_{pe}$, the "ion" surface wave instability is found to be very strong, and the stabilizing condition of $\omega_{ci} > \omega_{pi}$ is not easily attained in high density plasmas such as those in fusion machines. Thus, the unstable ion surface waves may have a serious effect on the containment of the fusion plasma.

UNCLASSIFIED

Security Classification

KEY WORDS	LINK A		LINK B		LINK C	
	ROLE	WT	ROLE	WT	ROLE	WT
ELECTROMAGNETIC WAVES						
PLASMA SCORE						
PLASMA COLUMN						
MARTELLIAS PLASMA						
SURFACE WAVES						

INSTRUCTIONS

1. ORIGINATING ACTIVITY: Enter the name and address of the contractor, subcontractor, grantee, Department of Defense activity or other organization (corporate author) issuing the report.

2a. REPORT SECURITY CLASSIFICATION: Enter the overall security classification of the report. Indicate whether "Restricted Data" is included. Marking is to be in accordance with appropriate security regulations.

2b. GROUP: Automatic downgrading is specified in DoD Directive 5200.10 and Armed Forces Industrial Manual. Enter the group number. Also, when applicable, show that optional markings have been used for Group 3 and Group 4 as authorized.

3. REPORT TITLE: Enter the complete report title in all capital letters. Titles in all cases should be unclassified. If a meaningful title cannot be selected without classification, show title classification in all capitals in parenthesis immediately following the title.

4. DESCRIPTIVE NOTES: If appropriate, enter the type of report, e.g., interim, progress, summary, annual, or final. Give the inclusive dates when a specific reporting period is covered.

5. AUTHOR(S): Enter the name(s) of author(s) as shown on or in the report. Enter last name, first name, middle initial. If military, show rank and branch of service. The name of the principal author is an absolute minimum requirement.

6. REPORT DATE: Enter the date of the report as day, month, year, or month, year. If more than one date appears on the report, use date of publication.

7a. TOTAL NUMBER OF PAGES: The total page count should follow normal pagination procedures, i.e., enter the number of pages containing information.

7b. NUMBER OF REFERENCES: Enter the total number of references cited in the report.

8a. CONTRACT OR GRANT NUMBER: If appropriate, enter the applicable number of the contract or grant under which the report was written.

8b, 8c, & 8d. PROJECT NUMBER: Enter the appropriate military department identification, such as project number, subproject number, system numbers, task number, etc.

9a. ORIGINATOR'S REPORT NUMBER(S): Enter the official report number by which the document will be identified and controlled by the originating activity. This number must be unique to this report.

9b. OTHER REPORT NUMBER(S): If the report has been assigned any other report numbers (either by the originator or by the sponsor), also enter this number(s).

10. AVAILABILITY/LIMITATION NOTICES: Enter any limitations on further dissemination of the report, other than those imposed by security classification, using standard statements such as:

1. "Qualified requesters may obtain copies of this report from DDC."
2. "Foreign announcement and dissemination of this report by DDC is not authorized."
3. "U. S. Government agencies may obtain copies of this report directly from DDC. Other qualified DDC users shall request through _____."
4. "U. S. military agencies may obtain copies of this report directly from DDC. Other qualified users shall request through _____."
5. "All distribution of this report is controlled. Qualified DDC users shall request through _____."

If the report has been furnished to the Office of Technical Services, Department of Commerce, for sale to the public, indicate this fact and enter the price, if known.

11. SUPPLEMENTARY NOTES: Use for additional explanatory notes.

12. SPONSORING MILITARY ACTIVITY: Enter the name of the departmental project office or laboratory sponsoring (paying for) the research and development. Include address.

13. ABSTRACT: Enter an abstract giving a brief and factual summary of the document indicative of the report, even though it may also appear elsewhere in the body of the technical report. If additional space is required, a continuation sheet shall be attached.

It is highly desirable that the abstract of classified reports be unclassified. Each paragraph of the abstract shall end with an indication of the military security classification of the information in the paragraph, represented as (TS), (S), (C), or (U).

There is no limitation on the length of the abstract. However, the suggested length is from 150 to 225 words.

14. KEY WORDS: Key words are technically meaningful terms or short phrases that characterize a report and may be used as index entries for cataloging the report. Key words must be selected so that no security classification is required. Identifiers, such as equipment model designation, trade name, military project code name, geographic location, may be used as key words but will be followed by an indication of technical context. The assignment of links, roles, and weights is optional.

DD FORM 1473

UNCLASSIFIED

Security Classification